Optimised Low Complexity Localisation in Wireless Sensor Networks

by

Naveed Salman

Submitted in accordance with the requirements for the degree of

Doctor of Philosophy

University of Leeds

School of Electronic and Electrical Engineering

August 2013

The candidate confirms that the work submitted is his own and that appropriate credit has been given where reference has been made to the work of others.

If we knew what it was we were doing, it would not be called research, would it?

Albert Einstein

Acknowledgments

I am most grateful to my supervisor, Dr Andrew Kemp, for his continuous encouragement and guidance. Working with Dr. Kemp was a pleasure, we had countless meetings and he always kept me motivated through ups and downs. I have learned a lot from Dr. Kemp and he played a key role in my professional and personal development over the past four years.

I am also grateful to my second supervisor Prof. Mounir Ghogho, a brilliant researcher and an inspiration to me. We had many fruitful meetings during which new ideas were discussed and my work was reviewed. I am also thankful to Dr. Des Mclernon, director of graduate studies for his help and support.

I also thank Prof. Jay Guo and Dr. Mark Hedley of CSIRO, Australia, with whom I discussed my research and we explored new areas in localisation for future research.

I would like to thank Dr. Nayef Alsindi and Dr. Basim Majeed of EBTIC, UAE, for giving me the opportunity to work with them.

I am thankful to Dr. Ismail Guvenc, associate editor, *IEEE Wireless Communication Letters*, who reviewed my letters and suggested valuable modifications.

Many thanks to my close friends and colleagues Ana Maria Popescu, Dr. Hemat Maheswari, Dr. Imtiaz Rasool and Waqas Khan.

Finally, above all, I thank my parents, my father Prof. Abdul Mutalib and my loving mother Naheeda Yasmin for their support. I know it must have been difficult for them to live away from me over these years as it was for me. But whatever I am now is because of them. Thank you.

Abstract

Wireless sensor networks (WSNs) consist of many small (up to several hundred) low powered sensing nodes. These nodes can be capable of sensing temperature, humidity, light intensity etc. In location aware WSNs, these nodes aside from sensing environmental conditions, can also locate themselves, thus promoting many new applications in the wireless communications industry. These applications may include firefighter tracking, cattle/wild life monitoring and logistics. One way to locate the nodes is to use global positioning system (GPS), however deploying a GPS chip on every sensor node is expensive and also they are power hungry. Moreover, GPS assisted nodes can only be located when a guaranteed line of sight (LoS) is present with the navigational satellites. On the other hand, nodes can also be located using low complexity and cheap local positioning systems (LPS).

Various techniques can be found in literature to locate wireless sensor nodes. Location algorithms, which are based on the absolute distance between nodes are known as range based algorithms. On the other hand, algorithms that do not require determination of the inter-node distance for localisation are called range-free positioning algorithms. Range free algorithms are based on the number of hops for communications between two nodes as a distance metric. Range based algorithms are however more accurate than range free algorithms.

In the context of range based algorithm, distance can be estimated between nodes by making use of the angle of the impinging signal, this technique is more commonly known as the angle of arrival (AoA) technique. Apart from being very sensitive to errors due to multipath, AoA is not favored for low complexity WSN localisation as an array of antennas or microphones is required on the sensor nodes to estimate the angle of the incoming signal. This increases the complexity and cost of the system. Absolute distance can be estimated using either the delay or attenuation of the signal. Systems capitalizing on the delay are more commonly known as time of arrival (ToA) systems. ToA localisation, although more accurate, requires highly accurate clocks and hence are high in complexity. On the other hand, received signal strength (RSS) based systems require no additional hardware and hence are more suitable for WSNs.

For location estimation via RSS (and ToA) the so called *trilateration* technique is used. A number of nodes, usually high in resources and with known locations known as anchor nodes (AN) are used to estimate the locations of target nodes (TN). The location of ANs can be determined using GPS or they can be placed at predetermined positions. Readings from the TN is received at the ANs and are transmitted to a central station for processing.

Due to its straightforward implementation, RSS has been an advantageous approach for low cost localisation systems such as WSN localisation. Thus a major part of this thesis focuses on RSS based localisation. The accuracy of location estimates via RSS is highly dependent on knowledge of the distance-power gradient or the so called path-loss exponent (PLE). Thus, degraded system performance is expected with an inaccurate PLE assumption. Although the propagation model is difficult to characterize in uncertain environments, the majority of current studies assume to have exact knowledge of the PLE. This is a gross oversimplification and hence this thesis looks into methods that considers the PLE as an unknown

variable in addition to the location coordinates of the target sensor node.

Thus the first part of this thesis deals with joint estimation of the PLE and location based on maximum likelihood (ML) and linear least squares (LLS) methods respectively. Error analysis of location estimates with incorrect PLE assumptions for both ML and LLS technique is done in their respective chapters. Furthermore, novel ideas such as assuming the PLE as an unknown random variable and development of a maximum a posteriori (MAP) estimator has also been discussed. While the hybrid Cramer Rao bound (CRB) is derived as benchmark for the MAP estimator. To further optimize the performance of the LLS technique, optimization such as optimal AN selection and weighted least squares (WLS) methods have also been proposed. Finally, a new linear CRB has been derived as a benchmark for the performance of the LLS.

The second part looks into another aspect of localisation that impacts the location accuracy i.e. AN/TN geometry. It is well known that the accuracy of TN location estimation depends on its relative angle with the ANs. Thus the placement of ANs has an impact on location accuracy. Optimal AN positions are achieved that guarantees best accuracy for the entire network area via extensive simulation. This is done via choosing the placement of ANs that offers the minimum mean CRB.

Finally, the impact of localisation error on upper layer applications i.e. routing of packets is studied. For location based routing, the fundamental assumption until recently was the absolute knowledge of the location of the forwarding nodes. This becomes unrealistic in localised networks and hence algorithms that are resilient to location error need to be developed. However, the first step is to recognise the impact of location on geographic routing parameters such as the packet delivery ratio (PDR) and loss rate (LR). Thus, via simulation, error analysis is done for

location error induced by ToA and RSS localisation. Furthermore, an algorithm is developed that reduces the performance degradation due to location error. The ascendancy of the proposed algorithm is proven via simulation.

Contents

List of Figures

List of Tables

Nomenclature

AN	Anchor node
aNm	Aditive noise model
AoA	Angle of Arrival
AWGN	Additive white Gaussian noise
C/A code	Coarse/Acquisition code
CCA	Clear channel assessment
CDF	Cumulative distribution function
CDMA	Code division multiple access
CMSER	Conditioned mean square error ratio
CRB	Cramer-Rao bound
CSMA/CA	Carrier Sense Multiple Access/Collision Avoidance
CW	Continuous waves
dB	Decibel
DoD	Department of defense

DP	Direct path
DSSS	Direct sequence spread spectrum
E911	Enhanced 911
FIM	Fisher information matrix
GHz	GigaHertz
GLONASS	Global navigation satellite system
GN	Gauss-Newton
GPS	Global positioning system
HCRB	Hybrid Cramer-Rao bound
HIM	Hybrid information matrix
JE	Joint estimator
kHz	kilo Hertz
LCJE	Low complexity joint estimator
LED	Least expected distance
LF	Low frequency
LJE	Linear joint estimator
LLS	Linear least squares
LLS-avg	Linear least squares-average
LLS-comb	Linear least squares-combination

LLS-ref	Linear least squares-reference
LM	Lavenberg-Marquardt
LOP	Line of position
LORAN	Long range navigation
LoS	Line of sight
LPS	Local positioning service
LR	Loss rate
MAI	Mutliple access interference
MAP	Maximum a posteriori
MDS	Multidimensional scaling
MEP	Maximum expectation progress
MER	Maximum expectation within transmission range
MFR	Most forward within range
MHz	MegaHertz
ML	Maximum likelihood
mNm	Multiplicative noise model
MSE	Mean square error
MSER	Mean square error ratio
NLoS	Non line of sight

NLS	Nonlinear least square
OW-ToA	One way time of arrival
P code	Precision code
pdf	Probability density function
PDR	Packet delivery ratio
PLE	Path-loss exponent
PPS	Precise positioning service
RF	Radio frequency
RMSE	Root mean square error
RSS	Received signal strength
RSSE	Received signal strength estimator
SNR	Signal-to-Noise Ratio
SNR	Signal-to-noise ratio
SPS	Standard positioning service
TDoA	Time difference of arrival
TN	Target Node
ToA	Time of arrival
TW-ToA	Two way time of arrival
UWB	Ultra wide band

VHF	Very high frequency
WLAN	Wireless local area network
WLS	Weighted least squares
WLS-avg	Weighted least squares-avg
WLS-comb	Weighted least squares-comb
WLS-ref	Weighted least squares-reference
WSN	Wireless sensor networks

List of Symbols

$\mathbf{A}^{\dagger}$ Moore–Penrose pseudoinverse

A Amplitude

$\mathbf{B}$ Bias

BW Bandwidth

$\mathbf{C}$ Covariance matrix

c speed of the electromagnetic wave ($3 \times 10^{8} m/s$)

d Euclidean distance

d_0 Reference distance (normally taken as 1 m)

E Expectation operator

f Frequency (Hertz)

G_t Transmitter antenna gain

G_r Receiver antenna gain

$h\,(t)$ Channel impulse response

$\mathbf{I}$ Fisher information matrix

$\mathbf{J}$ Jacobian matrix

ρ Number of iterations

$\mathscr{L}$ Path-loss

$\mathcal{N}$ Normal distribution

n Guassian noise

$p(.)$ Probability density function

P_t Transmit power

$\mathscr{R}^n$ Set of n dimensional real numbers

Tr Trace of matrix

δ Dirac function

τ Time delay

λ Wavelength

$\bar{\lambda}$ Newton step size

ϕ Phase

τ Time delay

ϵ_r Relative electrical permittivity

Θ Angle between TN and AN

μ Mean

σ^2 Variance

$\boldsymbol{\theta}$ Unknown parameters (to be estimated)

α PLE

$\Delta\alpha$ PLE error

$\check{\alpha}$ Incorrect PLE

α_0 Correct PLE

ε Cost function

w Shadowing noise

$\nabla_{\boldsymbol{\theta}}$ Gradient with respect to $\boldsymbol{\theta}$

$\tilde{\delta}$ Newton step

η Number of indepedent runs

ϱ Scaling factor

$\mathcal{B}$ Effective bandwidth

M Total number of ANs (chapter 4)

N Total number of ANs (chapter 2, 3, 5)

List of publications

Part of this thesis was published in the following papers.

Journal Publications

2013 N. Salman, M. Ghogho, and A. H. Kemp, "Optimized Low Complexity Sensor Node Positioning in Wireless Sensor Networks," *IEEE Sensors Journal.,*vol.14, no.1, pp.39,46, Jan. 2014.

2013 A. M. Popescu, N. Salman, and A. H. Kemp, "Geographic Routing Resilient to Location Errors," *IEEE Wireless Commun Lett.*, vol. 2, no. 2, pp. 203–206, April. 2013.

2012 N. Salman, M. Ghogho, and A. H. Kemp, "On the joint estimation of the RSS-based location and path-loss exponent," *IEEE Wireless Commun. Lett.*, vol. 1, no. 1, pp. 34–37, Feb. 2012.[1]

2012 N. Salman, M. Ghogho, and A. H. Kemp, "Low Complexity Joint Estimation of Location and Path-Loss Exponent," *IEEE Wireless Commun Lett.*, vol. 1, no. 4, pp. 364–367, Aug. 2012.

2012 A. M. Popescu, N. Salman, and A. H. Kemp, "Energy consumption of geographic routing with realistic localisation," *IET Networks,* Volume

[1]This paper won the Carter best paper award 2012 from the School of Electronic and Electrcial Engineering, University of Leeds.

1, issue3, September 2012, p. 126 – 135.

2013 I. Rasool, N. Salman, and A. H. Kemp, “RSSI-based Real-time Positioning in a 3-D Wireless Sensor Network,” accepted with revisions in *IET journal on Wireless Sensor Systems (WSS),* 2013.

Refereed Conferences

2012 N. Salman, M. Ghogho, J. Guo, A. H. Kemp, “Analysis of linear least square solution for RSS based localization” *12th International Symposium on Communications and Information Technologies (ISCIT), 2012.* pp. 1051 - 1054, Oct 2012.

2012 I. Rasool, N. Salman, and A. H. Kemp, "RSSI-based Positioning in Unknown Path-Loss Model for WSN” *Sensor Signal Processing for Defence (SSPD),*" Sept.2012.

2012 A. M. Popescu, N. Salman, and A. H. Kemp, “Energy consumption analysis of geographic routing in WSNs with location error," *8th European Wireless Conference, 2012.* pp.1-8, 18-20 April 2012.

2012 I. Rasool, Ion G. Tudorache, N. Salman, and A. H. Kemp , "Range Filtration Algorithm for Wireless Sensor Networks," *20th Telecommunications Forum TELFOR 2012,* pp. 180 - 185, 20-22 Nov. 2012.

2010 N. Salman, I. Rasool, and A. H. Kemp , "Overview of the IEEE 802.15.4 standards family for Low Rate Wireless Personal Area Networks," *7th International Symposium on Wireless Communication Systems (ISWCS),* 2010, pp.701-705, 19-22 Sept. 2010.

2010 I. Rasool, N. Salman, and A. H. Kemp , "GOF analysis for Gaussianity assumption of range errors in WSN," *7th International Symposium on*

Wireless Communication Systems (ISWCS), 2010, pp.154-158, 19-22 Sept. 2010.

2011 N. Salman, H. K. Maheshwari, A. H. Kemp, M. Ghogho, "Effects of anchor placement on mean-CRB for localization," *The 10th IFIP Annual Mediterranean Ad Hoc Networking Workshop (Med-Hoc-Net),* pp.115-118, 12-15, June 2011.

1 Introduction

Through out history man has always been curious to know where things are; from navigation by looking at stars to modern techniques such as local positioning service (LPS) and the global positioning system (GPS), locating objects has invariably been of great interest. However, in the last two decades, new technologies such as wireless sensor networks (WSN) have become very popular and localisation of nodes in such networks present new challenges. The next section presents a short history of wireless localisation systems.

1.1 A Short History of Wireless Localisation Systems

As with most technologies, positioning in wireless networks started in the military circles. Interest in navigation systems for military use dates back to the second world war when the Decca and LORAN (Long Range Navigation) systems were implemented. Later on new systems such as the Omega navigation system and GPS were developed. Here we give a brief overview of the historical and technical background of these systems.

1.1.1 The Decca navigation systems

The idea of the Decca systems was first conceived by W.J.O'Brien, an American researcher, in order to track the ground speed of aircrafts and called it API (Aircraft position Indicator). O'Brien however could not raise the interest of the American military officials for his system. After the war broke out in 1939 the British Decca Radio and Television Company carried out successful trials on the system. The British required an accurate navigation system for locating aircrafts and ships. The operation of the Decca system began one day before the invasion of France (D-Day) [1]. The Decca system is based on the phase comparison between continuous waves (CW) signals originating from a chain. A chain consists of a master station and three slave stations known as the red, green and purple stations. The slave stations are situated at the corners of an equilateral triangle and the master station is located at the center. The distance between the master and each slave station is around 92- 140 km. All stations transmit with frequencies that are harmonics of a common frequency f. On reception, the phase difference between the master and one of the slaves is measured and is translated into a hyperbolic line called a pattern. The three pairs of master-slave stations define three such patterns, which are drawn on nautical charts as shown in Fig. 1.1. The point of intersection of two patterns suggests the position of the receiver [1]. The Decca is a low frequency (LF) based system with a range up to 400 km and accuracy of about 50 m. 1.1 shows the harmonic frequencies of the masters and slave stations. Receiver with multiplying circuits receives the signals from a master/ slave pair. The signals are multiplied up to a common frequency on which the phase comparison is done. The common frequencies for each master/slave pair is given as follows:

- Master/Red $24f$

- Master/Green $18f$
- Master/Purple $30f$

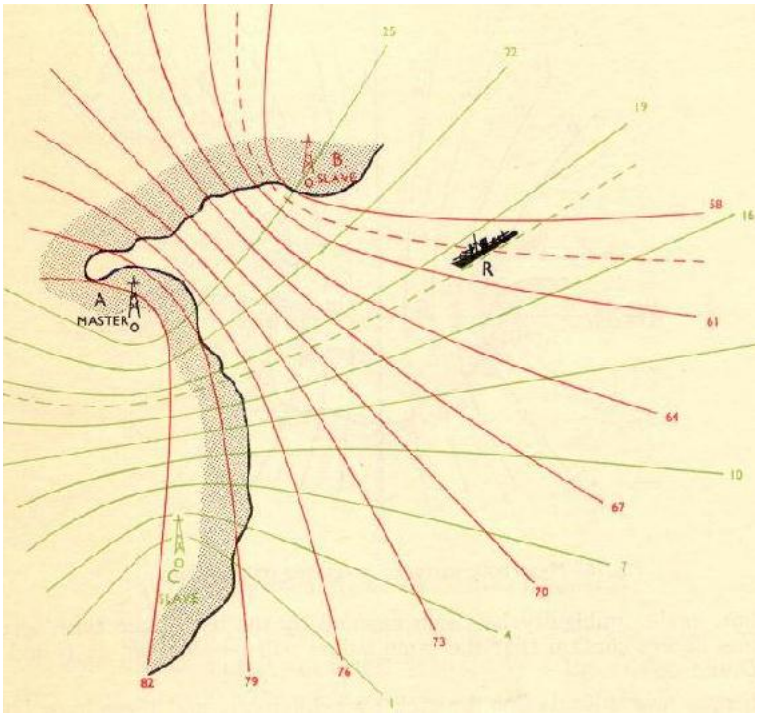

Figure 1.1: Decca lattice chart [1].

Station	Harmonic	Frequency
Master	$6f$	85 kHz
Red	$8f$	112 kHz
Green	$9f$	127 kHz
Purple	$5f$	71 kHz

Table 1.1: Harmonic frequencies of master/slave stations.

1.1.2 The LORAN systems

The LORAN systems were also developed during the Second World War. LORAN (initially known as LRN) was employed by the US and Royal Navy for navigation of marine ships. The Loran-A was the first less accurate system, which operated in the 1715-2000 kHz band and had a range of 1200 miles. LORAN-D was a

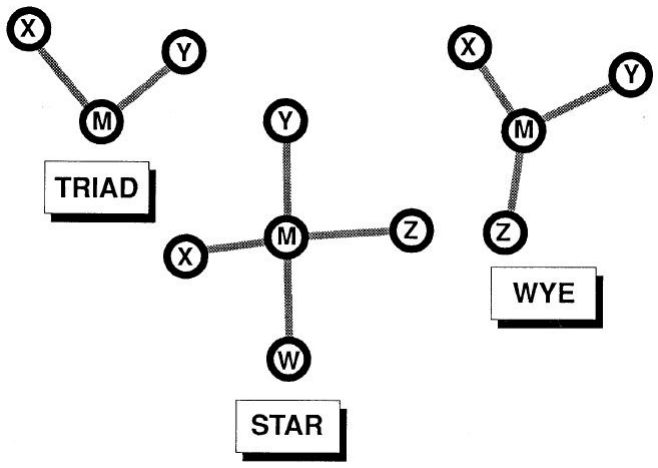

Figure 1.2: Master/slave topology for LORAN-C [2].

short-range system used for navigation of large air force planes. While Loran-F is employed for drone navigation. The LORAN-B differed from the other systems as it was based on the phase comparison of the incident signals [3], however, the LORAN-C was the most widely used system and will be discussed briefly here. Loran-C operates in the LF i.e. 90-110 kHz band and has a range around 1000 miles. The positioning accuracy for LORAN-C is around 500 meters. The LORAN-C like the Decca system is based on the principle of hyperbolic positioning. In the LORAN-C, instead of phase comparison, time difference of arrival (TDoA) of signals between stations is utilized to obtain position estimation. A Loran chain consists of at least three stations, consisting of one master and at least two secondary stations. The chain topology can be classified into three types; *triad*, *Wye* and *star*, this is shown in the Fig. 1.2.

TDoA at the receiver of one master and one secondary station signal defines one hyperbolic line of position (LOP). The transmitted signal from the master station consists of nine pulses while the secondary station signal is formed by a series of eight pulses. The difference of the number of pulses enables the receiver to distinguish between the master and secondary station signals. The master

station transmits its signal first; this signal when received by the receiver starts its clock. The secondary station also receives the transmission from the master in a time duration known as the baseline length (BLL) and then waits for a specific time duration known as the secondary coding delay (SCD) before transmitting its signal. The emission delay (ED) is BLL plus the SCD. The pulses from the master and the secondary stations are transmitted at a common group repetition rate (GRR). The time difference (TD) measurement is illustrated in Fig. 1.3.

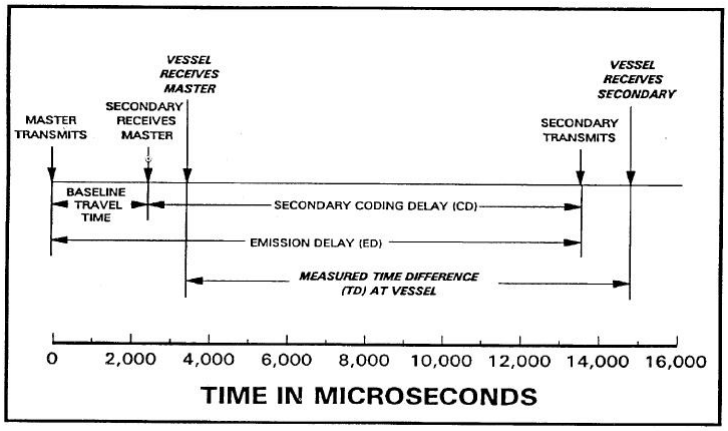

Figure 1.3: Time axis for LORAN-C localisation [2].

1.1.3 The OMEGA navigation system

The Omega navigation system was developed by the US navy for air craft navigation in 1968. Omega operates on a very low frequency (VLF) that ranges between 10-14 kHz. Similar to the Loran system, the Omega also is based on the hyperbolic positioning. The position estimation is achieved by phase comparison of the receiving signals. At the time of its operation, eight transmitters were placed strategically around the globe, and were used to provide worldwide coverage [4]. The Omega system achieved accuracies of 4 km. The Omega was the first world

wide navigation system which operated for 26 years. The system was shut down in 1997.

1.1.4 The global positioning system (GPS)

The GPS is the most widely used navigation system that provides three-dimensional positioning information at all times, all over the world. It has a wide range of applications including surveying, vehicle tracking, cellular positioning and aircraft tracking. GPS is an accurate satellite based navigation system, initially developed in the late 70's by the department of defense (DoD). A total of 27 satellites are in orbit with 24 operational and 3 spare, providing world wide positioning coverage. GPS satellites are at approximate altitudes of 20200 km above the earth. The first GPS satellite was sent into orbit in 1978 and by 1994, all 24 satellites were operational. The project cost an estimate of $12 billion [3, 5]. GPS positioning is based on the principle of trilateration, where at least three independent ranging between three satellites and user is carried out and then position of the user is estimated utilizing the ranging information. The structure of the GPS is broadly divided into three segments

- The space segment
- The control segment
- User

The control segment is formed by five land-based stations, their purpose is to monitor and control the satellite movement, clock correction and metrological data. The control segment is operated under the DoD. The space segment consists of the 24 operational satellites and is located in 6 orbital planes inclined at 55 degrees to the equator. The users include both military and commercial GPS devices. The GPS receiver can determine its position by first measuring its

distance with at least three satellites; this is done by calculating the time taken by signal to reach the user from each satellite. The exchange of information between the satellites and the receiver are done via codes. There are two types of carrier radio waves modulated by the codes. These two signals are known as L1 (1575.42 MHz) and L2 (1227.60 MHz). It must be noted here that these two signals are harmonically related to the fundamental frequency of 10.23 MHz that is generated by the atomic clocks (on board the satellites). These are extremely low powered signals and a direct line of sight (LoS) between the receiver and the satellites is required for accurate positioning. The L1 signal is modulated by two codes

- The Coarse/Acquisition code (C/A code)
- The Precision code (P code)

The L2 signal on the other hand is modulated only the P code. In addition, the satellite also transmits a navigation message that includes the satellites orbital and clock information, the general system status and the ionosphere model. The navigation code has a low frequency of 50 MHz and is modulated onto both L1 and L2 carrier waves, this is illustrated in Fig. 1.4. All the three codes mentioned are binary in nature and are known as PRN codes. Each satellite is provided with its unique PRN code. On the receiving side, the device, generates replicas of either the A/C or P codes and are slide across the received code. The sliding time taken by the locally generated code to completely match the received code is the time taken by the signal to reach from the satellite to the receiver. This in turn provides us with the distance information. There are two categories of GPS positioning;

- The Standard Positioning Service (SPS)
- The Precise Positioning Service (PPS)

The SPS makes use of the less precise C/A codes for location estimation. This has an accuracy of 100 m and is normally used for commercial applications. The PPS is based on the high pulse rate P code on both L1 and L2 carrier signals. The PPS is used for military applications and has sub 20 m accuracy.

Differential GPS is an enhancement to the GPS system to reduce timing errors. Differential GPS makes use of land based reference station or a control point with known coordinates. There is a data link between the user and the control point so that timing errors can be mitigated. Thus the error in positioning is reduced to 2-10 m accuracy if users are within 1000 km of the control point.

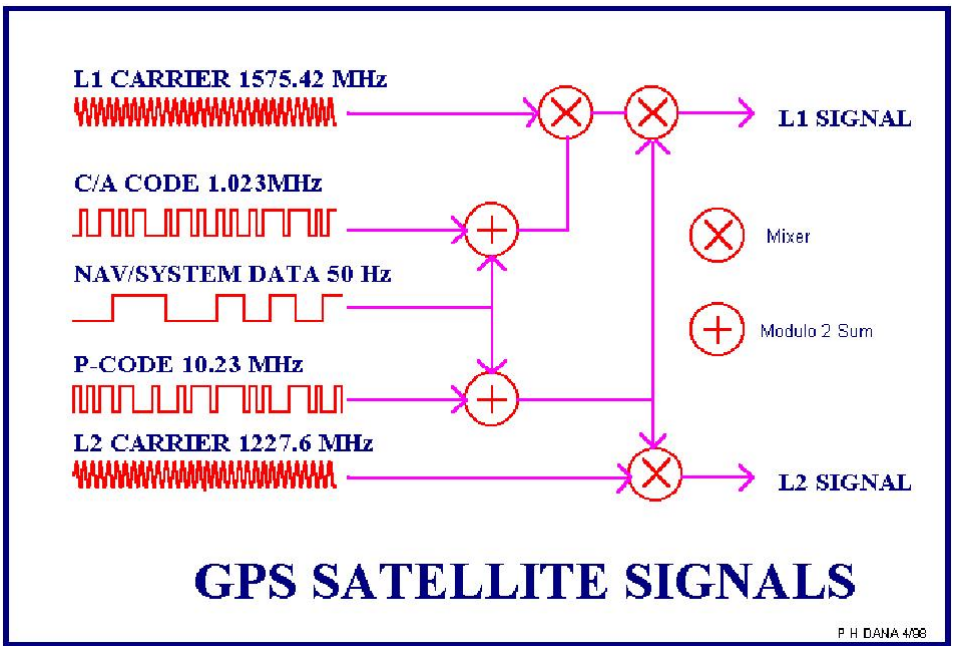

Figure 1.4: GPS sattelite signals [3].

1.1.5 Other positioning systems

Various other navigation and positioning systems were developed, they may include the British Gee system, which is a time based hyperbolic system and was employed in the Second World War. It offers an accuracy of 150 m when operated

at short ranges. Chayka is a Russian navigation system and is based on the Loran-C [6]. Another Russian system known as Alpha is a low frequency system, which is closely related to the America OMEGA system, phase difference of signals is utilized to determine the location [7]. In satellite navigation, GLONASS (Global Navigation Satellite System) is the Russian counterpart of the GPS. GLONASS became operational in 2010. It employs 24 satellites with 21 operational and 3 spares. The purpose of developing GLONASS was to provide navigational service to the Soviet military. It provides an accuracy of around 60 meters and vertical location accuracy of 70 meters [8]. The European Union's Galileo (named after the Italian astronomer) is an under development project and is expected to be operational in 2014. The need for a separate satellite navigation system for Europe was felt as GPS and GLONASS are controlled by the US and Russia and could be shut down in times of war or political unrest. Galileo promises better accuracies than the GPS and GLONASS i.e. up to 1 meter. Galileo will have 30 orbiting satellites, 27 operational and 3 spare in 3 orbital planes. Four atomic clocks (two-rubidium frequency stranded and two passive hydrogen masers) will be on board each satellite. Similar to the GPS, Galileo will be free to use to everyone, however high accuracy services will be charged a fee [9].

1.2 Classification of Localisation Systems

Localisation systems can be classified in various ways; referring to [10][11], following are some of the parameters by which these systems can be classified.

1.2.1 Classification based on the PHY employed

One way to class localisation systems is based on the signaling scheme employed. These schemes and their pros and cons are as follows.

1.2.1.1 Optical signals

Optical signals can provide accurate ranging and location. Optical signals are highly attenuated with distance and suffer drastically with non-line of sight (NLoS) errors, thus these systems are well suited for short range and LoS position/ranging. Furthermore optical signals suffer from interference due to sun light and light bulbs.

1.2.1.2 Infrared

Although infrared signals require low power transmitter, a perfect LoS is required. Infrared is also affected by sunlight.

1.2.1.3 Ultrasound

The relatively slower propagation speed of ultrasound waves eliminates the need for faster clocks. The disadvantage of using ultrasound is that they provide higher accuracies only at short ranges and requires high power transmitters.

1.2.1.4 Radio frequency (RF)

The accuracy of the RF location systems vary depending on the centre frequency of the signal, generally RF signals perform relatively well in non line of sight (NLoS) scenarios and can travel for longer range. The RF based system can

be further classified into ultra-wide band (UWB), code division multiple access (CDMA) etc.

1.2.2 Classification based on position estimation technique

Time of arrival (ToA), Time difference of Arrival (TDoA), Received Signal Strength (RSS) are some of the methods that can be employed to estimate the position of a target node.

1.2.3 Self positioning and remote positioning

Positioning of a cell phone over a CDMA network or via GPS, where the user estimates its own position is known as self-positioning. In remote positioning, the user's position is estimated by a network base station (BS), an example is the localisation of the caller to the enhanced 911 (E911) service. Indirect remote positioning is when the target node or user estimates its location and then sends its positioning information to the BS. Indirect self positioning refers to the positioning of the node by a BS and then transferring that information to the user.

1.2.4 Active and passive positioning

Active positioning refers to the systems where the network (BS or satellites) transmits positioning signals in order to estimate the location of a target. Passive positioning is when the network receives the positioning signals from the target node or user.

1.2.5 Centralized and distributed positioning

Centralized positioning collects location information at a BS before processing while in distributed positioning the location is calculated jointly with the neighboring nodes.

1.2.6 Single-hop/multi-hop algorithms

A direct communication link between two nodes is commonly referred to as a hop. Networks where there is only a single link between nodes for location purposes are called single-hop. GPS is an example of a single-hop positioning systems. On the other hand, if the node that is desired to be localised is out of range of an anchor or BS, a communication link using intermediate nodes is established, this is known as multi-hop. Single hop algorithms are simple and accurate but are not scalable, multihop algorithms are more scalable.

1.2.7 Range based and range free positioning

Location algorithms, which are based on the absolute distance between nodes, are known as range based algorithms. On the other hand, algorithms that do not require determining the actual inter-node distance for localisation are called range-free positioning algorithms [12, 13]. Range free algorithms are based on the number of hops for communications between two nodes as a distance metric. Range based algorithms are more accurate than range free algorithms.

1.2.8 Localisation coordinates

These can be sub-divided into the following:

1.2.8.1 Absolute Location.

This is the real global coordinates e.g. South 75 05.235'.

1.2.8.2 Relative location.

This involves the location of a target node with respect to a local reference (anchor).

1.2.8.3 Logical or semantic location.

These are simpler to understand, an example is Dr. Kemp's office, second floor, school of electronics.

1.3 Performance Metric

Accuracy of a location system is not the only benchmark of its performance; there are other criterion that should also be taken into consideration. The performance of positioning system can be determined by the following yardsticks.

1.3.1 Accuracy

Accuracy is the most important criterion for a location system. It is measured as the mean Euclidean distance between the true and the estimated location.

1.3.2 Precision

A good positioning system apart from being accurate should be persistent in estimating accurate location. If two systems have equal accuracy, the system,

which is more precise, is chosen. This decision is normally based on the cumulative distribution function (CDF) of the distance error, systems with high precision have steeper CDF graphs. Usually the precision is measured in percentile.

1.3.3 Complexity

Localisation in low power networks (such as sensor networks) is desired to be of low complexity. Nodes in such networks have lower computation power and algorithms requiring low processing are preferred. Other systems, where the calculations are carried out by an external base station can of course afford high complexity algorithms. The complexity of the system is normally measured in terms of the time taken by the network to localise a node.

1.3.4 Robustness

Systems that perform well in harsh conditions (such as ranging signals being blocked or highly cluttered environments) are preferred over systems which perform well only in accommodating scenarios. Thus, systems, which are able to perform localisation with incomplete information, are more robust.

1.3.5 Scalability

The scalability of a system can be measured in terms of geography and density. A system is geographically scalable if it can perform localisation at longer distance; generally, the performance of a system degrades as the distance between the nodes increases. On the other hand, the density of a network refers to the number of nodes per unit area/volume. The performance of systems deteriorates as more nodes are added into the network (due to multi-user interference (MUI)).

Furthermore, scalability also can be assessed wether a system can localise in two dimension (2D) or three dimension (3D).

1.3.6 Cost

Another important factor in choosing a positioning system is the cost. Cost can be in terms of money, energy consumption, size and weight. It might be desired to install low power and cheap positioning systems with little maintenance requirement. Such needs cannot be fulfilled by GPS and hence low cost systems are preffered.

1.4 Applications

Different applications have different requirements, as shown in 1.1 that all the location systems were used for military purposes (navigation of airplanes and ships). Although accuracy is an important factor in these systems, operation at longer range is vital. Thus systems utilizing the lower frequencies of the spectrum are employed. GPS on the other hand is a more accurate system outdoors where we have a direct LoS between the user and the satellite, it thus can be used as an efficient system for vehicle tracking etc. GPS, however deteriorates to achieve the desired accuracy indoors (NLoS) and in many instance it totally fails to locate the receiver. Furthermore, GPS receivers are extremely power hungry and costly. The focus of this thesis is to look into the localisation of nodes in sensor networks. WSNs which consist of independent nodes or devices that are capable of sensing and monitoring environmental conditions such as temperature, pressure and light intensity require low cost, very low power and low complexity [14]. Such nodes are designed to operate for several years without their batteries being replaced.

The applications of locating the nodes in such networks will be discussed in this section.

1.4.1 Wildlife tracking

Keeping track of wildlife has been of interest to zoologist, knowledge of animal movement over time can indicate animal behavior with other species and interaction with their own kind. The systems that are employed for such purposes are either using very high frequency (VHF) collars or using GPS chips. Since such observations are recorded over a long period, regular battery replacement in the collars becomes impractical. Low power sensor network localisation will improve battery life and guarantee little human interaction with the animals. ZebraNet is one such system and is demonstrated in [15].

1.4.2 Logistics

In order to locate boxes in a warehouse or goods in a factory, they are tagged with sensor. These sensors could monitor not only the temperature, pressure or humidity but also their location.

1.4.3 Secure buildings

In a highly secured building, where all individual cannot have access to certain areas of the building. Visitors can be tagged before entering the building, this will limit their movement. The tags can report to security when they are taken to a restricted area.

1.4.4 Search and rescue of avalanche victims

WSN localisation can be used in locating avalanche victims that are buried under the snow. The skiers are tagged with sensors that monitor their vital signs, the tags are also equipped with an accelerometer [16]. The accelerometer detects the orientation of the victims, so rescue team are aware while digging by shovels etc.

1.4.5 Aid to firefighters and police

Sensor network localisation can be used for detection of firefighters in a building on fire. Positioning of individuals in such situations is imperative, as visibility in a smoked filled building is extremely low. Firefighters could locate each other and can also be monitored from an external station. Similarly, police dogs trained to find explosives in a building could be located by tagging them with sensor-equipped collars.

1.4.6 Interactive gaming

Sensor location can also be brought into play in the gaming industry. In this regard, the first step was taken with the release of the Nintendo Wii in which the action in the game corresponds to the motion of a hand held controller. The gaming consol consists of a sensor bar, which is connected to the controller through an optical link. Although, the console can detect the 3D motion of the controller, a perfect LoS is must for proper operation, which is often a hindrance in the gaming experience. In the future, we will see more interactive gaming based on sensor location without the LoS constrained. Players can interact with each other in a three-dimensional environment viewed through special goggles or helmets, while their physical position and motion can be pinpointed.

1.5 Localisation

Since every node in the network cannot be equipped with a GPS chip, generally a small number of nodes which know their location (this can be achieved through GPS) called anchor nodes are deployed and the rest of the nodes estimate their coordinates by referencing to the anchor nodes. This can be done by first finding the range between the anchors and a target node and then manipulating that information to calculate the location [17, 18, 11]. The anchor nodes are often mains powered and are high in resources in terms of computational power and memory. The positioning techniques discussed in literature include the time-of-arrival (ToA), received signal strength (RSS) and the angle of arrival (AoA). A hybrid RSS-ToA can also be deployed. Another time based system is the time-difference-of-arrival (TDoA), which is a purely location based technique and does not involve the absolute ranging between the nodes.

1.5.1 Ranging techniques

The first step in most location techniques is to establish the absolute distance between two nodes. The received signal $r(t)$ can be represented by the following equation [19]

$$r(t) = h(t) * s(t) + n(t), \tag{1.1}$$

where * represents the convolution process, $n(t)$ is the thermal noise and $h(t)$ is the system (channel) impulse response

$$h\left(t\right) = A\left(d\right)\delta\left(t - \tau\left(d\right)\right), \tag{1.2}$$

where A is the amplitude or attenuation, and δ is the dirac function, thus

$$r(t) = A(d)\, s(t - \tau(d)) + n(t) \tag{1.3}$$

as seen from (1.3), the parameters that modify the received signal are the attenuation and the delay. Based on these parameters the ranging method is defined, and the distance d estimated.

1.5.1.1 Received signal strength (RSS)

The RSS technique is based on the emission at the transmitter side of a signal using fixed reference power known to the receiver while the receiver measures the power of the received signal and derives the distance from the calculated attenuation. The Frii formula provides us with the attenuation associated with free space propagation [20]

$$P_r = \frac{P_t G_t G_r \lambda^2}{(4\pi d)^2} \tag{1.4}$$

where P_t is the transmitted power, G_t, G_r are the transmitter and receive antenna gains respectively and λ is the wavelength associated with signal frequency. From (1.4) we notice that the received power P_r is inversely proportional to the square of the distance between the transmitter and receiver, thus it is evident that RSS technique offers accurate distance estimates at shorter distances. However, the accuracy decreases substantially with the increase in distance between the nodes. The RSS is a straightforward, inexpensive technique and requires no additional

hardware. The relation between distance and signal attenuation depends on channel behavior thus an accurate propagation model is required to reliably estimate the distance.

The relation between the received power P_r and the transmitted power P_t as in (1.4) is an over simplified form and is valid only for free space propagation. In real-world conditions there are two major sources of error while measuring the received signal strength, these are multipath and shadowing errors. Multipath errors are due to the reflection and scattering in NLoS environments. This results in multiple signals arriving at the receiver with varying amplitudes and phase [20]. These signals might interfere constructively or destructively resulting in fading. Shadowing is a result of attenuation of the signal due to hindrance by trees, walls etc. The shadowing effects are environment based and are generally modeled as random. The multipath effects can be mitigated by measuring the average of the received power over a sufficient period. The average receive power at distance d is given as [21]

$$P(d) = P_0 - 10\alpha \log_{10}\left(\frac{d}{d_0}\right), \tag{1.5}$$

where $P(d)$ is the average received power in dB.

d is the distance between transmitter and receiver.

P_0 is the received power at a reference distance d_0 (normally taken as 1 m).

α is the path-loss exponent (PLE), its value depends on the type of environment.

Due to the effects of shadowing the received signal power is distributed log-normal [18]. In other words, it is Gaussian distributed if the powers are taken in dB as follows

$$p(d) \sim \mathcal{N}(P(d), \sigma^2_{shadowing}).$$

Another major source of error is the incorrect PLE assumption. The impact of incorrect of PLE on location accuracy is detailed chapter 2 and 3.

1.5.1.2 Time based

The time-based systems utilize the delay in the transmitted signal when received. The underlying radios in use have a serious impact on the performance of a time-based system. Here we give a brief overview of the three classes of RF signals.

1) Underlying RF technology

a) Narrow band systems These systems determine the distance between nodes by calculating the difference in phase between the transmitted and received signal. The phase ϕ is related with delay τ of the signal as follows [20]

$$\phi = 2\pi f_c \tau \tag{1.6}$$

where f_c is the center frequency of the transmitted signal. In perfect LoS conditions, the narrow band systems can attain an accuracy of 1 m.

b) Wideband systems The frequency spectrum of these radios are spread often using pseudo-noise (PN) codes as in the case of the direct sequence spread spectrum (DSSS). This intentional increase in the bandwidth helps in combating interference. Also the increased bandwidth improves the accuracy of location as

evident from the equation of the estimated distance[19]

$$\hat{d} = \frac{c}{BW} \tag{1.7}$$

where $c = 3 \times 10^8 m/s$ is the speed of the electromagnetic wave and BW is the bandwidth. As a rule of thumb, in the absence of NLoS a wide band signal of 300 MHz will have an accuracy of 1 m.

c) Ultra wide band (UWB) systems The UWB provides an ideal PHY for ranging and localisation. A steep rise to the full power diminishes the uncertainty about the start time of the pulse. As time distance between nodes is measured as $d = time \times c$. Thus, the inaccuracy of distance is reduced by reducing the uncertainty in time. As stated before, the accuracy of the system increases with the BW, thus an UWB signal with a bandwidth greater than 3 GHz can achieve cm level accuracies. However, UWB systems can only be used for short distance as the higher frequencies face severe attenuation.

Next, commonly used ToA ranging protocols are discussed in brief.

2) Time based ranging protocols

Time based ranging can be classified into two techniques based on the number of packet transmission for range estimation.

a) One way time of arrival (OW-ToA)

Distance between two nodes, node A and B is estimated as follows. Node A transmits the time-stamped signal at t_1 and is received at node B at t_2, the

distance between the nodes is given by the equation [22]

$$d = c\,(t_2 - t_1) \tag{1.8}$$

The OW-ToA requires highly synchronized local clocks between the nodes. This method is not favored for WSN as the demand for highly accurate clocks increases the complexity and cost of the nodes

b) Two way time of arrival (TW-ToA)

In order to eliminate the requirement of clock synchronization between the nodes, the TW-ToA method is adopted. This method requires the nodes to exchange two packets for distance measurement. Node A transmits a ranging packet at t_{start} and records the time stamp. Node B on reception of this packet records the time and replies an acknowledgment signal after a delay of t_{reply}. Node A receives this signal at time t_{stop}. The propagation time t_p and hence the distance is calculated as [23]

$$d = c\left(\frac{t_{stop} - t_{start} - t_{reply}}{2}\right) \tag{1.9}$$

The node B's reply time t_{reply} can be known "a priori" to the network devices or this information can be sent by node B in the second packet exchange.

3) Major source of errors

The accuracy of location estimation is exceedingly dependent on the accuracy of range measurement. In this subsection, various sources of errors in time based range measurements are discussed.

a) Additive white Gaussian noise (AWGN) AWGN is due to the random vibration of atoms in the circuitry of the transceivers, which adds impairment to the ToA estimation. The accuracy of the ToA estimation in the presence of AWGN is discussed in [24].

b) Multipath propagation Multipath propagation (due to reflection and scattering) results into multiple copies of the transmitted pulse arriving at the receiver. This pulse might interfere constructively or destructively resulting in performance degradation. In narrowband systems where the pulse length is relatively longer, these multiple copies of the signal cannot be resolved. Generally, ToA calculation is carried out by correlating the received signal with its time-shifted template. However, due to multipath channel, the received signal is the result of the convolution of the transmitted signal and the impulse response of the channel. As a result, the correlation of the received signal with a pure template results in suboptimal performance. Furthermore, we can classify errors for the multipath ToA measurement into two categories.

- Early-arriving multipath.

The multiple copies due to reflection immediately follow the LoS signal, this results in the replicas partially overlapping the LoS signal. Thus, an isolated peak for location estimation at the receiver is not obtained. Fortunately, UWB systems with its immense bandwidth results in short natured pulses in the time domain. This also leads the UWB multipath pulses to be resolvable. Furthermore, a narrow autocorrelation peak gives us a precise ToA and making it easy to separate the LoS signal cross-correlation peak from the NLoS early arriving multipath signals.

- Attenuated LoS.

This is due to the attenuation of the LoS signal relative to the multipath component. In the worst case, the LoS signal is not picked by the receiver at all resulting in severe ranging errors. This error occurs mainly in networks where the nodes are located far apart from each other.

c) Direct path (DP) excess delay DP excess delay is the ToA error caused by the variable propagation speed of the radio signals. The speed of the electromagnetic waves is dependent on the material it propagates. The electromagnetic waves travel with the speed of light c in air. This speed decreases by a factor of $\sqrt{\epsilon_r}$ with respect to c when it travels in another material with ϵ_r being the relative electrical permittivity of the material. This can result in a positive bias in the range estimation. The DP excess delay $\triangle\tau$ is given by equation [25]

$$\triangle\tau = (\sqrt{\epsilon_r} - 1)\frac{d_w}{c} \tag{1.10}$$

where d_w is the thickness of the material.

d) NLoS propagation error NLoS propagation errors are due to the complete blockage of the DP. The ranging signals reach the receiver after covering an additional distance (resulting from reflection). Thus, the first arriving pulse does not correspond to the true distance between the nodes and a positive bias is introduced in the range measurement. Various methods have been proposed to mitigate the NLoS error. This includes identifying the NLoS signals and then discarding them completely. However [26, 27] suggests that NLoS can be utilized to improve the location accuracy.

e) Mutliple access interference (MAI) Multi-user scenarios can lead to interference with signals from other nodes resulting in suboptimal ToA estimation

and hence range measurement.

f) Clock drift and clock offset Accurate clocks are the basic requirement for ToA estimations. Commonly, nodes used in sensor networks have poor clock oscillators. The effects of the clock drifts, as the clock varies from the true time, thus should be taken into consideration. These errors can substantially affect the accuracy of the range estimation. Precise synchronization is also required for one way time of arrival, imperfection in the synchronization is an additional source of error in the ToA measurement and is termed as clock offset.

1.6 Positioning Techniques

The ranging techniques discussed in 1.5.1 can be utilized to estimate the location of a target node. This is known as *trilateration*, furthermore, range free positioning systems such as angle of arrival (AoA) have also been implemented. These positioning methods are discussed in the following subsections.

1.6.1 Angle of arrival (AoA)

This technique makes use of the incident angle of the signal transmitted by a target node on a pair of anchors. Though a minimum of two anchor nodes are required in two dimensional positioning, the accuracy can be increased by adding more anchors. A radial line is constructed joining the target node and the anchor, the target location is found at the intersection of these lines, this is illustrated in Fig. 1.5. The angle of the incident signal can be computed using one of the following techniques [17, 21].

The main beam of the receiver antenna is rotated mechanically or electronically,

and the angle which corresponds to highest receive power indicates the direction of the transmitter. Often a second non-rotating isotropic antenna is used to normalize the received signal power by the rotating antenna in case the transmitted signal is of varying power.

Another method uses an antenna array at the receiver and the angle is calculated by examining the phase differences at each element of the array. This method is similar to the time of arrival as the delay of the incoming signal is different at the array elements and is related to the phase delay $2\pi f_c t$. The phase delay scheme is often employed for narrowband signals.

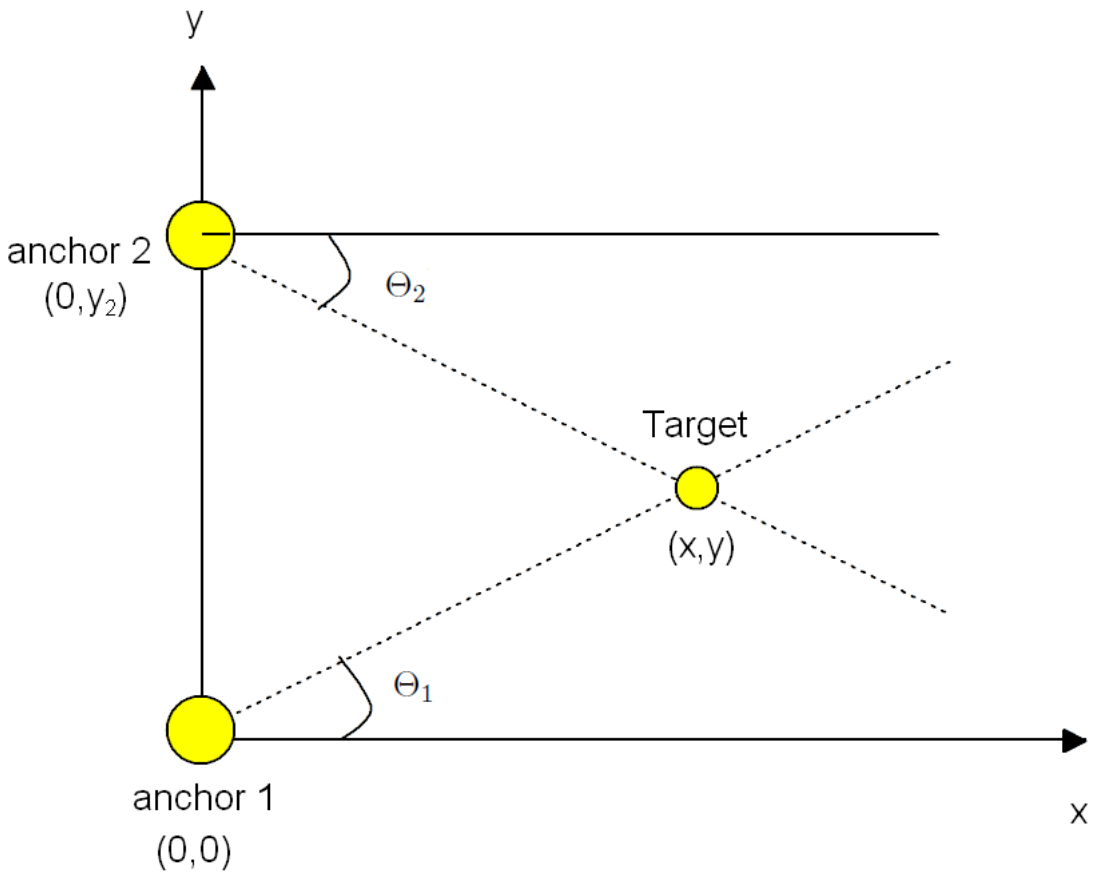

Figure 1.5: Positioning via AoA.

Finally, two directional antennas with overlapping main beams are used to esti-

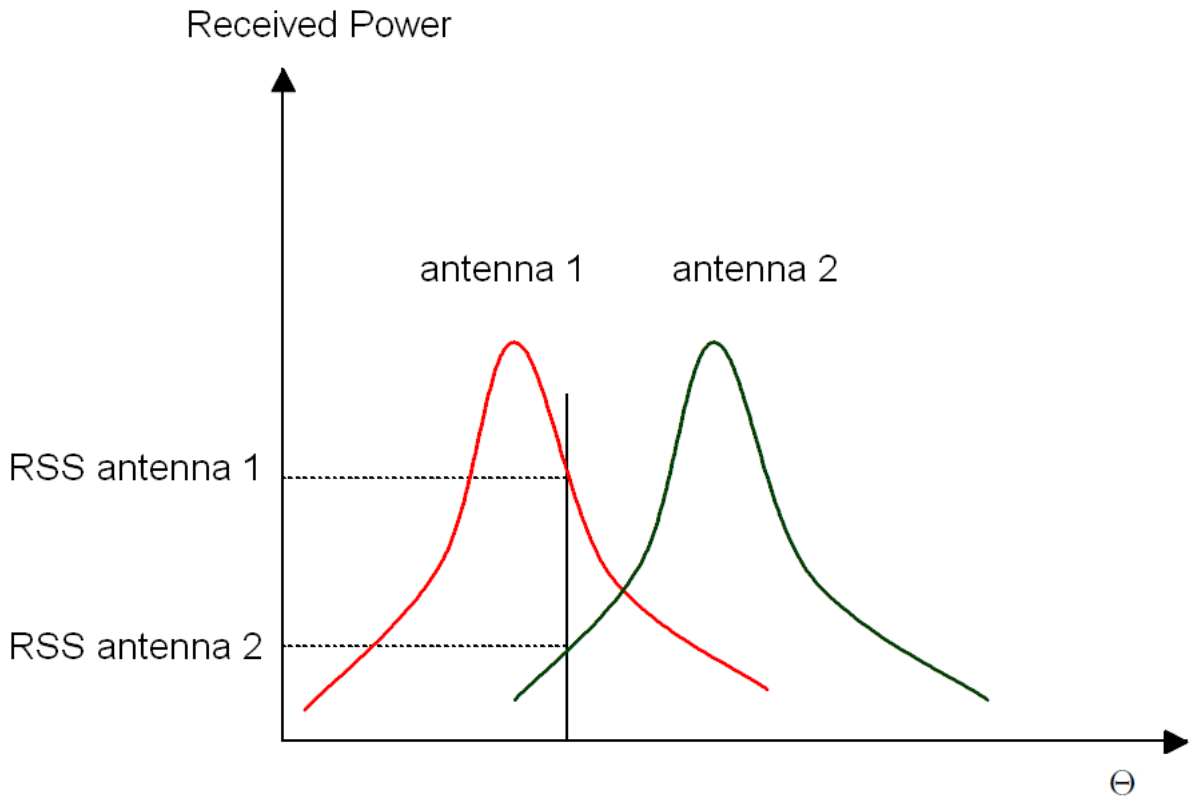

Figure 1.6: RSS ratio corresponding to angle of arrival.

mate the angle based on the RSS ratio between them. This is illustrated in Fig. 1.6 where the ratio between the signal strengths correspond to the arrival angle.

Once the arrival angle at the anchor nodes is established, locating the target follows a straight forward procedure. Let the anchor 1 be located at (0,0) and anchor 2 at (0,$y2$) and the transmission from the target node is making an angle Θ_1 and Θ_2 on anchor 1 and 2 respectively.

$$y = \tan(\Theta_1)\, x \tag{1.11}$$

$$y = \tan(\Theta_2)\, x + y_2 \tag{1.12}$$

Equating (1.11) and (1.12) will yield the location of the target on the x-axis

$$x = \frac{y_2}{\tan(\Theta_1) - \tan(\Theta_2)}. \tag{1.13}$$

Substituting value of x in (1.11) will give us the y coordinates. The AoA is not a favorable location approach for WSN localisation, as it requires additional hardware which increases the complexity and cost of the system.

1.6.1.1 Major sources of error.

The sources of error in AoA are similar to those in ToA i.e thermal noise and multipath. The angle measurement errors are generally Guassian distributed [17].

1.6.2 Trilateration

The estimated range between an anchor and a target node can be expressed as a circle, the center of which is where the anchor is located and its radius represents the distance. In order to locate a node in a two dimension plane, three such target and anchor pairs are required thus forming three circles. The point at which these circles coincide gives us the the location of the target node. In three dimensional space, at least four anchors are needed, and the target location in this case is the point of coincidence between four spheres.

The coordinates (x, y) of the target node shown in the Fig. 1.7 can be calculated from the following set of equations

$$d_1 = \sqrt{(x - x_1)^2 + (y - y_1)^2}$$

$$d_2 = \sqrt{(x - x_2)^2 + (y - y_2)^2}$$

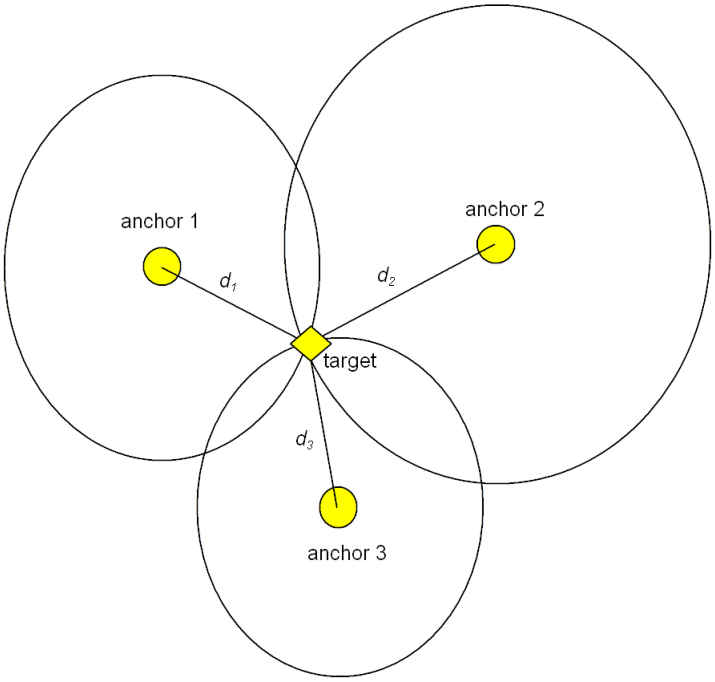

Figure 1.7: Trilateration.

$$d_3 = \sqrt{(x - x_3)^2 + (y - y_3)^2}. \tag{1.14}$$

1.6.3 Time difference of arrival (TDoA)

TDoA does not depend on the absolute time of arrival but rather the idea is to determine location of the target node by examining the difference in time at which a broadcast signal from the target node arrives at multiple measuring anchors. This difference in the arrival of time can be treated as a hyperbola, which has the two receiving anchors at its focii. Three anchor nodes are required for two dimensional positioning. The target node is located at the intersection of two hyperbolas as shown in Fig. 1.8. The equations for the two coinciding hyperbolas is given below

$$d_{31} = d_3 - d_1 = \sqrt{(x_3 - x)^2 + (y_3 - y)^2} - \sqrt{(x_1 - x)^2 + (y_1 - y)^2}$$

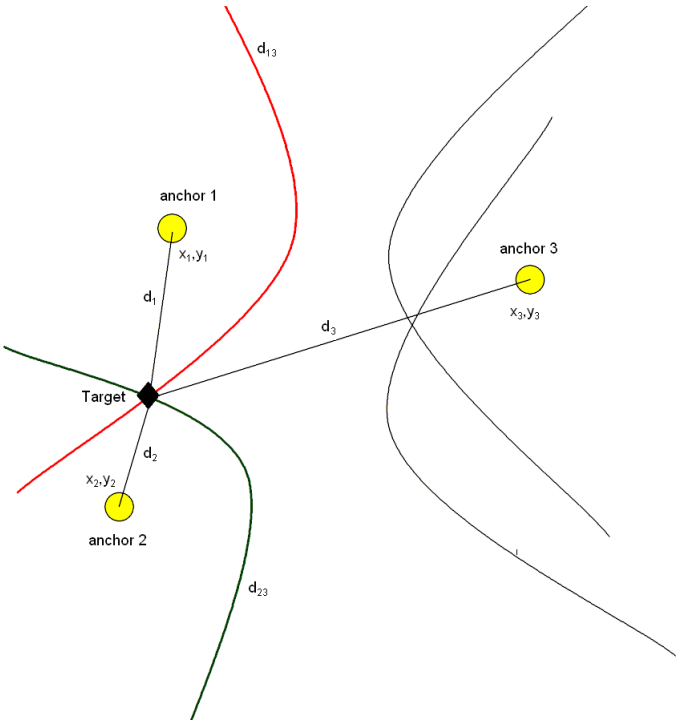

Figure 1.8: TDoA.

$$d_{32} = d_3 - d_2 = \sqrt{(x_3 - x)^2 + (y_3 - y)^2} - \sqrt{(x_2 - x)^2 + (y_2 - y)^2}. \quad (1.15)$$

TDoA can also be employed in an alternative mode, where the anchors broadcast the signal simultaneously while the target node receives it with different delays. In both cases, the anchor clocks should be accurately synchronized which are often wired to guarantee synchronization. The synchronization of the target node and anchors in this case is however not mandatory.

1.7 Major Contributions

The main contributions in thesis are as follows:

- Analytical expression for the mean square error (MSE) and bias of location

estimates for incorrect PLE assumption is derived for Maximum likelihood (ML) algorithm.

- A previously proposed RSS-PLE joint estimator (JE) is enhanced by reducing its complexity.
- A Maximum a posteriori (MAP) estimator which considers the PLE as an unknown random variable is proposed.
- Hybrid Cramer-Rao Bound (HCRB), a benchmark, for the MAP is derived.
- Analytical expression for the mean square error (MSE) and bias of location estimates for incorrect PLE assumption is derived for linear least squares (LLS) algorithm.
- Low complexity joint LLS algorithm for location and PLE is proposed.
- A RSS based weighted least squares (WLS) algorithm is proposed for location estimation.
- Optimal reference AN selection technique is proposed for better performance.
- Linear CRB to lower bound the performance of LLS algorithm is dervied.
- Technique to select optimal and worst AN positions based on the minimization of the mean CRB is proposed.
- A novel algorithm namely conditioned mean square error ratio (CMSER) is developed that is resilient to location error and performs considerably better than previously proposed geographic routing algorithms.

1.8 Thesis Outline

Following the introduction, in which a brief history of localisation systems, a classification of location systems, some performance metrics and some applications were described. The rest of the thesis is organised as follows:

Chapter 2 deals with RSS based localisation in an unknown path-loss model. First, an analytical expression for the mean square error (MSE) on location estimates for incorrect PLE assumption is derived and it is examined, via simulation, the effects of error in the PLE on the location accuracy. Second, a previously proposed RSS-PLE joint estimator (JE) is enhanced by reducing its complexity. Also a maximum a posteriori (MAP) estimator which considers the PLE as an unknown random variable is proposed. Finally, the Hybrid Cramer-Rao Bound (HCRB) as a benchmark for the MAP estimator is derived.

Chapter 3 This chapter also deals with the estimation of location coordinates in unknown path-loss model. First, the non-linear path-loss equations are linearized and the solution is obtained using linear least square (LLS) estimates. Second, in order to underline the effects of inaccurate PLE assumption in noisy channels on location coordinates, error analysis is done when incorrect PLE is assumed, hence a closed form expression is derived for MSE and bias. Next, the LLS problem is transformed into a single variable minimization problem to estimate jointly the location and PLE. In order to achieve higher accuracy, the obtained estimates are used as an initial estimate to the proposed iterative algorithm in chapter 2.

Chapter 4 In this chapter, the LLS method is further analysed and its performance is improved. Firstly, a weighted least squares (WLS) algorithm is proposed

which considerably improves the location estimation accuracy. Secondly, reference anchor optimization using a technique based on the minimization of the theoretical mean square error (MSE) is also proposed to further improve performance of LLS and WLS algorithms. Finally, in order to realistically bound the performance of any unbiased RSS location estimator based on the linear model, the linear Cramer-Rao bound (CRB) is derived.

Chapter 5 In this chapter, the effects of anchor placement on optimal target node positioning is investigated. The optimal and worst anchor positions are determined through extended simulation by comparing their mean CRB. Furthermore the ramifications of an additive and multiplicative noise model on the mean CRB are explored. Finally, the least squares (LS) method for localisation is used and its performance is compared with the lower bound for optimal anchor positions.

Chapter 6 In chapter 6, the effects of error in localised nodes on the geographic routing is discussed. Instead of assuming full knowledge of node location, nodes are first localised using ToA and RSS and then their estimated locations are use in the geographic routing algorithms. Furthermore, a novel algorithm namely conditioned mean square error ratio (CMSER) is developed that is resilient to location error and performs considerably better than previously proposed geographic routing algorithms with erroneous node locations.

Chapter 7 Chapter 7 concludes this thesis and briefly describes some future research directions in the field of localisation.

2 Joint Estimation of the RSS-Based Location and Path-Loss Exponent

The material in this chapter has been published in the paper:

- N. Salman, M. Ghogho, and A. H. Kemp, "On the joint estimation of the RSS-based location and path-loss exponent," *IEEE Wireless Commun. Lett.*, vol. 1, no. 1, pp. 34–37, Feb. 2012.

2.1 Overview

Two widely used techniques for distance estimation are time-of-arrival (ToA) [28] and received signal strength (RSS) [29, 30, 18]. Highly accurate clocks on-board the nodes are a requisite for ToA localisation. For low cost and low complexity positioning systems, RSS based localisation is the most attractive technique as no additional hardware is required. The accuracy of the location estimate via RSS is highly dependent on knowledge of the path-loss exponent (PLE). Thus, degraded system performance is expected with an inaccurate PLE assumption. In many studies, the distance relation with the received power is based on a

simplistic path-loss model [18, 31]. In these studies the PLE is assumed to be exactly known. This, in practical systems is an oversimplification as the PLE value can only be known when it is measured at multiple points prior to system implementation. Prior channel measurement is impractical in unfavourable scenarios and also its value is environment dependent, ergo its value needs to be estimated. In a recent publication [32], the authors address the same problem by first selecting the PLE from a values set by maximizing the *compatibility* of the distance estimates however compatible distance estimates might be highly inaccurate in noisy channels thus leading to inaccurate PLE estimation. The authors also put constraints on the estimated PLE values which are reasonable only in specific networks. More recently, in [33] a computationally intense two stage algorithm is used. In the first stage the location coordinates are estimated iteratively while keeping the PLE to any fixed value, in the second stage the PLE is estimated iteratively. This chapter focuses on the joint estimation of the PLE and location coordinates.

The signal model and problem statement is defined in section 2.2. In section 2.3, location error analysis when the PLE value is incorrect via Taylor series expansion is done while section 2.4 improves on an already proposed joint estimator (JE) [34]. Its implementation is improved by abating its complexity. In addition, any prior information regarding the PLE is utilized and a maximum a posteriori (MAP) estimator is developed in section 2.5 that also jointly estimates the PLE and location coordinates. Finally, the hybrid Cramer-Rao bound (HCRB) is derived in section 2.6 to lower bound the performance of an unbiased location estimator when the PLE is a random variable.

2.2 Signal Model

For later use, the following notations are defined. $\mathscr{R}^n$ represents the set of n dimensional real numbers. $Tr(M)$ represents the trace of the matrix M. $(.)^T$ represents the transpose operation. $E(.)$ represents the expectation operation. $(M)_{ij}$ represents the element at the i^{th} row and j^{th} column of matrix M. $\mathcal{N}(\mu, \sigma^2)$ denotes the normal distribution with mean μ and variance σ^2. A two dimensional network is considered with only one target node (TN) which has unknown co-ordinates $\boldsymbol{\theta} = [x, y]^T$ $(\boldsymbol{\theta} \in \mathscr{R}^2)$ that are to be estimated. The network consists of N anchor nodes (AN) with locations $\boldsymbol{\theta}_i = [x_i, y_i]^T (\boldsymbol{\theta}_i \in \mathscr{R}^2)$ for $i = 1, ..., N$. The distance between the TN and the i^{th} anchor, d_i, is related to the path-loss at the i^{th} anchor, $\mathscr{L}_i$, and the PLE, α, as [35, 36, 37]

$$\mathscr{L}_i = \mathscr{L}_0 + 10\alpha_i \log_{10} d_i + w_i, \tag{2.1}$$

where $\mathscr{L}_0$ being the path-loss at a reference distance d_0 and w_i is a zero-mean Gaussian random variable representing the log-normal shadowing effect, i.e.

$$w_i \sim \left(\mathcal{N}\left(0, \sigma_i^2\right)\right).$$

The path-loss is calculated as

$$\mathscr{L}_i = 10 \log_{10} P_t - 10 \log_{10} P_i, \tag{2.2}$$

where P_t is the transmit power at the TN and P_i is the received power at the i^{th} anchor. The distance d_i is given by

$$d_i = \sqrt{(x - x_i)^2 + (y - y_i)^2}. \tag{2.3}$$

The reference distance $d_0 < d_i$ is normally taken as 1 m. It is assumed that we do not have knowledge of α, thus the unknown vector is

$$\boldsymbol{\phi} = \left[\boldsymbol{\theta}^T, \alpha\right]^T.$$

The observed path-loss (in dB) from d_0 to d_i

$$z_i = \mathscr{L}_i - \mathscr{L}_0,$$

can be expressed as,

$$z_i = f_i(\boldsymbol{\phi}) + w_i,\ i = 1, ..., N, \tag{2.4}$$

where $f_i(\boldsymbol{\phi}) = 10\alpha \log_{10} d_i$. In a vector form,

$$\mathbf{z} = \mathbf{f}(\boldsymbol{\phi}) + \mathbf{w}, \tag{2.5}$$

where $\mathbf{z} = [z_1, ..., z_N]^T$ is the vector of the observed path-loss.

$\mathbf{f}(\boldsymbol{\phi}) = [f_1(\boldsymbol{\phi}), ..., f_N(\boldsymbol{\phi})]^T$represent the vector of the actual path-loss and $\mathbf{w} = [w_1, ..., w_N]^T$ is the noise vector. Since the noise is Gaussian and assuming independence of the noise components, the joint conditional probability density function (pdf) of z is given by

$$p(\mathbf{z} \mid \boldsymbol{\phi}) = \prod_{i=1}^{N} \frac{1}{\sqrt{2\pi\sigma_i^2}} \exp\left\{-\frac{(z_i - f_i(\boldsymbol{\phi}))^2}{2\sigma_i^2}\right\}. \tag{2.6}$$

Thus, the maximum likelihood (ML) estimate of (2.6) is equivalent to the non-linear least square (NLS) solution of the cost function

$$\varepsilon(\boldsymbol{\phi}) = (\mathbf{z} - \mathbf{f}(\boldsymbol{\phi}))^T (\mathbf{z} - \mathbf{f}(\boldsymbol{\phi})). \tag{2.7}$$

Since (2.5) represents a set of non-linear equations, an iterative method is required to estimate the unknown vector in an optimal fashion. Chapter 2 and 3 deals

with the sub-optimal (but low complexity) solution to (2.5).

2.3 Error Analysis

In this section, the effects of the error in α on location estimates that are obtained from an ideal unbiased location estimator are analysed .

The ML solution to the pdf (2.6) for any given value of the PLE α is obtained by minimizing the cost function

$$G\left(\boldsymbol{\theta}|\alpha\right) = \frac{1}{2\sigma^2}\sum_{i=1}^{N}\left(z_i - f_i\left(\boldsymbol{\theta}|\alpha\right)\right)^2 \tag{2.8}$$

Same shadowing variance for all ANs i.e. $\sigma_i^2 = \sigma^2 \,\forall\, i$ is considered. Next the gradient $\nabla_{\boldsymbol{\theta}}$ of $G\left(\boldsymbol{\theta}|\alpha\right)$ is taken such that $\nabla_{\boldsymbol{\theta}} = \begin{bmatrix} \frac{\partial}{\partial x} & \frac{\partial}{\partial y} \end{bmatrix}^T$ and applying the multivariate Taylor series expansion to $\nabla_{\boldsymbol{\theta}} G\left(\boldsymbol{\theta}|\alpha\right)$ around the true values $\boldsymbol{\theta}_0$ and α_0, while ignoring the higher terms to obtain (2.9),

$$\nabla_{\boldsymbol{\theta}} G\left(\boldsymbol{\theta}|\alpha\right) = \nabla_{\boldsymbol{\theta}} G\left(\boldsymbol{\theta}|\alpha\right)\Big|_{\substack{\boldsymbol{\theta}=\boldsymbol{\theta}_0 \\ \alpha=\alpha_0}} + \begin{bmatrix} \left[\frac{\partial}{\partial x}\nabla_{\boldsymbol{\theta}} G\left(\boldsymbol{\theta}|\alpha\right)\right]\Big|_{\substack{\boldsymbol{\theta}=\boldsymbol{\theta}_0 \\ \alpha=\alpha_0}} \\ \left[\frac{\partial}{\partial y}\nabla_{\boldsymbol{\theta}} G\left(\boldsymbol{\theta}|\alpha\right)\right]\Big|_{\substack{\boldsymbol{\theta}=\boldsymbol{\theta}_0 \\ \alpha=\alpha_0}} \end{bmatrix}^T \begin{bmatrix} (x - x_0) \\ (y - y_0) \end{bmatrix} +$$

$$\left[\left[\frac{\partial}{\partial \alpha}\nabla_{\boldsymbol{\theta}} G\left(\boldsymbol{\theta}|\alpha\right)\right]\Big|_{\substack{\boldsymbol{\theta}=\boldsymbol{\theta}_0 \\ \alpha=\alpha_0}}\right](\alpha - \alpha_0)\,, \tag{2.9}$$

where $\begin{bmatrix} \left[\frac{\partial}{\partial x}\nabla_{\boldsymbol{\theta}} G\left(\boldsymbol{\theta}|\alpha\right)\right]\Big|_{\substack{\boldsymbol{\theta}=\boldsymbol{\theta}_0 \\ \alpha=\alpha_0}} & \left[\frac{\partial}{\partial y}\nabla_{\boldsymbol{\theta}} G\left(\boldsymbol{\theta}|\alpha\right)\right]\Big|_{\substack{\boldsymbol{\theta}=\boldsymbol{\theta}_0 \\ \alpha=\alpha_0}} \end{bmatrix}$ can be replaced by its expected value [38]

$$E\left[\left[\frac{\partial}{\partial x}\nabla_{\boldsymbol{\theta}} G\left(\boldsymbol{\theta}|\alpha\right)\right]\Big|_{\substack{\boldsymbol{\theta}=\boldsymbol{\theta}_0 \\ \alpha=\alpha_0}} \quad \left[\frac{\partial}{\partial y}\nabla_{\boldsymbol{\theta}} G\left(\boldsymbol{\theta}|\alpha\right)\right]\Big|_{\substack{\boldsymbol{\theta}=\boldsymbol{\theta}_0 \\ \alpha=\alpha_0}}\right] = -\mathbf{I}\left(\boldsymbol{\theta}\right)$$

Here $\mathbf{I}(\boldsymbol{\theta})$ is the 2×2 Fisher information matrix (FIM) [39] of the localisation in terms of location coordinates (x, y) only and the expectation is w.r.t $p(\mathbf{z} \mid \phi)$. (2.9) is thus written as

$$\nabla_{\boldsymbol{\theta}} G(\boldsymbol{\theta}|\alpha) = \nabla_{\boldsymbol{\theta}} G(\boldsymbol{\theta}|\alpha)\Big|_{\substack{\boldsymbol{\theta}=\boldsymbol{\theta}_0 \\ \alpha=\alpha_0}} - \mathbf{I}(\boldsymbol{\theta}) \begin{bmatrix} (x - x_0) \\ (y - y_0) \end{bmatrix} + \left[\left[\frac{\partial}{\partial \alpha} \nabla_{\boldsymbol{\theta}} G(\boldsymbol{\theta}|\alpha)\right]\Big|_{\substack{\boldsymbol{\theta}=\boldsymbol{\theta}_0 \\ \alpha=\alpha_0}}\right] (\alpha - \alpha_0). \tag{2.10}$$

For the ML estimate $\hat{\boldsymbol{\theta}}$ with an incorrect PLE assumption $\check{\alpha}$, a necessary but not sufficient condition at the minima of the cost function is $\nabla_{\boldsymbol{\theta}} G(\boldsymbol{\theta}|\alpha)\Big|_{\substack{\boldsymbol{\theta}=\hat{\boldsymbol{\theta}} \\ \alpha=\check{\alpha}}} = o$, where o is a 2×1 null vector. Thus, (2.10) is written as

$$\begin{bmatrix} (\hat{x} - x_0) \\ (\hat{y} - y_0) \end{bmatrix} = \mathbf{I}(\boldsymbol{\theta}|\check{\alpha})^{-\mathbf{1}} \left[\nabla_{\boldsymbol{\theta}} G(\boldsymbol{\theta}|\alpha)\Big|_{\substack{\boldsymbol{\theta}=\boldsymbol{\theta}_0 \\ \alpha=\check{\alpha}}} + \left[\left[\tfrac{\partial}{\partial \alpha} \nabla_{\boldsymbol{\theta}} G(\boldsymbol{\theta}|\alpha)\right]\Big|_{\substack{\boldsymbol{\theta}=\boldsymbol{\theta}_0 \\ \alpha=\check{\alpha}}}\right](\Delta\alpha)\right], \tag{2.11}$$

where $\Delta\alpha = (\check{\alpha} - \alpha_0)$. Finally, location mean square error (MSE) is given by the trace of the covariance matrix[1]

$$E\begin{bmatrix} (\hat{x} - x_0) \\ (\hat{y} - y_0) \end{bmatrix} \begin{bmatrix} (\hat{x} - x_0) \\ (\hat{y} - y_0) \end{bmatrix}^T =$$

$$E\left[\left\{\mathbf{I}(\boldsymbol{\theta}|\check{\alpha})^{-\mathbf{1}} \left[\nabla_{\boldsymbol{\theta}} G(\boldsymbol{\theta}|\alpha)\Big|_{\substack{\boldsymbol{\theta}=\boldsymbol{\theta}_0 \\ \alpha=\check{\alpha}}} + \left[\left[\frac{\partial}{\partial \alpha} \nabla_{\boldsymbol{\theta}} G(\boldsymbol{\theta}|\alpha)\right]\Big|_{\substack{\boldsymbol{\theta}=\boldsymbol{\theta}_0 \\ \alpha=\check{\alpha}}}\right](\Delta\alpha)\right]\right\} \times\right.$$

[1] $\mathbf{I}(\boldsymbol{\theta})$ is symmetric.

$$\left\{\left[\nabla_{\boldsymbol{\theta}} G\left(\boldsymbol{\theta}|\alpha\right)\Big|_{\substack{\boldsymbol{\theta}=\boldsymbol{\theta}_0\\ \alpha=\check{\alpha}}} + \left[\left[\frac{\partial}{\partial\alpha}\nabla_{\boldsymbol{\theta}} G\left(\boldsymbol{\theta}|\alpha\right)\right]\Big|_{\substack{\boldsymbol{\theta}=\boldsymbol{\theta}_0\\ \alpha=\check{\alpha}}}\right](\Delta\alpha)\right]^T \mathbf{I}\left(\boldsymbol{\theta}|\check{\alpha}\right)^{-\mathbf{1}}\right\}\right], \quad (2.12)$$

since

$$E\left[\left(\nabla_{\boldsymbol{\theta}} G\left(\boldsymbol{\theta}|\alpha\right)\Big|_{\substack{\boldsymbol{\theta}=\boldsymbol{\theta}_0\\ \alpha=\check{\alpha}}}\right)\left(\nabla_{\boldsymbol{\theta}} G\left(\boldsymbol{\theta}|\alpha\right)\Big|_{\substack{\boldsymbol{\theta}=\boldsymbol{\theta}_0\\ \alpha=\check{\alpha}}}\right)^T\right] = \mathbf{I}\left(\boldsymbol{\theta}|\check{\alpha}\right), \quad (2.13)$$

then from (2.12)

$$MSE = Tr\left\{\mathbf{I}\left(\boldsymbol{\theta}|\check{\alpha}\right)^{-\mathbf{1}} E\left[\mathbf{I}\left(\boldsymbol{\theta}|\check{\alpha}\right) + \mathbf{X}.\boldsymbol{\Delta}\alpha + \mathbf{Y}.\Delta\alpha^{\mathbf{2}}\right]\mathbf{I}\left(\boldsymbol{\theta}|\check{\alpha}\right)^{-\mathbf{1}}\right\}, \quad (2.14)$$

where

$$\mathbf{X} = 2E\left[\nabla_{\boldsymbol{\theta}} G\left(\boldsymbol{\theta}|\alpha\right)\Big|_{\substack{\boldsymbol{\theta}=\boldsymbol{\theta}_0\\ \alpha=\check{\alpha}}}\left(\frac{\partial}{\partial\alpha}\nabla_{\boldsymbol{\theta}} G\left(\boldsymbol{\theta}|\alpha\right)\Big|_{\substack{\boldsymbol{\theta}=\boldsymbol{\theta}_0\\ \alpha=\check{\alpha}}}\right)^T\right]. \quad (2.15)$$

After derivation

$$\mathbf{X} = 2\begin{bmatrix} \frac{\check{\alpha}}{\sigma^2}\sum_{i=1}^{N}\left(\frac{\gamma\widetilde{x}_i}{d_i^2}\right)^2 & \frac{\check{\alpha}}{\sigma^2}\sum_{i=1}^{N}\left(\frac{\gamma}{d_i^2}\right)^2\widetilde{x}_i\widetilde{y}_i \\ \frac{\check{\alpha}}{\sigma^2}\sum_{i=1}^{N}\left(\frac{\gamma}{d_i^2}\right)^2\widetilde{x}_i\widetilde{y}_i & \frac{\check{\alpha}}{\sigma^2}\sum_{i=1}^{N}\left(\frac{\gamma\widetilde{y}_i}{d_i^2}\right)^2 \end{bmatrix}. \quad (2.16)$$

and

$$\mathbf{Y} = \left(\left[\frac{\partial}{\partial\alpha}\left[\nabla_{\boldsymbol{\theta}} G\left(\boldsymbol{\theta}|\alpha\right)\right]\right]\Big|_{\substack{\boldsymbol{\theta}=\boldsymbol{\theta}_0\\ \alpha=\check{\alpha}}}(\triangle\alpha)\right)\left(\left[\frac{\partial}{\partial\alpha}\left[\nabla_{\boldsymbol{\theta}} G\left(\boldsymbol{\theta}|\alpha\right)\right]\right]\Big|_{\substack{\boldsymbol{\theta}=\boldsymbol{\theta}_0\\ \alpha=\check{\alpha}}}\right)^T, \quad (2.17)$$

after derivation, $E\left[\mathbf{Y}\right]$ is given by

$$\mathbf{Y} = \begin{bmatrix} \sum_{i=1}^{N}\frac{\widetilde{x}_i^2\gamma^2}{\sigma^4 d_i^4}\left(\left(\ln d_i\check{\alpha}\gamma\right)^2+\sigma^2\right) & \sum_{i=1}^{N}\frac{\widetilde{x}_i\widetilde{y}_i\gamma^2}{\sigma^4 d_i^4}\left(\left(\ln d_i\check{\alpha}\gamma\right)^2+\sigma^2\right) \\ \sum_{i=1}^{N}\frac{\widetilde{x}_i\widetilde{y}_i\gamma^2}{\sigma^4 d_i^4}\left(\left(\ln d_i\check{\alpha}\gamma\right)^2+\sigma^2\right) & \sum_{i=1}^{N}\frac{\widetilde{y}_i^2\gamma^2}{\sigma^4 d_i^4}\left(\left(\ln d_i\check{\alpha}\gamma\right)^2+\sigma^2\right) \end{bmatrix}, \quad (2.18)$$

where $\gamma = \frac{10}{\ln 10}$, $\widetilde{x}_i = (x_0 - x_i)$ and $\widetilde{y}_i = (y_0 - y_i)$.

When the error in $\check{\alpha}$ is zero. When the error in $\check{\alpha}$ is zero, the MSE of the location reduces to the CRB[2] of location estimate. It is straightforward from (2.14)

$$MSE = Tr\left\{\left[\mathbf{I}\left(\boldsymbol{\theta}\right)^{-\mathbf{1}}\mathbf{I}\left(\boldsymbol{\theta}\right)\right]\mathbf{I}\left(\boldsymbol{\theta}\right)^{-\mathbf{1}}\right\} = Tr\left\{\mathbf{I}\left(\boldsymbol{\theta}\right)^{-\mathbf{1}}\right\}. \tag{2.19}$$

2.3.1 Bias of RSS estimator

For a "good" location geometry (i.e. the TN placed at the centre of the network while the ANs are at the edge) the RSS measurements are unbiased. Similarly, for high signal to noise ratio (SNR) i.e. when a large number of ANs are deployed, the estimation again is unbiased. However, for a "poor" geometry (i.e. the TN is near the edge of the network) or for low SNR, the RSS estimator exhibits a definite bias. This bias can unexpectedly lead to favourable results as the performance of the estimator can exceed the CRB. The CRB thus cannot tightly bound the estimator performance when it is unbiased. However, the CRB can still predict the performance of a general theoretical unbiased estimator.

2.3.1.1 Analytical expression of Bias due to incorrect PLE assumption

Rewriting (2.11),

$$\begin{bmatrix} (\hat{x}-x_0) \\ (\hat{y}-y_0) \end{bmatrix} = \mathbf{I}\left(\boldsymbol{\theta}|\check{\alpha}\right)^{-\mathbf{1}}\left[\nabla_{\boldsymbol{\theta}}G\left(\boldsymbol{\theta}|\alpha\right)\Big|_{\substack{\boldsymbol{\theta}=\boldsymbol{\theta}_0\\ \alpha=\check{\alpha}}} + \left[\left[\frac{\partial}{\partial\alpha}\nabla_{\boldsymbol{\theta}}G\left(\boldsymbol{\theta}|\alpha\right)\right]\Big|_{\substack{\boldsymbol{\theta}=\boldsymbol{\theta}_0\\ \alpha=\check{\alpha}}}\right](\Delta\alpha)\right]. \tag{2.20}$$

Bias $\mathbf{B}$ is given by $E\left(\hat{\boldsymbol{\theta}}-\boldsymbol{\theta}_0\right)=E\begin{bmatrix} (\hat{x}-x_0) \\ (\hat{y}-y_0) \end{bmatrix}$, thus (2.20) is written as

[2]The covariance matrix of an unbiased estimator is lower bounded by the CRB, and is given by $E\left[\left(\hat{\boldsymbol{\theta}}-\boldsymbol{\theta}\right)\left(\hat{\boldsymbol{\theta}}-\boldsymbol{\theta}\right)^{T}\right] \geq \left[\mathbf{I}\left(\boldsymbol{\theta}\right)\right]^{-1}$, where $\left[\mathbf{I}\left(\boldsymbol{\theta}\right)\right]$ is the Fisher information matrix (FIM).

$$\mathbf{B} = \mathbf{I}\left(\theta|\check{\alpha}\right)^{-\mathbf{1}} E\left[\left[\frac{\partial}{\partial\alpha}\nabla_{\boldsymbol{\theta}}\, G\left(\boldsymbol{\theta}|\alpha\right)\right]\Big|_{\substack{\boldsymbol{\theta}=\boldsymbol{\theta_0}\\ \alpha=\check{\alpha}}}\right](\Delta\alpha)$$

$$= \mathbf{I}\left(\theta|\check{\alpha}\right)^{-\mathbf{1}}\left[\begin{array}{cc} \gamma^2\check{\alpha}\sum_{i=1}^{N}\frac{\widetilde{x}_i \ln d_i}{\sigma^2 d_i^2} & \gamma^2\check{\alpha}\sum_{i=1}^{N}\frac{\widetilde{y}_i \ln d_i}{\sigma^2 d_i^2}\end{array}\right]^T(\Delta\alpha) \tag{2.21}$$

The Total Bias is given by

$$Total\ Bias = E\left[\ (\hat{x} - x_0)\ \right] + E\left[\ (\hat{y} - y_0)\ \right] = \mathbf{B}\left(1,1\right) + \mathbf{B}\left(2,1\right).$$

2.4 Low Complexity Joint Location and PLE Estimator

In [34], the author attempted to formulate a joint estimator (JE) to find the NLS estimate of the unknown vector $\boldsymbol{\phi}$. The solution was obtained iteratively using the Lavenberg-Marquardt (LM) method which is a modification to the Gauss-Newton (GN) method. The solution at the $(k+1)^{\,th}$ iteration is given by

$$\boldsymbol{\phi}^{k+1} = \boldsymbol{\phi}^k + \tilde{\delta}^k, \tag{2.22}$$

where $\tilde{\delta}^k$ is the newton step which is modified and given by [40]

$$\tilde{\delta}^k = \left(\left(\mathbf{J}^T\right)^k \mathbf{J}^k + \overline{\lambda}^k\mathbf{D}\right)^{-1}\left(\mathbf{J}^T\right)^k\left(\mathbf{z} - \mathbf{f}^k\left(\boldsymbol{\phi}\right)\right). \tag{2.23}$$

$\mathbf{D}$ is a positive diagonal matrix and for simplicity it is commonly taken as the

identity matrix[3]. $\mathbf{J}^k$ is the Jacobian matrix at the k^{th} step. The LM method differs from the conventional gradient descent algorithm as it has an adaptive step size. An initial step size $\bar{\lambda}_1$ is chosen. If at the k^{th} iteration, the error $\varepsilon(\boldsymbol{\phi})$ is reduced, the value of $\boldsymbol{\phi}^k$ is updated to $\boldsymbol{\phi}^{k+1}$ and the value of the step size is decreased by a factor $\bar{\lambda}^{k+1} = \frac{\bar{\lambda}^k}{\varrho}$, ϱ is some scaling factor. Its value is a trade-off between accuracy and computation complexity. A small ϱ offers more accuracy but higher computation. Conversely, if $\varepsilon(\boldsymbol{\phi})$ increases at the k^{th} iteration, then $\boldsymbol{\phi}^k$ is not updated and the value of the step size is increased by a factor $\bar{\lambda}^{k+1} = \varrho\bar{\lambda}^k$. For the estimator in [34], the Jacobian is a $N\times3$ matrix. Its elements are given by

$$\left[\mathbf{J}^1\right]_{ij} = \left.\frac{\partial f_i(\boldsymbol{\phi})}{\partial \boldsymbol{\phi}_j}\right|_{\boldsymbol{\phi}=\boldsymbol{\phi}_1}. \tag{2.24}$$

Described below is a simplified implementation of the JE which reduces the size of the Jacobian matrix from $N\times3$ to $N\times2$.

It is clear from (2.5) that although they form a set of non-linear equations in terms of TN coordinates (x, y), yet they are linear in terms of α and hence can be solved via classical ML method instead of an iterative algorithm. Taking the derivatives of (2.7) with respect to α and setting the result equal to zero yields

$$\frac{\partial\varepsilon(\boldsymbol{\phi})}{\partial\alpha} = -10\mathbf{z}^{\mathbf{T}}\log_{10}\mathbf{d} - 10\log_{10}\mathbf{d}^{\mathbf{T}}\mathbf{z} + 200\alpha\log_{10}\mathbf{d}^{\mathbf{T}}\log_{10}\mathbf{d} = 0. \tag{2.25}$$

Solving for the PLE yields

$$\hat{\alpha} = \frac{\mathbf{z}^T}{10\log_{10}\mathbf{d}^T}, \tag{2.26}$$

for $\mathbf{d} = [d_1, ..., d_N]^T$.

It is seen that (2.26) depends only on the observed path-loss and the distances

[3]The dimensions of $\mathbf{D}$ depend on the number of parameters to be estimated.

between the target and the ANs which in turn depend on the unknown x and y coordinates. This reduces the unknown vector to $\boldsymbol{\theta} = [x, y]^T$. Finally putting $\hat{\alpha}$ back in (2.7) and applying the LM algorithm produces the TN coordinates. This simplification shall be referred to as the low complexity joint estimator (LCJE). On the other hand, a simple RSS based location estimator which assumes to have accurate knowledge of α will be referred to as the received signal strength estimator RSSE.

2.5 Bayesian Estimation

2.5.1 Motivation

As mentioned before, knowledge of the exact value of the PLE is difficult to obtain. However, in general the value range is between 2-5 . In fact, many text books tabulate values of α for different environments based on empiric results [20]. Thus there is already a prior information about the PLE for different environments, therefore one could incorporate this information to estimate α instead of blind estimation as in JE. Hence, the PLE can be considered a random variable that is Gaussian distributed around a mean μ_a with variance σ_α^2. Empirical results in [41] validate this assumption. The value of the variance σ_a^2 indicates the confidence in the available data. In this section, a MAP estimator is formulated that iteratively estimates the location coordinates and also capitalizes on the prior information about α.

2.5.2 Maximum a posteriori estimator

Using the signal model in (2.5) and the *a priori* information on α, the MAP estimator of $\boldsymbol{\phi}$ is given by [42]

$$\tilde{\boldsymbol{\phi}}_{\text{MAP}} \equiv \arg\max_{\boldsymbol{\phi}} \left\{ \ln p\left(\boldsymbol{\phi} \mid \mathbf{z}\right) \right\}, \tag{2.27}$$

where $p\left(\boldsymbol{\phi} \mid \mathbf{z}\right)$ is posterior probability of $\boldsymbol{\phi}$ given the obserivation $\mathbf{z}$, and is given by

$$\ln p\left(\boldsymbol{\phi} \mid \mathbf{z}\right) = \ln p\left(\mathbf{z} \mid \boldsymbol{\phi}\right) + \ln p\left(\boldsymbol{\phi}\right).$$

Thus,

$$\tilde{\boldsymbol{\phi}}_{\text{MAP}} \equiv \arg\max_{\boldsymbol{\phi}} \left\{ \ln p\left(\mathbf{z} \mid \boldsymbol{\phi}\right) + \ln p\left(\boldsymbol{\phi}\right) \right\}. \tag{2.28}$$

Since in the unknown vector $\boldsymbol{\phi} = \left[\boldsymbol{\theta}^T, \alpha\right]^T$, only α is a random variable, thus (2.28) can be written as

$$\tilde{\boldsymbol{\phi}}_{\text{MAP}} \equiv \arg\max_{\alpha} \left\{ \ln p\left(\mathbf{z} \mid \alpha, \boldsymbol{\theta}\right) + \ln p\left(\alpha\right) \right\}. \tag{2.29}$$

where

$$p\left(\alpha\right) = \frac{1}{\sqrt{2\pi\sigma_\alpha^2}} \exp\left\{ -\left(\frac{\left(\alpha - \mu_\alpha\right)^2}{2\sigma_\alpha^2} \right) \right\}.$$

(2.29) can be equivalently represented by

$$\tilde{\boldsymbol{\phi}}_{\text{MAP}} \equiv \arg\min_{\alpha} \left\{ \frac{1}{2} \sum_{i=1}^{N} \left(\frac{z_i - f_i\left(\boldsymbol{\theta}\right)}{\sigma_i} \right)^2 + \frac{\left(\alpha - \mu_\alpha\right)^2}{2\sigma_\alpha^2} \right\}. \tag{2.30}$$

Differentiating w.r.t α and equating the outcome to zero yields

$$\sum_{i=1}^{N} -\frac{\left(z_i - f_i\left(\boldsymbol{\theta}\right)\right) 10 \log_{10} d_i}{\sigma_i^2} + \frac{\left(\alpha - \mu_\alpha\right)}{\sigma_\alpha^2} = 0. \tag{2.31}$$

Solving (2.31) for α,

$$\hat{\alpha} = \mu_\alpha + \frac{\sum_{i=1}^{N} (K_i - \mu_\alpha L_i) L_i}{\frac{1}{\sigma_\alpha^2} + \sum_{i=1}^{N} L_i^2}, \tag{2.32}$$

where

$$K_i = \frac{z_i}{\sigma_i},$$

and

$$L_i = \frac{10 \log_{10} d_i}{\sigma_i}.$$

The variance σ_α^2 is choosen by doing some prior measurement in an environment. A small σ_α^2 will suggest that the PLE value is uniform for different channel links in the environment. As can be seen, L_i depends on d_i, which is unknown. The values of $\hat{\alpha}$ can now be updated jointly with the coordinates (x, y) using the LM algorithm. Hence, the available information about α is capitalized in addition to the observed data.

2.6 Hybrid Cramer-Rao Bound

In order to compare the MSEs of estimators, the CRB has been extensively used as a benchmark. The CRB puts a lower bound on any unbiased estimator.

The classical CRB in [34] cannot be used as a benchmark for the performance of the MAP estimator given in subsection 2.5.2. This is because the classical CRB does not consider the available information of the parameters to be estimated. For a set of all random parameters, the Bayesian CRB can be used as a bound [42]. However, if some of the unknown parameters are random while others are deterministic, then the hybrid CRB is used.

In this section, the HCRB is derived when considering the PLE as a random variable. The hybrid information matrix (HIM) is defined as [42].

$$\mathbf{I_H} = \mathbf{I_D} + \mathbf{I_P}, \tag{2.33}$$

where $\mathbf{I_D}$ is the 3×3 matrix that represents the contribution from the observed data. Its elements are given by

$$[\mathbf{I_D}] = E\left[\mathbf{I}\left(\alpha, \boldsymbol{\theta}\right)\right], \tag{2.34}$$

where the expectation is w.r.t $p\left(\alpha\right)$ and

$$\left[\mathbf{I}\left(\alpha, \boldsymbol{\theta}\right)\right]_{ij} = -E\left[\frac{\partial^2 \ln p\left(\mathbf{z} \mid \alpha, \boldsymbol{\theta}\right)}{\partial \boldsymbol{\theta}_i \partial \boldsymbol{\theta}_j}\right], \tag{2.35}$$

the expectation here is w.r.t $p\left(\mathbf{z} \mid \alpha, \boldsymbol{\theta}\right)$. $\mathbf{I_P}$ shows the prior information and is given by

$$\mathbf{I_P} = -E\left[\frac{\partial^2 \ln p\left(\alpha\right)}{\partial \alpha^2}\right], \tag{2.36}$$

where the expectation is w.r.t $p\left(\alpha\right)$ only. After some derivation, $\mathbf{I_H}$ is given by

$$\mathbf{I_H} = \frac{1}{\sigma^2}\begin{bmatrix} \sum_{i=1}^{N}\left(\frac{\widetilde{\gamma x_i}}{d_i^2}\right)^2\Psi & \sum_{i=1}^{N}\left(\frac{\gamma}{d_i^2}\right)^2\widetilde{x}_i\widetilde{y}_i\Psi & \sum_{i=1}^{N}\left(\frac{\gamma}{d_i}\right)^2\widetilde{x}_i \ln d_i\boldsymbol{\Phi} \\ \sum_{i=1}^{N}\left(\frac{\gamma}{d_i^2}\right)^2\widetilde{x}_i\widetilde{y}_i\Psi & \sum_{i=1}^{N}\left(\frac{\widetilde{\gamma y_i}}{d_i^2}\right)^2\Psi & \sum_{i=1}^{N}\left(\frac{\gamma}{d_i}\right)^2\widetilde{y}_i \ln d_i\boldsymbol{\Phi} \\ \sum_{i=1}^{N}\left(\frac{\gamma}{d_i}\right)^2\widetilde{x}_i \ln d_i\boldsymbol{\Phi} & \sum_{i=1}^{N}\left(\frac{\gamma}{d_i}\right)^2\widetilde{y}_i \ln d_i\boldsymbol{\Phi} & \sum_{i=1}^{N}(\gamma \ln d_i)^2+\sigma_\alpha^{-2} \end{bmatrix}, \tag{2.37}$$

where $\boldsymbol{\Phi}$ and Ψ are the first and second moments of $p\left(\alpha\right)$. Now, the localisation MSE for any unbiased location estimator is bounded by

$$MSE\left(\hat{\boldsymbol{\theta}}\right) \geq \left[\mathbf{I_H}\right]_{11}^{-1} + \left[\mathbf{I_H}\right]_{22}^{-1}, \tag{2.38}$$

where

$$MSE\left(\hat{\boldsymbol{\theta}}\right)=E\left[\left(\hat{\boldsymbol{\theta}}-\boldsymbol{\theta}_0\right)^T\left(\hat{\boldsymbol{\theta}}-\boldsymbol{\theta}_0\right)\right] \tag{2.39}$$

and

$$\hat{\boldsymbol{\theta}}-\boldsymbol{\theta}_0=\left[\begin{array}{cc}(\hat{x}-x_0) & (\hat{y}-y_0)\end{array}\right]^T, \tag{2.40}$$

$\boldsymbol{\theta}_0$ being the true values.

On the other hand, the MSE of the estimated $\hat{\alpha}$ is bounded by

$$MSE\left(\hat{\alpha}\right)\geq\left[\mathbf{I_H}\right]_{33}^{-1}. \tag{2.41}$$

2.7 Simulation Results

In all the simulations a circular deployment of ANs with radius (R) is considered. (x^1, y^1) is the initial seed given to the LM algorithm which iterates ρ number of times. Simulations are run independently η number of times.

2.7.1 Error Analysis

2.7.1.1 MSE

Fig. 2.1 compares the location error analysis with RSSE simulation for incorrect PLE assumption. The root mean square error (RMSE) is compared with different values of $\Delta\alpha$. The TN is placed at the centre of the network at (0,0). It is observed that the simulations follow the error analysis results. However, both the error analysis and the simulation exhibit larger error for $\breve{\alpha}<\alpha_0$ as compared to $\breve{\alpha}>\alpha_0$. The large error shown by the simulation is due to the divergence of

the iterative algorithm due to incorrect PLE assumption. It is also observed that RMSE decreases as the number of ANs are increased, however even for larger number of ANs the incorrect PLE assumption produces unacceptable location error.

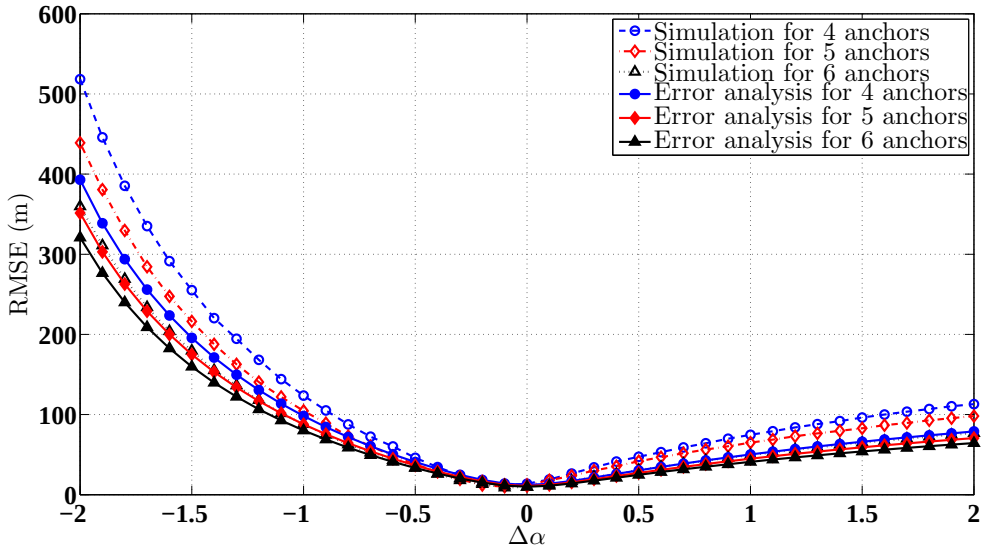

Figure 2.1: Comparison between error analysis and RSSE simulation. $\sigma_i^2 = 5$, $\rho = 10$, $\alpha_0 = 3$, R=50 m, $\eta = 500$, $(x_0, y_0) = (0, 0)$, $(x^1, y^1) = (24, -24)$.

2.7.1.2 Bias

A circular deployment of 6 ANs is considered in Fig. 2.2 and the target node is placed at different positions. The noise variance is $\sigma^2 = 1$. The total bias is compared with different values of $\triangle\alpha$. It is interesting to note that when the target node is placed at the centre, i.e. equal distance from all ANs, then no Bias is recorded. Once again, it is noted that the simulation closely follow the theoretical results.

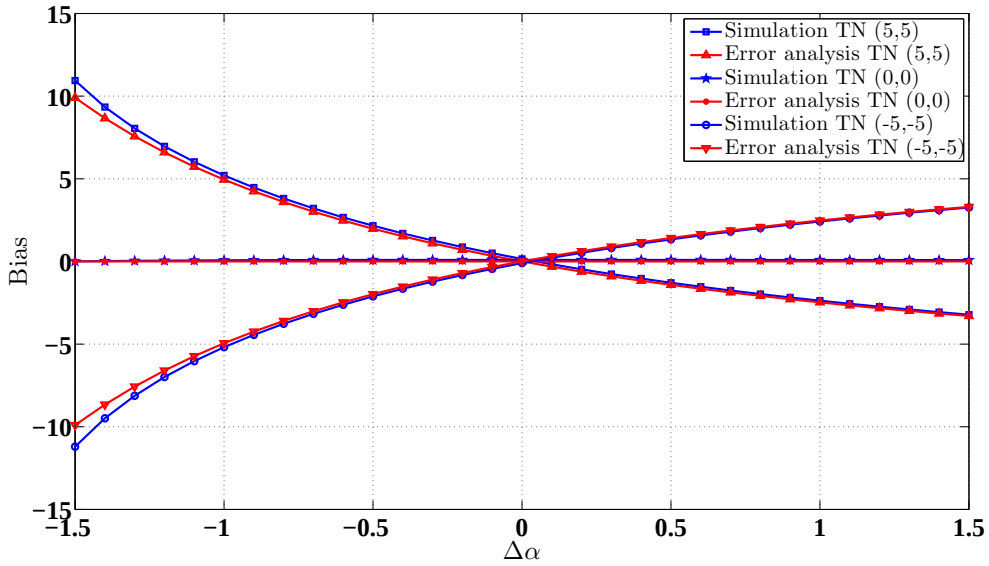

Figure 2.2: Comparison between theoretical Bias and RSSE simulation. $\sigma_i^2 = 1$, $\rho = 10$, $\alpha_0 = 3$, R=50 m, $N = 6$.

2.7.2 Comparison between JE and LCJE

In the simulation shown in Fig. 2.3, the performance of JE and LCJE is compared. As can be seen both implementation show similar performance. Thus the decrease in complexity in LCJE does not have any negative impact on the performance of the algorithm.

2.7.3 Performance comparison between JE and MAP (estimation of α)

Fig. 2.4 shows the comparison between performance of the RSSE, JE and the MAP estimator in estimating α at TN position (0,0). Two different values of σ_α= 0.1 and 0.05 are used. It is observed that as the noise variance increases (or at low SNR) the MAP performs considerably better than the JE. It is noticed that CRB and the HCRB bound the performance of the iterative algorithm as it is unbiased

at this geometry. However, at other geometries when the estimator is biased, the CRB/HCRB does not tightly bound the performance of the estimator. It should be noted that all algorithm parameters such as (x^1, y^1), $\bar{\lambda}^1$, ϱ and ρ in the LM algorithm are kept the same for both methods.

2.7.4 Performance comparison between JE and MAP (estimation of (x, y))

In Fig. 2.5, the performance of the RSSE, JE and MAP algorithms is compared. The RMSE is compared with the number of iteration ρ. It is observed that all three algorithms asymptotically converge to the same minimum. However, due to no prior information the JE has a slower convergence rate than the MAP. Thus the MAP exhibits superior performance for a smaller ρ. Indeed, the performance of the MAP estimator depends on σ_α, a smaller value of σ_α shows better performance.

2.7.5 Location CRB/HCRB comparison

Fig. 2.6 shows the performance of the CRB and HCRB on the location estimation for the three different cases, i.e. when α is known, α is unknown and deterministic and when α is unknown and random. It is interesting to note, that at a good geometry when the TN is at (0,0) the performance of HCRB and CRB is the same. For other geometries the HCRB shows smaller error than the CRB. This is expected due to the additional information available about α.

2.8 Summary

In this chapter, the issue of RSS based location estimation for an unknown path-loss model was addressed. First, error analysis for incorrectly assumed PLE was

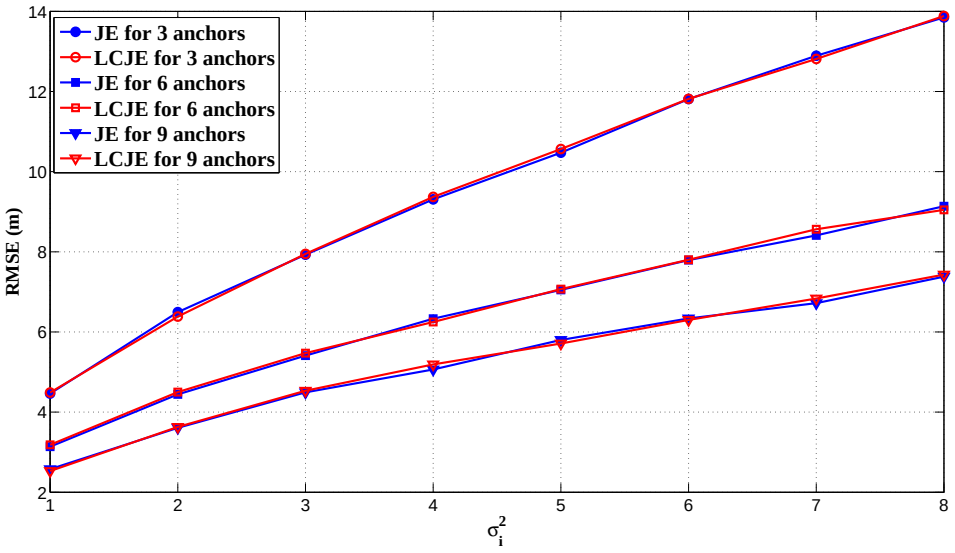

Figure 2.3: Performance comparison between JE and LCJE. R=50, $\alpha_0 = 3$, $\lambda^1 = 1$, $\varrho = 1.1$, $\rho = 15$, $\eta = 1500$, $(x_0, y_0) = (0, 0)$, $(x^1, y^1) = (25, 25)$.

done. It was shown that the simulation results are in agreement with the error analysis results and that both show degraded performance when α is incorrectly assumed. Performance degradation is even worse for negative $\Delta\alpha$. Second, a low complexity implementation of the JE by decreasing the elements of the Jacobian matrix was proposed. Simulation results prove that this simplification has no affect on the performance. In order to utilize the on hand data available about the PLE, the PLE is considered as a random variable and a MAP estimator was proposed. Simulation results prove that the MAP performs better in estimating α at low SNR and has a faster convergence in location estimation. Finally, the HCRB for a random α was derived and it was shown that in general it is lower than the CRB due to the additional information provided about α. Yet when the TN is at equal distance from all anchors both bounds are the same.

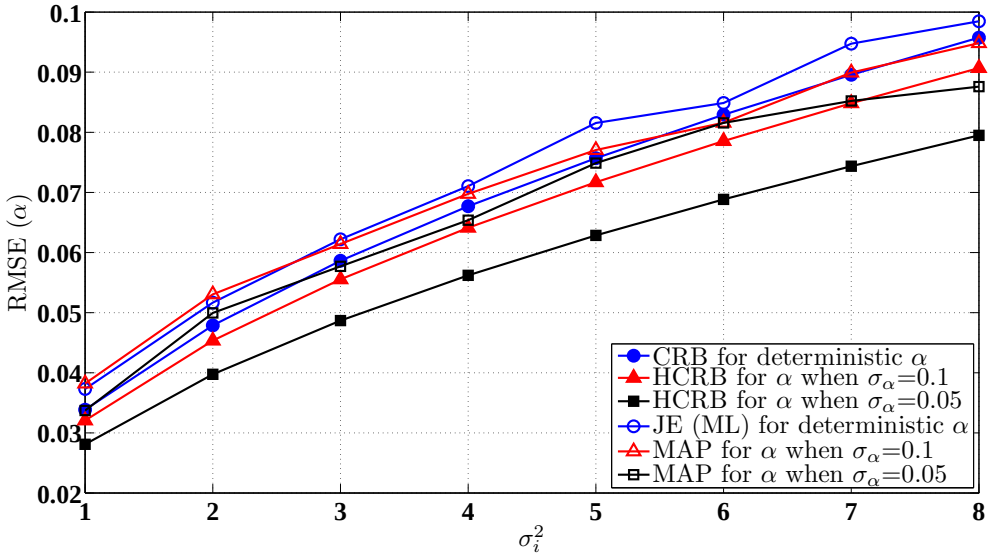

Figure 2.4: Comparison between theoretical Bias and RSSE simulation. $\sigma_i^2 = 1$, $\rho = 10$, $\alpha_0 = 3$, R=50 m, $N = 6$.

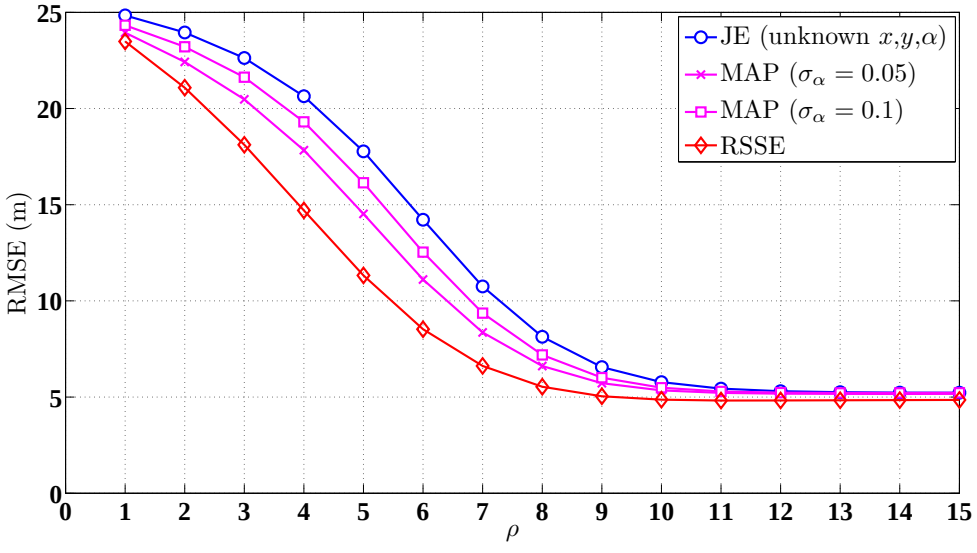

Figure 2.5: Performance comparison between RSSE, JE and MAP estimator. $\sigma_i^2 = 5$, R=30 m, $\alpha_0 = 3$, $\bar{\lambda}^1 = 1$, $\varrho = 1.1$, $\eta = 1500$, $N = 4$, $(x_0, y_0) = (0, 0)$, $(x^1, y^1) = (18, 18)$.

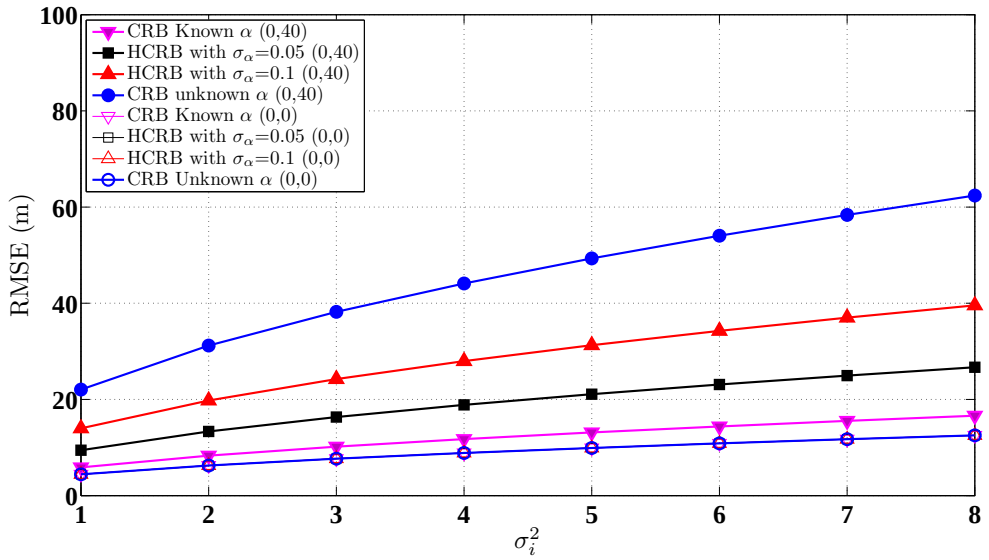

Figure 2.6: Location CRB/HCRB comparison for $(x_0, y_0) = (0, 0)$, $(0, 40)$, $N = 3$, $\alpha_0 = 3$, $R = 50$ m.

3 Low Complexity RSS based Localisation

The material in this chapter has been published in the papers:

- N. Salman, M. Ghogho, and A. H. Kemp, "Low Complexity Joint Estimation of Location and Path-Loss Exponent," *IEEE Wireless Commun Lett.*, vol. 1, no. 4, pp. 364–367, Aug. 2012.
- N. Salman, M. Ghogho, J. Guo, A. H. Kemp, "Analysis of linear least square solution for RSS based localization" *12th International Symposium on Communications and Information Technologies (ISCIT), 2012.* pp. 1051 - 1054, Oct 2012.

3.1 Overview

Chapter 2 dealt with the RSS based localisation using the iterative LM method and developed the LCJE. Although the LCJE reduces the number of unknowns and hence the size of the Jacobian matrix, it suffers from issues which are inherent with iterative techniques. These may include ill-conditioning and divergence [40]. Furthermore a close initial estimate is required to guarantee convergence to the global minima. In many cases, guessing a close initial estimate is not

possible, which can result in the iterative algorithms to converge to the local minima. To by pass these difficulties, in this chapter, the non-linear path-loss observations are first linearised and then solved via simple linear least squares (LLS) method. The chapter also deals with the joint estimation of PLE and location using the LLS. The approach here is opposite to LCJE in chapter 2, where first the PLE was determined in terms of location coordinates which were then estimated. However, in this chapter, the PLE is first estimated as it is dependent on the location coordinates, which results into a single variable minimization problem. The PLE is estimated via a simple line search followed by the location estimation. Furthermore in this chapter, using the linearised set of equations a closed form expression is developed for the mean square error (MSE) and bias of the location estimates for incorrect PLE assumption. For further increased accuracy the obtained results are used as the initial estimate to our proposed iterative algorithm i.e. LCJE. This results in optimum performance with a small number of iterations and guaranteed convergence. To sum up, the main contributions of this chapter are as follows:

- Introducing LLS technique to solve RSS based location.
- Error analysis of LLS technique with PLE in error.
- Joint estimation of PLE and location using LLS.
- Demonstration of superior performance when the LLS solution is used as the initial estimate for LCJE.

The rest of the chapter is organized as follows. Section 3.2 presents the problem statement and the system model. In section 3.3, the non-linear path-loss equations are linearised and the linear least squares (LLS) solution is presented. In section 3.4, location error analysis for incorrect PLE is carried out. In section 3.5, the linear joint estimator (LJE) for PLE and location estimation is developed.

Finally in section 3.6, the simulation results are discussed which are followed by conclusions.

3.2 System Model

Unless otherwise specified, same notations as in chapter 2 are used in this chapter. The signal model (before linearisation) is similar to that in chapter 2, and will be rewritten here for easy understanding.

A two dimensional network is considered bearing target node (TN) which has unknown coordinates $\boldsymbol{\theta} = [x, y]^T$ ($\boldsymbol{\theta} \in \mathscr{R}^2$) that are to be estimated. The network consists of N anchor nodes (ANs) with locations $\boldsymbol{\theta}_i = [x_i, y_i]^T (\boldsymbol{\theta}_i \in \mathscr{R}^2)$ for $i = 1, ..., N$. The distance d_i between the TN and the i^{th} AN, is related to the path-loss at the i^{th} AN, $\mathscr{L}_i$, and the PLE, α, as [35]

$$\mathscr{L}_i = \mathscr{L}_0 + 10\alpha \log_{10} d_i + w_i, \tag{3.1}$$

where $\mathscr{L}_0$ is the path-loss at the reference distance d_0 ($d_0 < d_i$, and is normally taken as 1 m) and w_i is a zero-mean Gaussian random variable representing the multipath log-normal shadowing effect, i.e.

$$w_i \sim \left(\mathcal{N}\left(0, \sigma_i^2\right)\right).$$

The different delay of the multipaths are irrelevant in RSS location systems. Thus shadowing in this only fluctuates the received power due to constructive and destructive interference at the receiver.

The path-loss is calculated as

$$\mathscr{L}_i = 10 \log_{10} P_t - 10 \log_{10} P_i, \tag{3.2}$$

where P_t is the transmit power at the TN and P_i is the received power at the i^{th} AN. The distance d_i is given by

$$d_i = \sqrt{(x - x_i)^2 + (y - y_i)^2}.$$

The observed path-loss (in dB) from d_0 to d_i,

$$z_i = \mathscr{L}_i - \mathscr{L}_0, \tag{3.3}$$

can be expressed as

$$z_i = f_i(\boldsymbol{\theta}) + w_i, \tag{3.4}$$

where

$$f_i(\boldsymbol{\theta}) = \gamma\alpha \ln d_i, \tag{3.5}$$

and

$$\gamma = \frac{10}{\ln 10}. \tag{3.6}$$

In a vector form,

$$\mathbf{z} = \mathbf{f}(\boldsymbol{\theta}) + \mathbf{w}, \tag{3.7}$$

where $\mathbf{z} = [z_1, ..., z_N]^T$ is the vector of the observed path-loss.

$\mathbf{f}(\boldsymbol{\theta}) = [f_1(\boldsymbol{\theta}), ..., f_N(\boldsymbol{\theta})]^T$is the actual path-loss vector and $\mathbf{w} = [w_1, ..., w_N]^T$ is the noise vector. It is evident from (3.7) that it forms a set of non-linear equations and hence are normally solved using iterative methods such as the Gauss-Newton (GN) method. However, the solution can also be found non-iteratively by first linearising the system as shown in the next section.

3.3 Linear Model

The idea of linearising the non-linear set of distance equations was first proposed for ToA systems in [43] while its detailed analysis is present in [44]. Here a similar approach is used to linearise the non-linear path-loss equations as follows. Let $\hat{z}_i$ be the noisy path-loss measurements. Then from (3.7),

$$\frac{\hat{z}_i}{\gamma\alpha} = \ln \hat{d}_i \tag{3.8}$$

or

$$\left(\exp \frac{2\hat{z}_i}{\gamma\alpha}\right) = \hat{d}_i^2. \tag{3.9}$$

Each distance equation can now be subtracted from a reference distance equation d_r^2.

$$d_r^2 - d_i^2 = \left(\exp \frac{2\hat{z}_r}{\gamma\alpha}\right) - \left(\exp \frac{2\hat{z}_i}{\gamma\alpha}\right) \tag{3.10}$$

or

$$(x_i - x_r)\, x + (y_i - y_r)\, y = 0.5 \left[\left(\exp \frac{2\hat{z}_r}{\gamma\alpha}\right) - \left(\exp \frac{2\hat{z}_i}{\gamma\alpha}\right) - \left(x_r^2 + y_r^2\right) + \left(x_i^2 + y_i^2\right)\right]. \tag{3.11}$$

The obtained results can be written in matrix form

$$\mathbf{A}\boldsymbol{\theta} = 0.5\mathbf{b}_\alpha, \tag{3.12}$$

where

$$\mathbf{A} = \begin{bmatrix} x_1 - x_r & y_1 - y_r \\ x_2 - x_r & y_2 - y_r \\ \vdots & \vdots \\ x_{N-1} - x_r & y_{N-1} - y_r \end{bmatrix}, \boldsymbol{\theta} = \begin{bmatrix} x \\ y \end{bmatrix} \tag{3.13}$$

and

$$\mathbf{b}_\alpha = \begin{bmatrix} \left(\exp\frac{2\hat{z}_r}{\gamma\alpha}\right) - \left(\exp\frac{2\hat{z}_1}{\gamma\alpha}\right) - \varphi_r + \varphi_1 \\ \left(\exp\frac{2\hat{z}_r}{\gamma\alpha}\right) - \left(\exp\frac{2\hat{z}_2}{\gamma\alpha}\right) - \varphi_r + \varphi_2 \\ \vdots \\ \left(\exp\frac{2\hat{z}_r}{\gamma\alpha}\right) - \left(\exp\frac{2\hat{z}_{N-1}}{\gamma\alpha}\right) - \varphi_r + \varphi_{N-1} \end{bmatrix},$$

where $\varphi_r = x_r^2 + y_r^2$ and $\varphi_i = x_i^2 + y_i^2$ for $i = 1, ..., N-1$. The solution is given by [39]

$$\hat{\boldsymbol{\theta}} = 0.5\mathbf{A}^\dagger \mathbf{b}_\alpha, \tag{3.14}$$

where $\mathbf{A}^\dagger = (\mathbf{A}^T\mathbf{A})^{-\mathbf{1}}\mathbf{A}^T$.

This approach is referred to as the linear least squares (LLS) method. The reference distance d_r can be obtained by choosing a reference node. This will be referred to as LLS-ref. Alternatively d_r can be the average of all distance equations i.e. $d_r^2 = \frac{1}{N}\sum_{i=1}^{N} d_i^2$, this implementation will be referred as LLS-avg. Finally instead of subtracting a reference distance, each distance equation is subtracted from every other (combination of pair of equations) resulting in $N \times \left(\frac{N-1}{2}\right)$ equations. This shall be known as LLS-comb. It is noted however that the number of equations increases substantially with LLS-comb for larger number of ANs.

3.4 Error Analysis

In order to appreciate the effects of an incorrect PLE assumption on location error, the MSE and bias expressions for location error due to incorrect PLE and noisy path-loss estimates are derived. Let the LS solution

$$\check{\boldsymbol{\theta}} = 0.5\mathbf{A}^{\dagger}\mathbf{b}_{\check{\alpha}} \tag{3.15}$$

be the solution of the TN location for incorrect PLE assumption. The observed vector $\mathbf{b}_{\check{\alpha}}$ contains path-loss $\check{z}_i$ with associated noise that has variance σ^2 and PLE

$$\check{\alpha} = \alpha_0 + \Delta\alpha, \tag{3.16}$$

α_0 is the true value of the PLE and $\Delta\alpha$ is the error. On the other hand if $\boldsymbol{\theta}_0$ is the solution obtained for accurate PLE α_0 resulting in observed vector $\mathbf{b}_{\boldsymbol{\alpha_0}}$ then

$$\boldsymbol{\theta}_0 = 0.5\mathbf{A}^{\dagger}\mathbf{b}_{\boldsymbol{\alpha_0}}, \tag{3.17}$$

and for $\boldsymbol{\epsilon} = (\mathbf{b}_{\check{\alpha}}) - (\mathbf{b}_{\boldsymbol{\alpha_0}})$,

$$\check{\boldsymbol{\theta}} - \boldsymbol{\theta}_0 = \left(0.5\mathbf{A}^{\dagger}\left(\boldsymbol{\epsilon}\right)\right). \tag{3.18}$$

3.4.1 MSE

The mean square error (MSE) is given by the trace of the covariance matrix

$$MSE = Tr\left\{E\left[\left(\check{\boldsymbol{\theta}} - \boldsymbol{\theta}_0\right)\left(\check{\boldsymbol{\theta}} - \boldsymbol{\theta}_0\right)^{T}\right]\right\}. \tag{3.19}$$

Putting (3.17) and (3.18) in (3.19), it follows

$$MSE = Tr\left\{0.25\Big[\mathbf{A}^{\dagger}E\left[\boldsymbol{\epsilon}\boldsymbol{\epsilon}^{T}\right]\left(\mathbf{A}^{\dagger}\right)^{T}\Big]\right\}. \tag{3.20}$$

$$\left\{E\left[\boldsymbol{\epsilon}\boldsymbol{\epsilon}^T\right]\right\}_{ii} = \exp\frac{4\left(\gamma\breve{\alpha}f_r(\boldsymbol{\theta})+2\sigma^2\right)}{\left(\gamma\breve{\alpha}\right)^2} + \exp\frac{4f_i(\boldsymbol{\theta})}{\gamma\alpha_0} + \exp\frac{4f_r(\boldsymbol{\theta})}{\gamma\alpha_0} - 2\exp\frac{2(f_i(\boldsymbol{\theta})+f_r(\boldsymbol{\theta}))}{\left(\gamma\alpha_0\right)^2} - 2\exp\frac{2\left(\gamma\breve{\alpha}(f_r(\boldsymbol{\theta})+f_i(\boldsymbol{\theta}))+2\sigma^2\right)}{\left(\gamma\breve{\alpha}\right)^2} - 2\exp\left(\frac{2\left(\gamma\breve{\alpha}f_r(\boldsymbol{\theta})+\sigma^2\right)}{\left(\gamma\breve{\alpha}\right)^2} + \frac{2f_r(\boldsymbol{\theta})}{\gamma\alpha_0}\right) + \exp\frac{4\left(\gamma\breve{\alpha}f_i(\boldsymbol{\theta})+2\sigma^2\right)}{\left(\gamma\breve{\alpha}\right)^2} + 2\times \exp\left(\frac{2\left(\gamma\breve{\alpha}f_r(\boldsymbol{\theta})+\sigma^2\right)}{\left(\gamma\breve{\alpha}\right)^2}+\frac{2f_i(\boldsymbol{\theta})}{\gamma\alpha_0}\right)+2\exp\left(\frac{2\left(\gamma\breve{\alpha}f_i(\boldsymbol{\theta})+\sigma^2\right)}{\left(\gamma\breve{\alpha}\right)^2}+\frac{2f_r(\boldsymbol{\theta})}{\gamma\alpha_0}\right) - 2\exp\left(\frac{2\left(\gamma\breve{\alpha}f_i(\boldsymbol{\theta})+\sigma^2\right)}{\left(\gamma\breve{\alpha}\right)^2} + \frac{2f_i(\boldsymbol{\theta})}{\gamma\alpha_0}\right). \tag{3.21}$$

$$\begin{aligned}&\left\{E\left[\boldsymbol{\epsilon}\boldsymbol{\epsilon}^T\right]\right\}_{ij}= \\ &\exp\frac{4\left(\gamma\breve{\alpha}f_r(\boldsymbol{\theta})+2\sigma^2\right)}{\left(\gamma\breve{\alpha}\right)^2} - \exp\frac{2\left(\gamma\breve{\alpha}(f_r(\boldsymbol{\theta})+f_j(\boldsymbol{\theta}))+2\sigma^2\right)}{\left(\gamma\breve{\alpha}\right)^2} - 2\exp\left(\frac{2\left(\gamma\breve{\alpha}f_r(\boldsymbol{\theta})+\sigma^2\right)}{\left(\gamma\breve{\alpha}\right)^2}+\frac{2(f_r(\boldsymbol{\theta}))}{\gamma\alpha_0}\right) + \\ &\exp\left(\frac{2\left(\gamma\breve{\alpha}f_r(\boldsymbol{\theta})+\sigma^2\right)}{\left(\gamma\breve{\alpha}\right)^2}+\frac{2(f_j(\boldsymbol{\theta}))}{\gamma\alpha_0}\right) - \exp\frac{2\left(\gamma\breve{\alpha}(f_i(\boldsymbol{\theta})+f_r(\boldsymbol{\theta}))+2\sigma^2\right)}{\left(\gamma\breve{\alpha}\right)^2} - \exp\left(\frac{2(f_i(\boldsymbol{\theta})+f_r(\boldsymbol{\theta}))}{\gamma\alpha_0}\right) + \\ &\exp\frac{2\left(\gamma\breve{\alpha}(f_i(\boldsymbol{\theta})+f_j(\boldsymbol{\theta}))+2\sigma^2\right)}{\left(\gamma\breve{\alpha}\right)^2} + \exp\left(\frac{2\left(\gamma\breve{\alpha}f_i(\boldsymbol{\theta})+\sigma^2\right)}{\left(\gamma\breve{\alpha}\right)^2} + \frac{2(f_r(\boldsymbol{\theta}))}{\gamma\alpha_0}\right) - \\ &\exp\left(\frac{2\left(\gamma\breve{\alpha}f_i(\boldsymbol{\theta})+\sigma^2\right)}{\left(\gamma\breve{\alpha}\right)^2} + \frac{2(f_j(\boldsymbol{\theta}))}{\gamma\alpha_0}\right) + \exp\left(\frac{2(f_i(\boldsymbol{\theta})+f_j(\boldsymbol{\theta}))}{\gamma\alpha_0}\right) + \exp\left(\frac{2\left(\gamma\breve{\alpha}f_j(\boldsymbol{\theta})+\sigma^2\right)}{\left(\gamma\breve{\alpha}\right)^2} + \frac{2(f_r(\boldsymbol{\theta}))}{\gamma\alpha_0}\right) + \\ &\exp\frac{4(f_r(\boldsymbol{\theta}))}{\gamma\alpha_0} - \exp\left(\frac{2(f_j(\boldsymbol{\theta})+f_r(\boldsymbol{\theta}))}{\gamma\alpha_0}\right) + \exp\left(\frac{2\left(\gamma\breve{\alpha}f_r(\boldsymbol{\theta})+\sigma^2\right)}{\left(\gamma\breve{\alpha}\right)^2} + \frac{2(f_i(\boldsymbol{\theta}))}{\gamma\alpha_0}\right) - \\ &\exp\left(\frac{2\left(\gamma\breve{\alpha}f_j(\boldsymbol{\theta})+\sigma^2\right)}{\left(\gamma\breve{\alpha}\right)^2} + \frac{2(f_i(\boldsymbol{\theta}))}{\gamma\alpha_0}\right).\end{aligned} \tag{3.22}$$

On the other hand when $i \neq j$, then $\left\{E\left[\boldsymbol{\epsilon}\boldsymbol{\epsilon}^T\right]\right\}_{ij}$ can be given by (3.22).
The diagonal elements of $E\left[\boldsymbol{\epsilon}\boldsymbol{\epsilon}^T\right]$ are given by (3.21) where $f_r\left(\boldsymbol{\theta}\right) = \gamma\alpha \ln d_r$.

3.4.2 BIAS

The total bias is given by

$$E\left[\ \left(\breve{x} - x_0\right)\ \right] + E\left[\ \left(\breve{y} - y_0\right)\ \right] = \mathbf{B}\left(1,1\right) + \mathbf{B}\left(2,1\right) \tag{3.23}$$

where

$$\mathbf{B} = 0.5\mathbf{A}^{\dagger}E\left(\boldsymbol{\epsilon}\right) \tag{3.24}$$

and the elements of $E\left(\boldsymbol{\epsilon}\right)$ are given as

$$E(\boldsymbol{\epsilon}) = \exp\left(\frac{2\left(\gamma\check{\alpha}f_r(\boldsymbol{\theta})+\sigma^2\right)}{(\gamma\check{\alpha})^2}\right) - \exp\left(\frac{2\left(\gamma\check{\alpha}f_i(\boldsymbol{\theta})+\sigma^2\right)}{(\gamma\check{\alpha})^2}\right)$$

$$- \left(\exp\frac{2f_r(\boldsymbol{\theta})}{\gamma\alpha_0}\right) + \left(\exp\frac{2f_i(\boldsymbol{\theta})}{\gamma\alpha_0}\right). \tag{3.25}$$

The total bias expression (3.23) could be misleading at times, as the bias in the x-axis and y-axis could cancel out each other if they are of the same magnitude but opposite sign. In which case the bias can be zero however it does not mean that the estimates are error free. Although, in our simulation the trend is that the bias in both x and y axis has the same sign, in order to avoid confusion, the abolute value of bias can be taken instead i.e.

Total Bias

$$= \left|E\left[\ (\check{x} - x_0)\ \right]\right| + \left|E\left[\ (\check{y} - y_0)\ \right]\right|.$$

3.5 Location Estimation in Unknown Path-Loss Model

For unknown path-loss model, the least squares (LS) problem for the observed vector $\mathbf{b}_\alpha$ with any unknown α is obtained by minimizing the cost function $\mathrm{C}(\boldsymbol{\theta}, \alpha)$

$$\mathrm{C}(\boldsymbol{\theta}, \alpha) = \|\mathbf{A}\boldsymbol{\theta} - \mathbf{0.5}\mathbf{b}_\alpha\|^2, \tag{3.26}$$

where the LS solution is given by

$$\hat{\boldsymbol{\theta}}_{\mathrm{LS}} = 0.5\mathbf{A}^\dagger\mathbf{b}_\alpha \tag{3.27}$$

Putting (3.27) in (3.26), it follows

$$\mathrm{C}(\alpha) = \mathbf{b}_\alpha^T \left(\mathbf{A}\mathbf{A}^\dagger\right)^T \mathbf{A}\mathbf{A}^\dagger \mathbf{b}_\alpha + \mathbf{b}_\alpha^T \mathbf{b}_\alpha - \mathbf{2}\mathbf{b}_\alpha^T \left(\mathbf{A}\mathbf{A}^\dagger\right)^T \mathbf{b}_\alpha, \tag{3.28}$$

using $\left(\mathbf{A}\mathbf{A}^\dagger\right)^T \mathbf{A}\mathbf{A}^\dagger = \mathbf{A}\mathbf{A}^\dagger$ and $\left(\mathbf{A}\mathbf{A}^\dagger\right)^T = \mathbf{A}\mathbf{A}^\dagger$ to get

$$\mathrm{C}(\alpha) = \mathbf{b}_\alpha^T \mathbf{b}_\alpha - \mathbf{b}_\alpha^T \left(\mathbf{A}\mathbf{A}^\dagger\right) \mathbf{b}_\alpha \tag{3.29}$$

or

$$\mathrm{C}(\alpha) = \left[0.25 \left(\mathbf{b}_\alpha^T \left(\mathbf{I} - \mathbf{A}\mathbf{A}^\dagger\right) \mathbf{b}_\alpha\right)\right], \tag{3.30}$$

which is now only a single variable optimization problem. Finally

$$\hat{\alpha} = \arg\min_\alpha \mathrm{C}(\alpha). \tag{3.31}$$

Solution to (3.31) is straightforward as the values of α are between 2-5 for most environments [20]. Incremental values of α between these limits are inserted in (3.31) and the one that minimizes $\mathrm{C}(\alpha)$ is selected. The value of the increment depends on the desired accuracy. Thus $\mathbf{b}_{\hat{\alpha}}$ obtained is used to obtain the location coordinates such as

$$\hat{\boldsymbol{\theta}}_{LJE} = 0.5\mathbf{A}^\dagger \mathbf{b}_{\hat{\alpha}}. \tag{3.32}$$

This technique will be referred to as linear joint estimator (LJE).

3.5.1 $\hat{\theta}_{LJE}$ as the initial estimate

In order to achieve higher accuracy at the expense of higher computation, $\hat{\boldsymbol{\theta}}_{LJE}$ can be used as an initial estimate to a more computationally complex iterative algorithm such as maximum a posteriori (MAP) and LCJE in chapter 2. Both of these algorithms operate iteratively such as $\boldsymbol{\theta}^{k+1} = \boldsymbol{\theta}^{k} + \tilde{\delta}$, where $\tilde{\delta}$ is a small step and $\boldsymbol{\theta}^{k}$ is the estimate at the k^{th} iteration. Although both of these algorithms are optimal, they still require a close initial estimate $\boldsymbol{\theta}^{1}$ for convergence to the global minima. For initial estimates that are far away from the actual location coordinates, iterative algorithm can converge into a local minima. Hence by keeping $\boldsymbol{\theta}^{1}$=$\hat{\boldsymbol{\theta}}_{LJE}$ convergence to the global minima can be guaranteed. Furthermore for $\boldsymbol{\theta}^{1} = \hat{\boldsymbol{\theta}}_{LJE}$ convergence can be achieved with smaller k.

3.5.2 Cramer-Rao bound (CRB)

The CRB lower bounds the MSE of any unbiased estimator. The CRB for unknown location coordinates with known PLE is derived in [18]. When the PLE is also unknown the the CRB-α is derived in [34].

3.6 Simulation Results

For the performance comparison. two different anchor/target node deployments are considered.

3.6.1 Circular deployment of ANs with correct PLE.

In the first case, a circular deployment of ANs around the origin with radius (R) is considered. Also randomly deployed 20 TNs are considered in the network

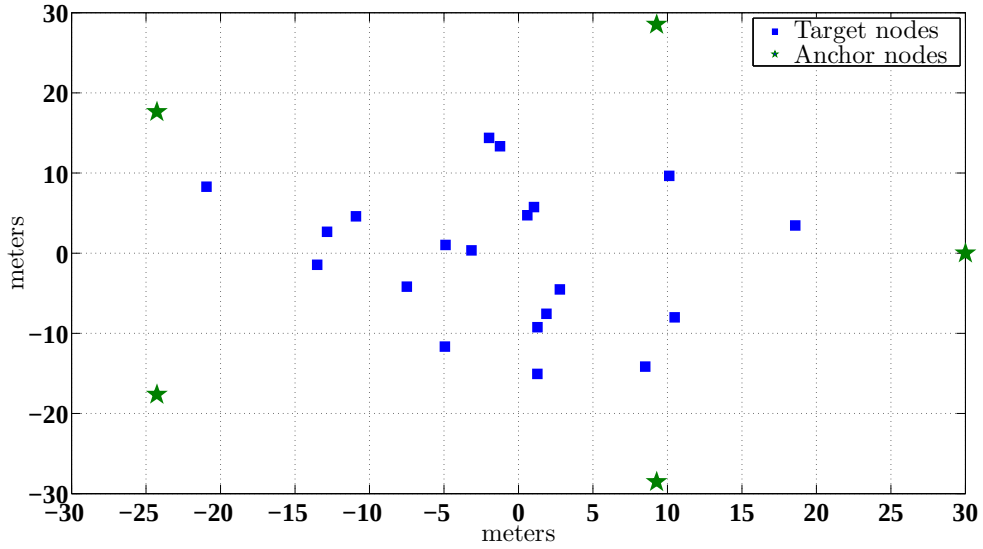

Figure 3.1: Network setup.

and average performance is analyzed. This network is illustrated in Fig. 3.1. Equal noise variance for all ANs i.e. $\sigma_i^2 = \sigma_r^2 = \sigma^2$ is assumed. Where σ_r^2 is the shadowing variance associated with the path-lose estimate of the reference AN. The simulations are run η number of times independently. For this scenario only the LLS-ref approach is used. For the MSE and Bias due to shadowing error only (accurate PLE), (3.20) is used with $\Delta\alpha = 0$.

In Fig. 3.2, the root mean square error (RMSE) of location estimates is compared while increasing the variance in the path-loss estimates σ_i^2. Simulation and theoretical RMSE is plotted for 5, 7 and 9 ANs. The radius (R) of the circular deployment is 50 m and the PLE value is 3. As expected lower RMSE is observed for larger number of ANs. It is also noted that the theoretical analysis accurately predicts the performance of the LLS estimator.

Fig. 3.3 demonstrates the performance of the LLS estimator and the theoretical error analysis for different values of the PLE while other simulation conditions are the same as for Fig. 3.2. It is observed that the performance is improved

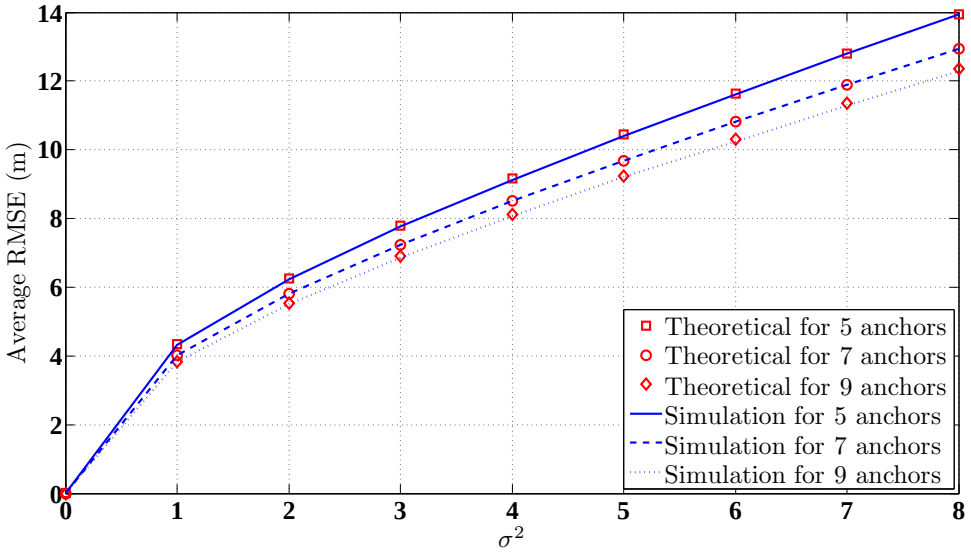

Figure 3.2: Simulation and theoretical RMSE. $\eta = 1000$, $\alpha = 3$, $R = 50$ m.

σ^2	0	1	2	3	4	5
LJE-ref	3.0000	3.0505	3.0981	3.1437	3.1846	3.2203
LJE-avg	3.0000	3.0582	3.1081	3.1541	3.2021	3.2349
LJE-comb	3.0000	3.0555	3.1078	3.1586	3.1979	3.2369

Table 3.1: Average of estimated $\hat{\alpha}$ at different values of noise variance σ^2, actual value $\alpha_0 = 3$.

for large values of the PLE, this improved performance seems encouraging for large PLE values however this could be misleading for real time implementation. The reason is that in real time systems the TN transmits with a finite transmit power, for a larger PLE (and longer distance) the received power at the AN might fall below the detection threshold. However, the system model employed in this chapter does not impose such limitations. Nevertheless, for practical system with high transmit power, larger PLE values could still lead to better accuracy.

In Fig. 3.4, variance σ^2 in the path-loss estimate is kept constant at 5 while the radius is increased from 30 m to 100 m. The results are obtained for 5, 7 and 9 ANs. The theoretical analysis and simulation show large error at longer distances.

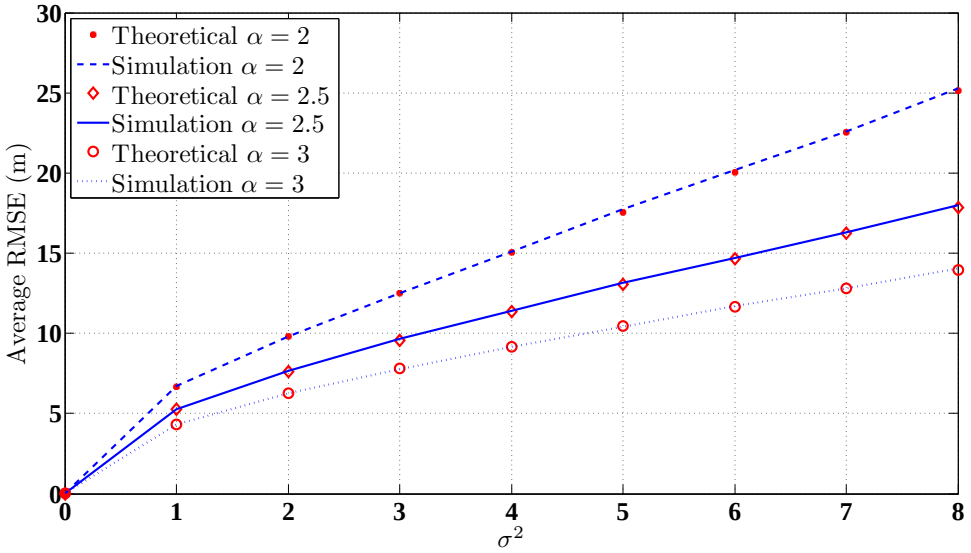

Figure 3.3: Simulation and theoretical RMSE. $\eta = 1000$, $N = 5$, $R = 50$ m.

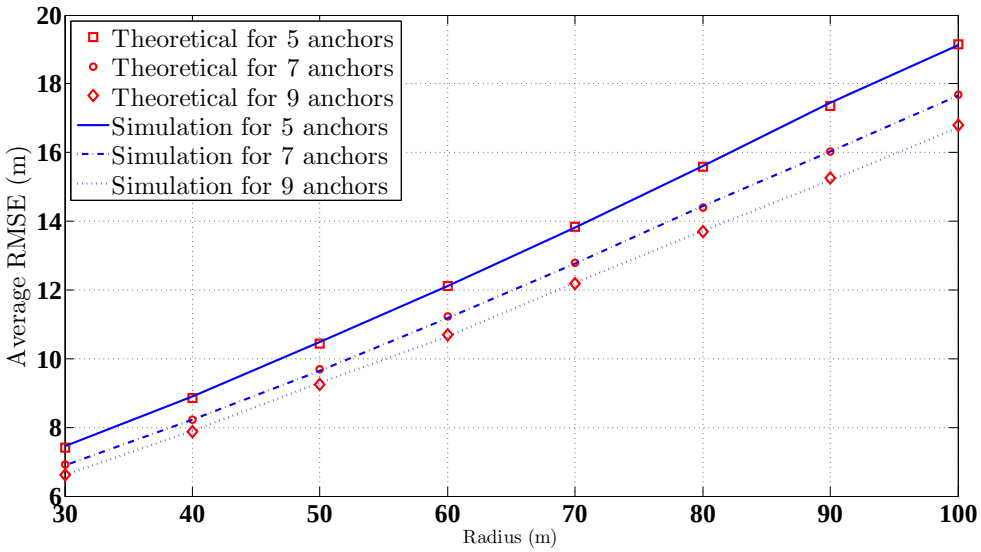

Figure 3.4: Simulation and theoretical RMSE. $\eta = 1000$, $\alpha = 3$, $\sigma^2 = 5$.

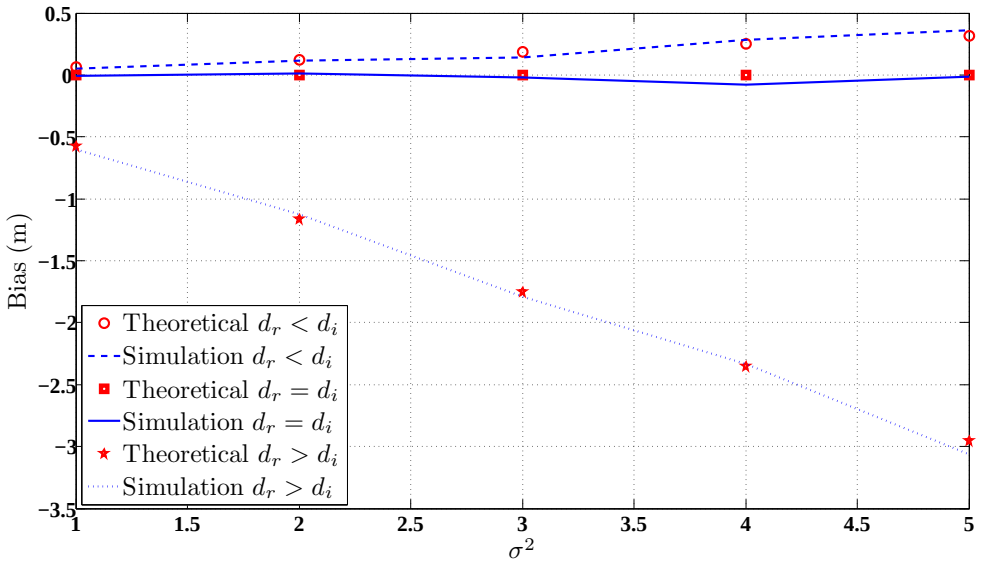

Figure 3.5: Simulation and theoretical bias $\eta = 1000$, $\alpha = 3$, $R = 50$ m.

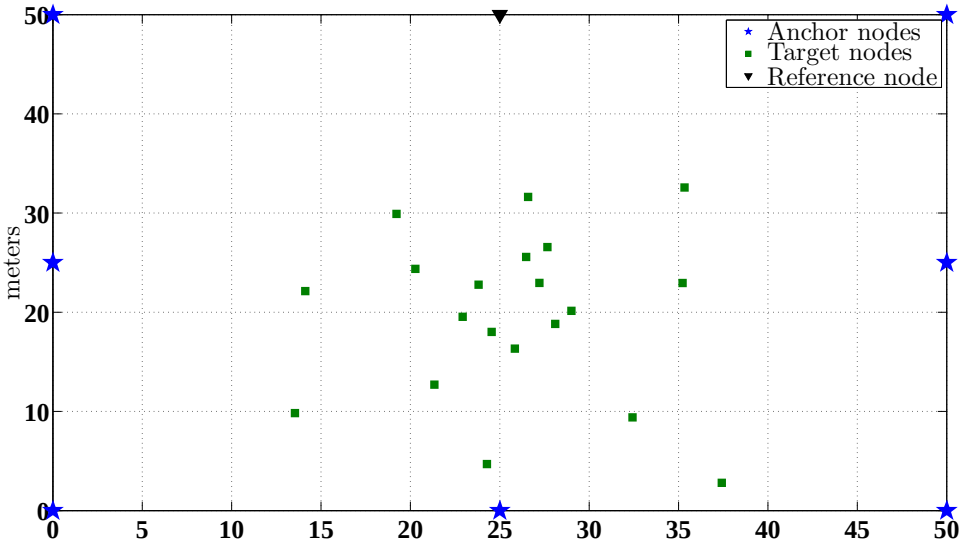

Figure 3.6: Network setup.

Fig. 3.5 illustrates the bias of the LLS estimator and theoretical results. In order to observe the bias, a single TN is considered at the origin (0,0) while 5 ANs are deployed in a circular arrangement with $R = 50$ m. The impact of reference node placement on the bias is seen by first placing the reference AN at equal distance as all other ANs from the TN i.e. $d_r = d_i = 50$ m. In this setup the bias in the estimator and theoretical bias is zero. Second, the reference AN is placed inside the network with $d_r = 10$ m, with this geometry, a positive bias is observed in the simulation and analysis. Finally, the reference AN is placed outside the circular deployment of the AN's at $d_r = 70$ m resulting in substantial negative bias. A negative bias indicates that the biased estimate of the target node is localized towards the negative x or y axis.

3.6.2 Square area with ANs around the edges with incorrect PLE

In the second scenario, a 2-D area with dimensions $50\,\mathrm{m} \times 50\,\mathrm{m}$ is considered with 8 ANs around the edge at $[0, 0], [50, 0], [50, 50], [0, 50], [25, 0], [50, 25], [0, 25],$ $[25, 50]$. Again instead of assuming a single TN, 20 TNs are assumed within the network to observe the average performance. This is illustrated in Fig. 3.6. For the LJE-ref, LLS-ref implementation, $[25, 50]$ is taken as the reference AN. The simulation is executed $\eta = 300$ times independently. Equal noise variance for all $\hat{z}_i$ i.e. $\sigma_i^2 = \sigma^2$ is assumed and the actual value of PLE $\alpha_0 = 3$. The incremental step to estimate $\hat{\alpha}$ in (3.31) is 0.1.

3.6.2.1 Bias of $\hat{\alpha}$

For the network described above, simulations to estimate α are done for 20 TNs. Table 3.1 shows the average of the obtained $\hat{\alpha}$ values for various levels of noise in

the observed $\hat{z}_i$. It is evident that although the estimated values are close to the actual PLE α_0, yet there is a positive bias in the estimates. This bias effects the estimation of the location coordinates and is described in subsection 3.6.2.3.

3.6.2.2 Error analysis

In Fig. 3.7, simulation and error analysis results are shown, error in terms of the RMSE subject to incorrect PLE assumption and noise is given. The error analysis accurately predicts the performance of the estimator (LLS-ref). It is evident that inaccurate PLE assumption can result in substantial error in location estimates. In Fig. 3.8, the bias due to incorrect PLE and noise is shown. It is also observed that comparatively degraded performance in terms of both RMSE and the bias is observed for $\check{\alpha} < \alpha_0$ than for $\check{\alpha} > \alpha_0$. These results confirm the error analysis results obtained in chapter 2 for the ML technique.

3.6.2.3 Performance comparison of LJE and LLS

Fig. 3.9 shows the performance comparison between the variants of LLS and LJE. The RMSE of all estimators is compared while increasing the variance in the path-loss noise. It is observed that there is no considerable performance difference between the three different approaches of LLS. It is also observed that performance of LJE is close to LLS with LJE-avg and LJE-comb performing slightly better than LJE-ref. However, it is also observed that at certain points due to the bias of the LJE in estimating $\hat{\alpha}$, its performance exceeds that of the LLS. This is a counter intuitive phenomenon but is inherent with biased estimators. There is considerable gap between the performance of the estimators and the CRB, the reason for this is discussed in the Chapter 4.

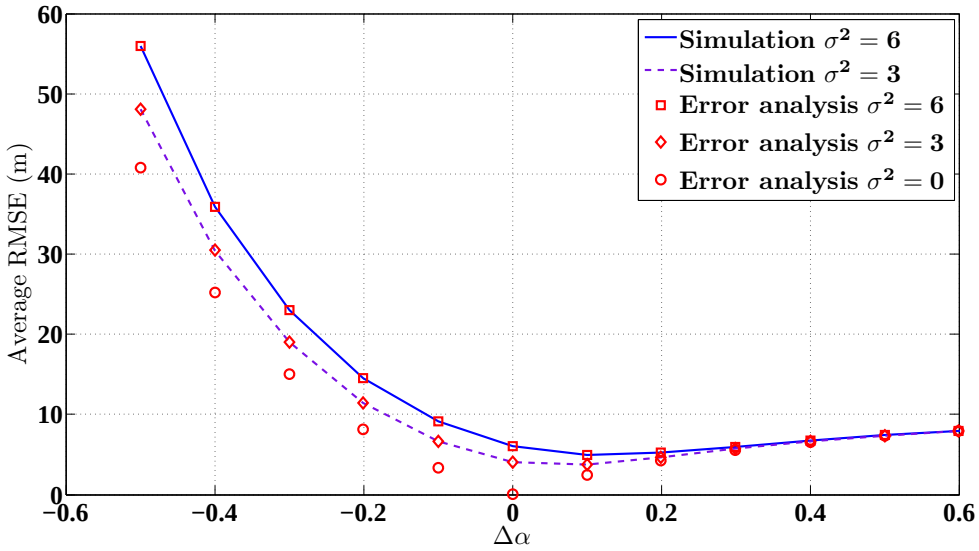

Figure 3.7: Error analysis: RMSE and simulation for incorrect PLE.

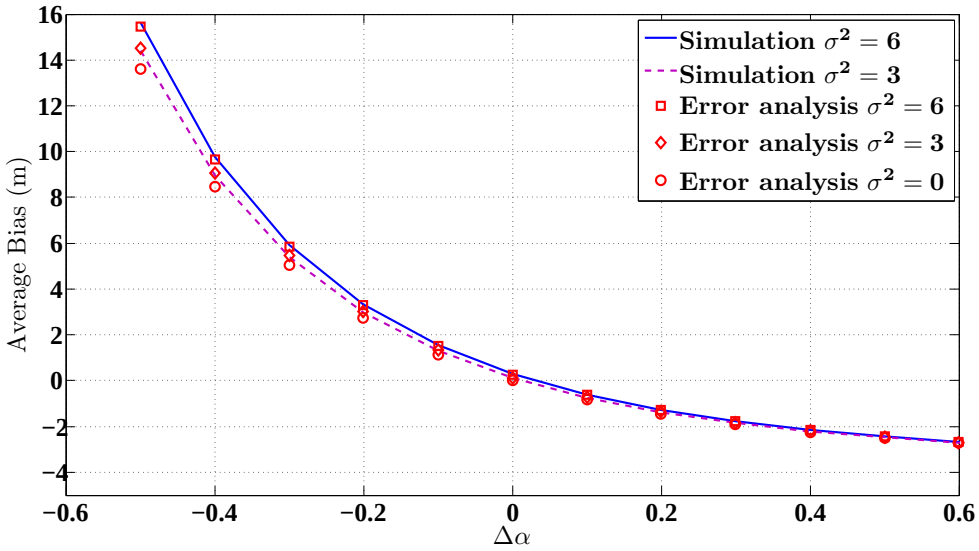

Figure 3.8: Error analysis: Bias and simulation for incorrect PLE.

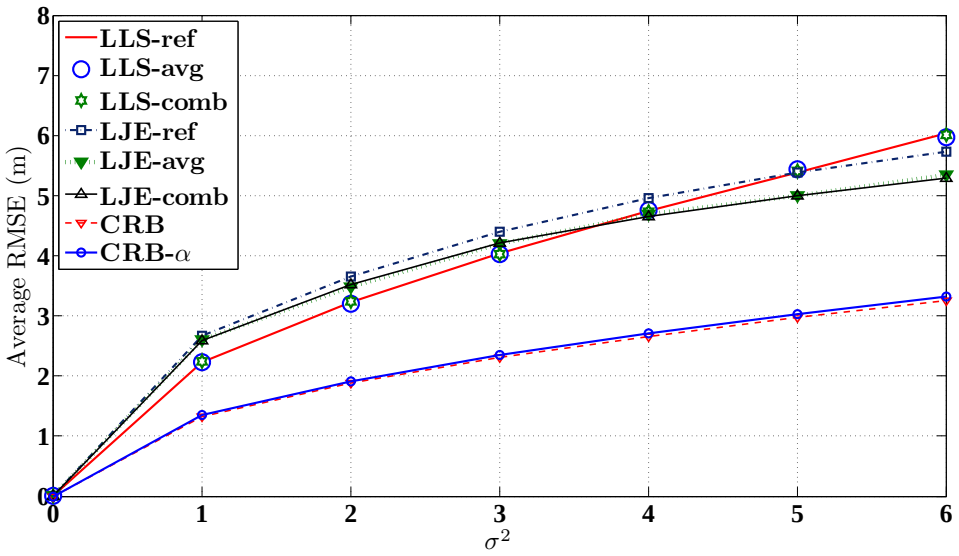

Figure 3.9: Performance comparison between variants of LLS and LJE, the CRB (with known α) and the CRB-α (estimated α).

3.6.2.4 LJE as initial estimate for LCJE

In the simulation shown in the Fig. 3.10, the performance of the LCJE is compared when given a random value as the initial estimate $\boldsymbol{\theta}^1$ and when the estimated value of LJE, $\hat{\boldsymbol{\theta}}_{LJE}$, is selected as $\boldsymbol{\theta}^1$. It is seen that there is considerable performance improvement when $\boldsymbol{\theta}^1 = \hat{\boldsymbol{\theta}}_{LJE}$. Indeed the performance of LCJE with a random $\boldsymbol{\theta}^1$ can be improved by taking more iterations. Nevertheless, it is seen that only with $k = 3$ iterations, for $\boldsymbol{\theta}^1 = \hat{\boldsymbol{\theta}}_{LJE}$ reach near optimal performance. On the other hand, for an arbitrarily chosen initial estimate, there is degraded performance even for $k = 6$ iterations. Thus the advantages of this approach are twofold; i) there is obvious performance improvement in terms of power consumption and computational time taken with smaller number of iterations. ii) the requirement for the selection of a close initial point to avoid convergence to local minima is bypassed.

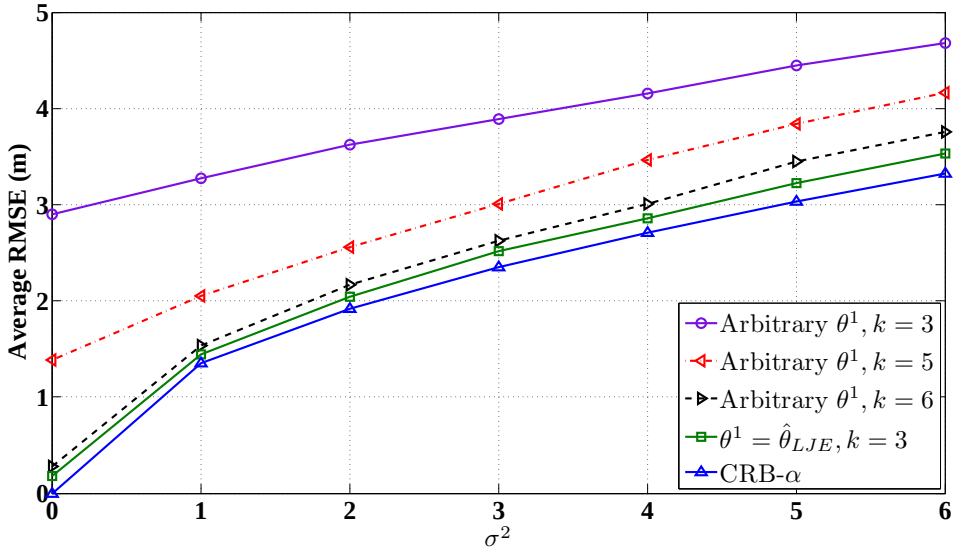

Figure 3.10: Performance of LCJE for arbitrary $\boldsymbol{\theta}^1$and $\boldsymbol{\theta}^1 = \hat{\boldsymbol{\theta}}_{LJE}$.

3.7 Summary

In this chapter, a simplified low complexity RSS based location estimator for unknown path-loss model is proposed. The error analysis for incorrect PLE assumption was done. Based on the linear model, analytical expressions for the RMSE and bias were derived. It was seen via simulation that analysis results accurately predicts the performance of the linear estimator. For correct PLE assumption, the performance of the estimator is unbiased if the TN is at equal distance from all ANs. It was also observed that use of an incorrect PLE has dramatic impact on the accuracy of location estimates. Both the MSE and bias are large for $\check{\alpha} < \alpha_0$ than for $\check{\alpha} > \alpha_0$. Next, a simplistic technique to estimate the PLE by optimizing a single variable function was devised. Simulation results show that this technique has acceptable performance though the estimates are biased. In order to achieve even better accuracy, the LJE results are used as the initial estimate for more computationally intense but optimal algorithm

and showed via simulation that this performs considerably better with a smaller number of iterations in comparison with an arbitrary initial estimate. For future work, the joint estimation of different PLE for each link and the location will be investigated. Furthermore, in such scenario the geometry of ANs and its impact on location accuracy will be studied.

4 Optimising Linear Least Squares Solution to RSS Localisation

The material in this chapter has been published in the paper:

- N. Salman, M. Ghogho, and A. H. Kemp, "Optimized Low Complexity Sensor Node Positioning in Wireless Sensor Networks," *EEE Sensors Journal.,*vol.14, no.1, pp.39,46, Jan. 2014.

4.1 Overview

It was shown in chapter 2 that due to the non-linear nature of the localisation problem, location estimation via RSS (and also for ToA) can be achieved using maximum likelihood (ML) techniques that commonly operate in an iterative fashion. Generally, a close initial estimate of location is required for the ML algorithm. Furthermore, the ML technique due to its iterative nature is high in complexity. On the other hand, location can also be estimated by employing a low complexity linear least squares (LLS) approach as discussed in chapter 3. The LLS technique does not require a close initial estimate and is of low complexity as it does not require multiple iterations. However it was noticed that the LLS technique performs sub-optimally. Hence the LLS technique needs further

optimization to achieve acceptable results. In addition it was also noted from 3.9 that the conventional CRB does not tightly bound the performance of the LLS. Hence a new bound needs to be derived.

In this chapter the performance of the LLS RSS location estimator is analysed and improvement is proposed. The linear model in this chapter is modified to account for different PLEs and noise variance for each link. The basic concept behind the LLS technique is that instead of using individual readings from ANs, readings from AN pairs are first formulated (subtracted from each other) to linearise the non-linear system of equations. Generally, a reference node has to be chosen and paired with all other ANs. However, random selection of an AN as a reference can cause performance degradation. Other techniques to linearise the system include averaging the readings from all ANs and then pairing them with individual AN. Finally, pairing each AN with every other AN can be used for linearisation. The system performance can be optimized by choosing an optimal reference AN and pairing it with all other ANs. In this chapter, a technique for optimal reference AN selection using the RSS signals is devised. In order to further improve the performance, the correlation between the (now linear) RSS readings is used and a weighted least squares (WLS) algorithm is proposed. For optimized performance the optimal AN selection for the WLS method is also given in the chapter.

In order to compare the MSEs of estimators, the Cramer-Rao bound has been extensively used as a benchmark. For ML algorithms, the CRB on location estimated has been derived for ToA in [45, 46] and for RSS systems in [18]. However, since the LLS method is not based on individual readings, the CRB given in [18] does not tightly bound the performance of the LLS-RSS estimator. For ToA LLS technique the CRB is given in [44]. The ToA linear CRB in [44] does not lower bound the performance of the RSS system due to different signal and noise model. In this chapter, the linear CRB is derived to tightly bound the

performance of the LLS and WLS algorithm based on RSS range estimation.

To sum up, the main contributions of this chapter are as follows:

- WLS algorithm for the linear model is proposed.
- Optimal anchor selection for both LLS and WLS methods is proposed.
- Linear CRB for RSS systems is derived.

Simulation results show that the linear CRB is significantly larger than the exact CRB and is thus more realistic in lower bounding the performance of RSS systems using the linear model. It is shown via simulations that the performance of the LLS estimator improves considerably when the optimal reference AN is used. The system performance is further improved using the WLS algorithm with optimal AN selection.

The rest of the chapter is organized as follows. Section 4.2 presents the problem statement and the system model. In section 4.3, the modified linear RSS model and the LLS solution is presented. In section 4.4, the WLS algorithm is proposed. In section 4.5, the optimal reference AN selection technique is presented. In section 4.6, linear CRB is derived. Finally, in section 4.7, the simulation results are discussed which are followed by conclusions.

4.2 System Model

Unless otherwise specified, same notations as in chapter 2 are used in this chapter. The signal model (before linearisation) is similar to that in chapter 2, with a different PLE α_i used for each anchor now. The signal model will be rewritten here for easy understanding.

A two dimensional (2-D) network is considered, consisting of a TN which has unknown coordinates $\boldsymbol{\theta} = [x, y]^T$ ($\boldsymbol{\theta} \in \mathscr{R}^2$) that are to be estimated, and M ANs

with known locations $\boldsymbol{\theta}_i = [x_i, y_i]^T (\boldsymbol{\theta}_i \in \mathscr{R}^2)$ for $i = 1, ..., M$. The received power at the ANs due to random shadowing is log-normally distributed. This model is based on empirical results obtained in [36, 37]. Thus the distance d_i between the TN and the i^{th} AN, is related to the path-loss at the i^{th} AN, $\mathscr{L}_i$, and the PLE, α_i, as [35]

$$\mathscr{L}_i = \mathscr{L}_0 + 10\alpha_i \log_{10} d_i + w_i, \tag{4.1}$$

where $\mathscr{L}_0$ is the path-loss at the reference distance d_0 ($d_0 < d_i$, and is normally taken as 1 m) and w_i is a zero-mean Gaussian random variable with known variance representing the log-normal shadowing effect, i.e. $w_i \sim (\mathcal{N}(0, \sigma_i^2))$. The PLEs are assumed to be known via prior channel modelling or accurate estimation [32]. The path-loss is calculated as

$$\mathscr{L}_i = 10 \log_{10} P_t - 10 \log_{10} P_i \tag{4.2}$$

where P_t is the transmit power at the TN and P_i is the received power at the i^{th} AN. The distance d_i is given by

$$d_i = \sqrt{(x - x_i)^2 + (y - y_i)^2}. \tag{4.3}$$

The observed path-loss (in dB) from d_0 to d_i, $z_i = \mathscr{L}_i - \mathscr{L}_0$, can be expressed as

$$z_i = f_i(\boldsymbol{\theta}) + w_i, \qquad i = 1, ..., M \tag{4.4}$$

where $f_i(\boldsymbol{\theta}) = \gamma \alpha_i \ln d_i$ and $\gamma = \frac{10}{\ln 10}$. In a vector form,

$$\mathbf{z} = \mathbf{f}(\boldsymbol{\theta}) + \mathbf{w}, \tag{4.5}$$

where $\mathbf{z} = [z_1, ..., z_M]^T$ is the vector of the observed path loss.

$\mathbf{f}(\boldsymbol{\theta}) = [f_1(\boldsymbol{\theta}), ..., f_M(\boldsymbol{\theta})]^T$is the actual path-loss vector and $\mathbf{w} = [w_1, ..., w_M]^T$ is the noise vector.

Since the noise is Gaussian and assuming independence of the noise components, the joint conditional probability density function (pdf) of $\mathbf{z}$ is given by

$$p(\mathbf{z} \mid \boldsymbol{\theta}) = \prod_{i=1}^{M} \frac{1}{\sqrt{2\pi\sigma_i^2}} \exp\left\{-\frac{(z_i - f_i(\boldsymbol{\theta}))^2}{2\sigma_i^2}\right\}. \tag{4.6}$$

Thus, the maximum likelihood (ML) estimate of (4.6) is equivalent to the non-linear least square (NLS) solution of the cost function

$$\varepsilon(\boldsymbol{\theta}) = (\mathbf{z} - \mathbf{f}(\boldsymbol{\theta}))^T (\mathbf{z} - \mathbf{f}(\boldsymbol{\theta})). \tag{4.7}$$

The solution to (4.7) is obtained using high complexity iterative techniques such as the Gauss-Newton (GN) or Levenberg-Marquardt (LM) techniques. Due to its iterative nature, the ML techniques can converge to local minimum instead of global minimum if given an initial seed that is far from the actual node location. Hence a close initial guess is essential to the reliability of the ML technique. In addition to the high complexity of the ML method, it can suffer from various other challenging issues detailed in [40].

In order to bypass the close initial estimate requirement and high complexity of the ML method, location coordinates can be estimated using a low complexity LLS technique explained in the next section.

4.3 Modified Linear Model

The idea behind the LLS is to first linearise the RSS measurements and then use ordinary least squares (OLS) to estimate the unknown parameters. This idea was first introduced for ToA systems in [43] and analysed for the same in

[44]. However, for RSS measurements the linearisation is somewhat different due to additional parameters such as the PLEs. The non-linear system of path-loss equations can be linearised as follows. From (4.4), it can be readily shown that

$$E\left(\frac{1}{\beta_i}\exp\left(\frac{2z_i}{\gamma\alpha_i}\right)\right) = d_i^2, \tag{4.8}$$

where $\beta_i = \exp\left(\frac{2\sigma_i^2}{(\gamma\alpha_i)^2}\right)$. Similarly choosing a reference AN, it can be shown

$$E\left(\frac{1}{\beta_r}\exp\left(\frac{2z_r}{\gamma\alpha_r}\right)\right) = d_r^2, \tag{4.9}$$

where $\beta_r = \exp\left(\frac{2\sigma_r^2}{(\gamma\alpha_r)^2}\right)$.

Proof Proof of (4.8) is presented here, proof of (4.9) is similar.

$$E\left[\frac{1}{\beta_i}\exp\left(\frac{2z_i}{\gamma\alpha_i}\right)\right] = \frac{1}{\beta_i}\int\left(\exp\left(\frac{2z_i}{\gamma\alpha_i}\right)\right)\frac{1}{\sigma_i^2\sqrt{2\pi}}\exp\left(-\frac{\left(z_i - f_i\left(\boldsymbol{\theta}\right)\right)^2}{2\sigma_i^2}\right)dz_i$$

$$= \frac{1}{\beta_i}\int\frac{1}{\sigma_i^2\sqrt{2\pi}}\exp\left\{-\left(\frac{z_i^2 + f_i^2\left(\boldsymbol{\theta}\right) - 2z_i f_i\left(\boldsymbol{\theta}\right)}{2\sigma_i^2}\right) + \left(\frac{2z_i}{\gamma\alpha_i}\right)\right\}dz_i.$$

By completing squares method,

$$= \frac{1}{\beta_i}\int \frac{1}{\sigma_i^2\sqrt{2\pi}} \exp\left\{ -\left(\frac{z_i^2 + f_i^2(\boldsymbol{\theta}) - 2z_i f_i(\boldsymbol{\theta}) - 2\left(\frac{2\sigma_i^2}{(\gamma\alpha_i)}\right) z_i + \left(\frac{2\sigma_i^2}{(\gamma\alpha_i)}\right)^2 + 2\left(\frac{2\sigma_i^2}{(\gamma\alpha_i)}\right) f_i(\boldsymbol{\theta})}{2\sigma_i^2} \right) \right\}$$
$$\exp\left(\frac{\left(\frac{2\sigma_i^2}{(\gamma\alpha_i)}\right)^2 + 2\left(\frac{2\sigma_i^2}{(\gamma\alpha_i)}\right) f_i(\boldsymbol{\theta})}{2\sigma_i^2} \right) dz_i.$$

$$= \frac{1}{\beta_i}\int \frac{1}{\sigma_i^2\sqrt{2\pi}} \exp - \left(\frac{\left(z_i - f_i(\boldsymbol{\theta}) - \frac{2\sigma_i^2}{(\gamma\alpha_i)}\right)^2}{2\sigma_i^2} \right) \exp\left(\frac{\left(\frac{2\sigma_i^2}{(\gamma\alpha_i)}\right)^2 + 2\left(\frac{2\sigma_i^2}{(\gamma\alpha_i)}\right) f_i(\boldsymbol{\theta})}{2\sigma_i^2} \right) dz_i. \tag{4.10}$$

The first part of the (4.10) is a pdf and its integral is equal 1. Thus we have

$$E\left[\frac{1}{\beta_i}\exp\left(\frac{2z_i}{\gamma\alpha_i}\right)\right] = \frac{1}{\beta_i}\exp\left(\frac{\left(\frac{2\sigma_i^2}{(\gamma\alpha_i)}\right)^2 + 2\left(\frac{2\sigma_i^2}{(\gamma\alpha_i)}\right) f_i(\boldsymbol{\theta})}{2\sigma_i^2} \right)$$
$$= \frac{1}{\beta_i}\exp\left(\frac{2\sigma_i^2}{(\gamma\alpha_i)^2}\right)\exp(2\ln d_i)$$
$$= d_i^2$$

For linearisation, the square of each distance equation is subtracted from the square of a reference distance equation d_r^2. This results in a linear system which is represented in matrix form as

$$\mathbf{b} = \mathbf{A}\boldsymbol{\theta} + \mathbf{v}, \tag{4.11}$$

where $\mathbf{b} = [b_1, ..., b_N]^T$, is the observation vector and is given by

$$\mathbf{b} = \begin{bmatrix} \bar{\delta}_r - \bar{\delta}_1 - \varphi_r + \varphi_1 \\ \bar{\delta}_r - \bar{\delta}_2 - \varphi_r + \varphi_2 \\ \vdots \\ \bar{\delta}_r - \bar{\delta}_N - \varphi_r + \varphi_N \end{bmatrix} \tag{4.12}$$

for $\bar{\delta}_r = \frac{1}{\beta_r} \exp\left(\frac{2z_r}{\gamma\alpha_r}\right)$ and $\bar{\delta}_i = \frac{1}{\beta_i} \exp\left(\frac{2z_i}{\gamma\alpha_i}\right)$. While

$$\varphi_r = x_r^2 + y_r^2 \text{ and } \varphi_i = x_i^2 + y_i^2$$

for $i \neq r$, $i = 1, ..., N$ and $N = M - 1$ and $\mathbf{A}$ is the $N \times 2$ data matrix

$$\mathbf{A} = 2 \begin{bmatrix} x_1 - x_r & y_1 - y_r \\ x_2 - x_r & y_2 - y_r \\ \vdots & \vdots \\ x_N - x_r & y_N - y_r \end{bmatrix}. \tag{4.13}$$

$\mathbf{v}$ is the noise vector which has zero mean and variance given by

$$\breve{\sigma} = E\left[\left(\bar{\delta}_r - \bar{\delta}_i - d_r^2 + d_i^2\right)^2\right]$$

$$= d_i^4 \exp\left(\frac{4\sigma_i^2}{(\gamma\alpha_i)^2}\right) - d_i^4 + d_r^4 \exp\left(\frac{4\sigma_r^2}{(\gamma\alpha_r)^2}\right) - d_r^4 \tag{4.14}$$

and covariance

$$E\left[\left(\bar{\delta}_r - \bar{\delta}_i - d_r^2 + d_i^2\right)\left(\bar{\delta}_r - \bar{\delta}_j - d_r^2 + d_j^2\right)\right]$$

$$= \left\{ d_r^4 \exp\left(\frac{4\sigma_r^2}{(\gamma\alpha_r)^2}\right) - d_r^4 \right\}. \tag{4.15}$$

The solution to the LLS problem is obtained by minimizing the cost function

$$\varepsilon_{LLS}(\boldsymbol{\theta}) = (\mathbf{b} - \mathbf{A}\boldsymbol{\theta})^T (\mathbf{b} - \mathbf{A}\boldsymbol{\theta}) \tag{4.16}$$

and is given as [39]

$$\hat{\boldsymbol{\theta}}_{LLS} = \mathbf{A}^{\dagger}\mathbf{b}, \tag{4.17}$$

where $\mathbf{A}^{\dagger}$ is Moore–Penrose pseudoinverse i.e. $\mathbf{A}^{\dagger} = (\mathbf{A}^T\mathbf{A})^{-1}\mathbf{A}^T$. The LLS can be implemented in three different ways:

4.3.1 LLS-ref

In this implementation, d_r is the distance of the TN from a reference AN as shown above.

4.3.2 LLS-avg

Instead of choosing a reference distance, d_r is taken as the average of all distances from the ANs. Thus in this case, $d_r^2 = \frac{1}{M}\sum_{i=1}^{M} d_i^2$.

4.3.3 LLS-comb

In this case, combination of all pairs of ANs is considered and subtracted from each other. This results in $M\left(\frac{M-1}{2}\right)$ equations. This technique is studied for the

ToA case in [47]. The elements of data matrix $\mathbf{A}$ are now given by

$$\mathbf{A} = 2 \begin{bmatrix} x_1 - x_2 & y_1 - y_2 \\ \vdots & \vdots \\ x_1 - x_N & y_1 - y_N \\ x_2 - x_3 & y_2 - y_3 \\ \vdots & \vdots \\ x_{N-1} - x_N & y_{N-1} - y_N \end{bmatrix}. \tag{4.18}$$

Similarly element of vector $\mathbf{b}$ are given as $\mathbf{b}_{ij} = \left[\bar{\delta}_i - \bar{\delta}_j - \varphi_i + \varphi_j \right]$ for $i, j = 1, ..., M$ and $i < j$. It should be noted that the number of equations increase considerably for a large number of ANs. Hence LLS-comb is not favourable for large a number of ANs.

The performance of all variants of the LLS algorithm are compared in the simulation section.

4.4 Weighted Least Squares Algorithm

For the LLS solution obtained in (4.17), no knowledge about the reliability of each measurement is used. If this information is present, links that are more reliable are given more weight than others. Thus utilizing the information present in the covariance matrix, a weighted least square (WLS) algorithm is proposed in this section.

For a given covariance matrix $\mathbf{C}(\boldsymbol{\theta})$ the WLS solution is obtained by minimizing the cost function

$$\varepsilon_{WLS}(\boldsymbol{\theta}) = (\mathbf{b} - \mathbf{A}\boldsymbol{\theta})^T \mathbf{C}(\boldsymbol{\theta})^{-1} (\mathbf{b} - \mathbf{A}\boldsymbol{\theta}), \tag{4.19}$$

where the elements of $\mathbf{C}(\boldsymbol{\theta})$ are given by (4.14) and (4.15). It is however noted that the elements of the $\mathbf{C}(\boldsymbol{\theta})$ are dependent on the actual distance of the target node from the anchors, which is unknown, hence the estimated distance is used to estimate the covariance matrix $\mathbf{C}\left(\hat{\boldsymbol{\theta}}\right)$. The WLS estimate is obtained as follows

$$\hat{\boldsymbol{\theta}}_{WLS} = \mathbf{A}^{\ddagger}\mathbf{b}^{\ddagger}, \tag{4.20}$$

where $\mathbf{A}^{\ddagger} = \left\{\mathbf{A}^{T}\left[\mathbf{C}\left(\hat{\boldsymbol{\theta}}\right)\right]^{-1}\mathbf{A}\right\}^{-1}\mathbf{A}^{T}$ and $\mathbf{b}^{\ddagger} = \left[\mathbf{C}\left(\hat{\boldsymbol{\theta}}\right)\right]^{-1}\mathbf{b}$.

It is noted that similar to LLS, the WLS algorithm can also be implemented in three different modes i.e. WLS-ref, WLS-avg and WLS-comb. It is however seen that the covariance matrix is different for the three implementations. For WLS-ref, the diagonal and non diagonal terms of $\mathbf{C}(\boldsymbol{\theta})$ are given by (4.14) and (4.15). For WLS-avg, where the reference anchor is the mean of all anchors, the $M \times M$ covariance matrix is given below.

$$\begin{aligned}\mathbf{C}(\boldsymbol{\theta}) = \\ \operatorname{diag}\left\{d_1^4 \exp\left(\tfrac{4\sigma_1^2}{(\gamma\alpha_1)^2}\right) - d_1^4 +, ..., + d_N^4 \exp\left(\tfrac{4\sigma_N^2}{(\gamma\alpha_N)^2}\right) - d_N^4\right\} \\ + \mathbf{1}_{M\times M}\left\{\overline{d}_r^4 \exp\left(\frac{4\overline{\sigma}_r^2}{(\gamma\overline{\alpha}_r)^2}\right) - \overline{d}_r^4\right\},\end{aligned} \tag{4.21}$$

where

$$\overline{d}_r^4 = \frac{1}{M}\sum_{i=1}^{M} d_i^4, \tag{4.22}$$

$$\overline{\sigma}_r^2 = \frac{1}{M}\sum_{i=1}^{M} \sigma_i^2 \tag{4.23}$$

and

$$\overline{\alpha}_r = \frac{1}{M}\sum_{i=1}^{M}\alpha_i, \tag{4.24}$$

where $\mathbf{1}_{M\times M}$ represents the $(M \times M)$ matrix of all ones.

For the WLS-comb, development of the $\left(\frac{M^2-M}{2}\right) \times \left(\frac{M^2-M}{2}\right)$ covariance matrix becomes slightly complicated. As for WLS-ref and WLS-avg, the non-diagonal elements are the same, however this does not hold for WLS-comb for which the diagonal terms are given as

$$\tilde{\sigma}_i^2 = E\left[\left(\bar{\delta}_i - \bar{\delta}_j - d_i^2 + d_j^2\right)^2\right]$$

$$= d_i^4 \exp\left(\frac{4\sigma_i^2}{(\gamma\alpha_i)^2}\right) - d_i^4 + d_j^4 \exp\left(\frac{4\sigma_j^2}{(\gamma\alpha_j)^2}\right) - d_j^4, \tag{4.25}$$

for $i, j = 1, ..., M \quad$ and $i < j$.

Conversely, the non-diagonal terms are given by

$$E\left[\left(\bar{\delta}_i - \bar{\delta}_j - d_i^2 + d_j^2\right)\left(\bar{\delta}_k - \bar{\delta}_l - d_k^2 + d_l^2\right)\right] =$$

$$\begin{cases} \left\{d_i^4 \exp\left(\frac{4\sigma_i^2}{(\gamma\alpha_i)^2}\right) - d_i^4\right\} & \text{for } i = k \\ \left\{d_j^4 \exp\left(\frac{4\sigma_j^2}{(\gamma\alpha_j)^2}\right) - d_j^4\right\} & \text{for } i = k \\ -\left\{d_i^4 \exp\left(\frac{4\sigma_i^2}{(\gamma\alpha_i)^2}\right) - d_i^4\right\} & \text{for } i = l \\ -\left\{d_j^4 \exp\left(\frac{4\sigma_j^2}{(\gamma\alpha_j)^2}\right) - d_j^4\right\} & \text{for } j = k \\ 0 & \text{for } i \neq l \text{ and } j \neq k \end{cases}$$

for $i, j = 1, ..., M \quad$ and $i < j$

and $k, l = 1, ..., M \quad$ and $k < l$.

$$\left\{E\left(\mathbf{b}\mathbf{b}^T\right)\right\}_{ii} = \varphi_r^2 + \varphi_i^2 + \frac{d_r^4}{\beta_r^2}\exp\left(\frac{8\sigma_r^2}{(\gamma\alpha_r)^2}\right) + \frac{d_i^4}{\beta_i^2}\exp\left(\frac{8\sigma_i^2}{(\gamma\alpha_i)^2}\right) - \frac{2d_r^2}{\beta_r}\exp\left(\frac{2\sigma_r^2}{(\gamma\alpha_r)^2}\right) - \frac{2d_i^2}{\beta_i}\exp\left(\frac{2\sigma_i^2}{(\gamma\alpha_i)^2}\right) - 2\varphi_r\varphi_i - \frac{2d_i^2 d_r^2}{\beta_i\beta_r}\exp\left(\frac{2\sigma_r^2}{(\gamma\alpha_r)^2}\right)\exp\left(\frac{2\sigma_i^2}{(\gamma\alpha_i)^2}\right) + \frac{2d_r^2\varphi_i}{\beta_r}\exp\left(\frac{2\sigma_r^2}{(\gamma\alpha_r)^2}\right) + \frac{2d_i^2\varphi_r}{\beta_i}\exp\left(\frac{2\sigma_i^2}{(\gamma\alpha_i)^2}\right). \tag{4.28}$$

4.5 Optimal Reference Anchor Node Selection

Generally, the performance of LLS-avg and LLS-comb is slightly better than LLS-ref implementation due to the averaging effect of all ANs. Similarly, the performance of WLS-avg and WLS-comb is better than WLS-ref. However, in its basic form, LLS/WLS-ref randomly selects a reference AN. This could at times lead to degraded system performance as the accuracy of the location estimate depends on factors such as the true distance d_r from the TN, shadowing noise variance σ_r^2 and the PLE α_r of a particular reference AN. In this section, a technique to select the optimal reference AN is proposed. The optimal reference AN is chosen to be the AN that minimizes the MSE of the location estimates. Thus

$$\boldsymbol{\theta}_{i_{opt}} = \arg\min_{\boldsymbol{\theta_i}}\left(MSE\right). \tag{4.26}$$

where

$$MSE\left(\hat{\boldsymbol{\theta}}\right) = Tr\left\{E\left[\left(\hat{\boldsymbol{\theta}} - \boldsymbol{\theta}_0\right)\left(\hat{\boldsymbol{\theta}} - \boldsymbol{\theta}_0\right)^T\right]\right\}, \tag{4.27}$$

where $\hat{\boldsymbol{\theta}}$ is the estimated location via LLS or WLS and $\boldsymbol{\theta}_0$ is the true location coordinates. The theoretical MSE is given for the LLS and WLS algorithm in the following subsections.

$$\left\{E\left(\mathbf{b}\mathbf{b}^T\right)\right\}_{ij} = \varphi_r^2 + \frac{d_r^4}{\beta_r^2}\exp\left(\frac{8\sigma_r^2}{(\gamma\alpha_r)^2}\right) - \frac{d_j^2 d_r^2}{\beta_j\beta_r}\exp\left(\frac{2\sigma_j^2}{(\gamma\alpha_j)^2}\right)\exp\left(\frac{2\sigma_r^2}{(\gamma\alpha_r)^2}\right) - \frac{d_i^2 d_r^2}{\beta_i\beta_r}\exp\left(\frac{2\sigma_i^2}{(\gamma\alpha_i)^2}\right)\exp\left(\frac{2\sigma_r^2}{(\gamma\alpha_r)^2}\right) + \frac{d_i^2 d_j^2}{\beta_i\beta_j}\exp\left(\frac{2\sigma_i^2}{(\gamma\alpha_i)^2}\right)\exp\left(\frac{2\sigma_j^2}{(\gamma\alpha_j)^2}\right) - \frac{2d_r^2\varphi_r}{\beta_r}\exp\left(\frac{2\sigma_r^2}{(\gamma\alpha_r)^2}\right) + \frac{d_r^2\varphi_j}{\beta_r}\exp\left(\frac{2\sigma_r^2}{(\gamma\alpha_r)^2}\right) + \frac{d_j^2\varphi_r}{\beta_j}\exp\left(\frac{2\sigma_j^2}{(\gamma\alpha_j)^2}\right) + \frac{d_r^2\varphi_i}{\beta_r}\exp\left(\frac{2\sigma_r^2}{(\gamma\alpha_r)^2}\right) + \frac{d_i^2\varphi_r}{\beta_i}\exp\left(\frac{2\sigma_i^2}{(\gamma\alpha_i)^2}\right) - \frac{d_i^2\varphi_j}{\beta_i}\exp\left(\frac{2\sigma_i^2}{(\gamma\alpha_i)^2}\right) - \frac{d_j^2\varphi}{\beta_j}\exp\left(\frac{2\sigma_j^2}{(\gamma\alpha_j)^2}\right) - \varphi_r\varphi_i - \varphi_r\varphi_j + \varphi_i\varphi_j. \tag{4.29}$$

Theoretical MSE for LLS

For LLS, the estimated location $\hat{\boldsymbol{\theta}}$ is given by $\hat{\boldsymbol{\theta}}_{LLS} = \mathbf{A}^{\dagger}\mathbf{b}$ while $\boldsymbol{\theta}_0$ can be represented by $\boldsymbol{\theta}_0 = \mathbf{A}^{\dagger}\mathbf{b}_0$, where $\mathbf{b}_0$ represents the noise free observation vector and is given by

$$\mathbf{b}_0 = \begin{bmatrix} d_r^2 - d_1^2 - \varphi_r + \varphi_1 \\ d_r^2 - d_2^2 - \varphi_r + \varphi_2 \\ \vdots \\ d_r^2 - d_2^2 - \varphi_r + \varphi_N \end{bmatrix}.$$

Putting elements of $\hat{\boldsymbol{\theta}}_{LLS}$ and $\boldsymbol{\theta}_0$ in (4.27) and after some manipulation, it follows

$$MSE\left(\hat{\boldsymbol{\theta}}_{LLS}\right) = Tr\left\{\mathbf{A}^{\dagger}\mathbf{K}\left(\mathbf{A}^{\dagger}\right)^T\right\}, \tag{4.30}$$

where

$$\mathbf{K} = E\left(\mathbf{b}\mathbf{b}^T\right) - 2E\left(\mathbf{b}\right)\mathbf{b}_0^T + \mathbf{b}_0\mathbf{b}_0^T \tag{4.31}$$

where $E\left(\mathbf{b}\right) = \mathbf{b}_0$. The diagonal and off diagonal elements of $E\left(\mathbf{b}\mathbf{b}^T\right)$ are given

by (4.28) and (4.29) respectively.

Theoretical MSE for WLS

For the MSE of the WLS algorithm the estimated $\hat{\boldsymbol{\theta}}_{WLS}$ (4.20) is used in (4.27) to obtain the following MSE expression

$$MSE\left(\hat{\boldsymbol{\theta}}_{WLS}\right) = Tr\Bigg\{\left[\mathbf{A}^{\ddagger}\mathbf{C}\left(\boldsymbol{\theta}\right)^{-1}E\left(\mathbf{b}\mathbf{b}^{T}\right)\left[\mathbf{C}\left(\boldsymbol{\theta}\right)^{-1}\right]^{T}\left(\mathbf{A}^{\ddagger}\right)^{T}\right] - 2\left[\mathbf{A}^{\ddagger}\mathbf{C}\left(\boldsymbol{\theta}\right)^{-1}\mathbf{b}_0\mathbf{b}_0^{T}\left(\mathbf{A}^{\dagger}\right)^{T}\right] + \left[\mathbf{A}^{\dagger}\mathbf{b}_0\mathbf{b}_0^{T}\left(\mathbf{A}^{\dagger}\right)^{T}\right]\Bigg\}. \quad (4.32)$$

It is noted that the theoretical MSE depends on the actual distances which are unknown, hence their estimates are used to estimate the MSE in (4.30) and (4.32). Once the optimal AN is selected, it is used again in the LLS solution (4.17) or WLS solution (4.20) to provide the final estimate of the TN location. This will be referred to as LLS-opt and WLS-opt respectively.

The following results were obtained via simulations.

Case 1. Equal PLEs and equal distances In case of equal PLEs and equal distances of the TN from all ANs i.e. $\alpha_i = \alpha$, $d_i = d \; \forall \; i$, the AN with the smallest noise variance σ_i^2 is selected as the reference AN.

Case 2. Equal PLEs and equal noise variance For equal PLEs and equal noise variance from all ANs i.e. $\alpha_i = \alpha$, $\sigma_i^2 = \sigma^2 \; \forall i$, the AN with the shortest distance d_i from the TN is selected as the reference AN.

Case 3. Equal distance and equal noise variance For equal noise variance and equal distances of the TN from all ANs i.e. $\sigma_i^2 = \sigma^2$, $d_i = d \,\forall\, i$, the AN with the largest PLE α_i is chosen as the reference AN. Choosing reference AN with the largest PLE might seem counter intuitive, however if the PLE is reduced to zero, then no distance information can be extracted. Since, we do not consider a lower receiver threshold power in the signal model, hence a larger PLE will give us better performance and hence the AN with largest PLE is considered as the reference AN.

4.6 Performance Bound

The CRB lower bounds the MSE performance of any unbiased estimator. For 2-D TN location, the CRB on the estimation MSE is given by

$$MSE\left(\hat{\boldsymbol{\theta}}\right) \geq \frac{\left[\mathbf{I}\left(\boldsymbol{\theta}\right)\right]_{11} + \left[\mathbf{I}\left(\boldsymbol{\theta}\right)\right]_{22}}{\det\left[\mathbf{I}\left(\boldsymbol{\theta}\right)\right]}, \tag{4.33}$$

where $[\mathbf{I}(\boldsymbol{\theta})]$ is the Fisher information matrix (FIM), and its elements are given by [39]

$$\left[\mathbf{I}\left(\boldsymbol{\theta}\right)\right]_{ij} = -E\left[\frac{\partial^2 \ln p\left(\mathbf{z} \mid \boldsymbol{\theta}\right)}{\partial \boldsymbol{\theta}_i \partial \boldsymbol{\theta}_j}\right]. \tag{4.34}$$

To lower bound the ML algorithms, the elements of the FIM are given by

$$\left[\mathbf{I}\left(\boldsymbol{\theta}\right)\right] = \begin{bmatrix} \sum_{i=1}^{M} \frac{\gamma^2 \alpha_i^2 (x-x_i)^2}{d_i^4 \sigma_i^2} & \sum_{i=1}^{M} \frac{\gamma^2 \alpha_i^2 (x-x_i)(y-y_i)}{d_i^4 \sigma_i^2} \\ \sum_{i=1}^{M} \frac{\gamma^2 \alpha_i^2 (x-x_i)(y-y_i)}{d_i^4 \sigma_i^2} & \sum_{i=1}^{M} \frac{\gamma^2 \alpha_i^2 (y-y_i)^2}{d_i^4 \sigma_i^2} \end{bmatrix}. \tag{4.35}$$

The CRB as obtained from the FIM in (4.35) only tightly bounds the performance

of ML type algorithms. Since the LLS method is different from the ML approach, the exact CRB for RSS-based localisation in [18] does not accurately predict the performance of estimators based on the linear model. Unlike the conventional CRB, which is based on the observations taken from individual ANs, the linear CRB is based on the observations

$$p_i = \frac{1}{\beta_r} \exp\left(\frac{2z_r}{\gamma\alpha_r}\right) - \frac{1}{\beta_i} \exp\left(\frac{2z_i}{\gamma\alpha_i}\right). \tag{4.36}$$

Clearly, $\frac{1}{\beta_{r,i}} \exp\left(\frac{2z_{r,i}}{\gamma\alpha_{r,i}}\right)$ represents a log-normal distribution; a closed form expression for the difference of two log-normal random variables is however not known. Although the summation of two log-normal random variables can be approximated by another log-normal random variable [48, 49], p_i can be approximated by a Gaussian random variable i.e.

$$p_i \sim \mathcal{N}\left(\mu_i, \breve{\sigma}_i^2\right)$$

where

$$\mu_i = d_r^2 - d_i^2 \tag{4.37}$$

and

$$\breve{\sigma}_i^2 = d_r^4 \exp\left(\frac{4\sigma_r^2}{(\gamma\alpha_r)^2}\right) - d_r^4 + d_i^4 \exp\left(\frac{4\sigma_i^2}{(\gamma\alpha_i)^2}\right) - d_i^4. \tag{4.38}$$

In vector form,

$$p(\mathbf{p} \mid \boldsymbol{\theta}) \sim \mathcal{N}\left(\boldsymbol{\mu}\left(\boldsymbol{\theta}\right), \mathbf{C}\left(\boldsymbol{\theta}\right)\right), \tag{4.39}$$

where $\boldsymbol{\mu}(\boldsymbol{\theta}) = [\mu_1(\boldsymbol{\theta}), \mu_2(\boldsymbol{\theta}), ..., \mu_N(\boldsymbol{\theta})]^T$ is the vector constituting the means, and $\mathbf{C}(\boldsymbol{\theta})$ is the $N \times N$ covariance matrix whose elements are given by (4.14) and (4.15).

In order to prove the validity of the Gaussian assumption, the empirical cumulative distribution function (CDF) of p_i and the theoretical Gaussian CDF are plotted in Fig. 4.1. It is observed that even for a relatively large variance of $\sigma_i^2 = \sigma_r^2 = 6$, the empirical CDF closely fits the Gaussian CDF. The plot shows two cases, for $d_r > d_i$ and for $d_r < d_i$. It is clear that for both cases the Gaussian assumption holds true.

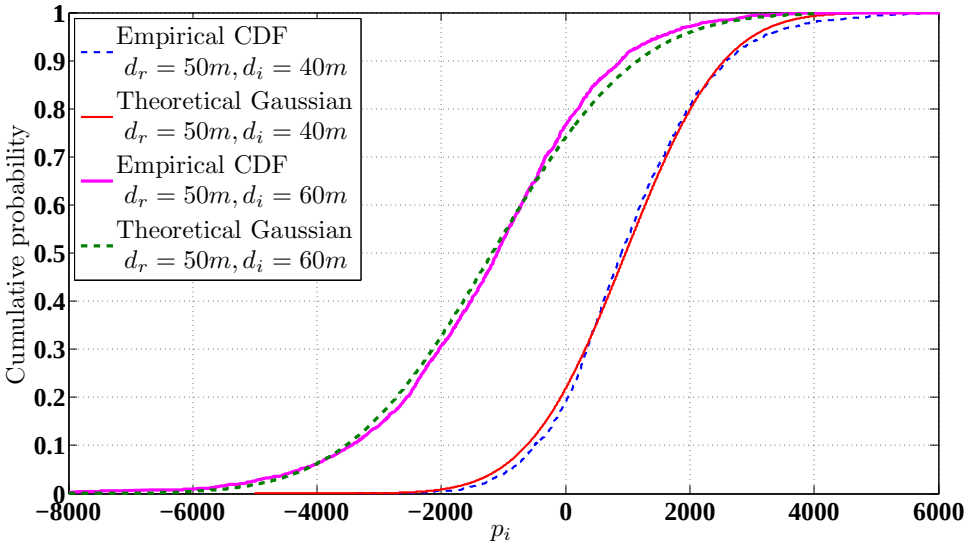

Figure 4.1: Empirical CDF of p_i and theoretical Gaussian CDF. $\sigma_i^2 = \sigma_r^2 = 6$

For the multivariate Gaussian distribution in (4.39), the elements of the FIM are given by[1]

[1] In this thesis, the linear CRB is derived for the the LLS-ref model, for other variants similar procedure can be followed.

$$\left[\mathbf{I}\left(\boldsymbol{\theta}\right)\right]_{ij}=\left(\frac{\partial\boldsymbol{\mu}\left(\boldsymbol{\theta}\right)}{\partial\boldsymbol{\theta}_{i}}\right)^{T}\mathbf{C}^{-1}\left(\boldsymbol{\theta}\right)\left(\frac{\partial\boldsymbol{\mu}\left(\boldsymbol{\theta}\right)}{\partial\boldsymbol{\theta}_{j}}\right)+0.5Tr\left(\mathbf{C}^{-1}\left(\boldsymbol{\theta}\right)\frac{\partial\mathbf{C}\left(\boldsymbol{\theta}\right)}{\partial\boldsymbol{\theta}_{i}}\mathbf{C}^{-1}\left(\boldsymbol{\theta}\right)\frac{\partial\mathbf{C}\left(\boldsymbol{\theta}\right)}{\partial\boldsymbol{\theta}_{j}}\right). \tag{4.40}$$

where

$$\frac{\partial\boldsymbol{\mu}_{i}\left(\boldsymbol{\theta}\right)}{\partial x}=2\left(x-x_{r}\right)-2\left(x-x_{i}\right)$$

and

$$\frac{\partial\boldsymbol{\mu}_{i}\left(\boldsymbol{\theta}\right)}{\partial y}=2\left(y-y_{r}\right)-2\left(y-y_{i}\right). \tag{4.41}$$

The derivatives of $\mathbf{C}\left(\boldsymbol{\theta}\right)$ are given by (4.42) and (4.43).

$$\frac{\partial\mathbf{C}(\boldsymbol{\theta})}{\partial x}=\operatorname{diag}\left\{4d_{1}^{2}\left(x-x_{1}\right)\left[\exp\left(\frac{4\sigma_{1}^{2}}{\left(\gamma\alpha_{1}\right)^{2}}\right)-1\right]+,...,+4d_{N}^{2}\left(x-x_{N}\right)\left[\exp\left(\frac{4\sigma_{N}^{2}}{\left(\gamma\alpha_{N}\right)^{2}}\right)-1\right]\right\}$$

$$+\mathbf{1}_{N\times N}\left\{4d_{r}^{2}\left(x-x_{r}\right)\left[\exp\left(\frac{4\sigma_{r}^{2}}{\left(\gamma\alpha_{r}\right)^{2}}\right)-1\right]\right\}. \tag{4.42}$$

$$\frac{\partial\mathbf{C}(\boldsymbol{\theta})}{\partial y}=\operatorname{diag}\left\{4d_{1}^{2}\left(y-y_{1}\right)\left[\exp\left(\frac{4\sigma_{1}^{2}}{\left(\gamma\alpha_{1}\right)^{2}}\right)-1\right]+,...,+4d_{N}^{2}\left(y-y_{N}\right)\left[\exp\left(\frac{4\sigma_{N}^{2}}{\left(\gamma\alpha_{N}\right)^{2}}\right)-1\right]\right\}$$

$$+\mathbf{1}_{N\times N}\left\{4d_{r}^{2}\left(y-y_{r}\right)\left[\exp\left(\frac{4\sigma_{r}^{2}}{\left(\gamma\alpha_{r}\right)^{2}}\right)-1\right]\right\}. \tag{4.43}$$

4.7 Simulation Results

For performance comparison, a circular deployment of 5 ANs around the origin of a 2-D coordinate system is considered with radius R. To evaluate the average

performance at various TN positions, 20 TNs are randomly deployed inside the network. For simplicity, the noise variance associated with all ANs is kept the same i.e. $\sigma_i^2 = \sigma_r^2 = \sigma^2$. A different PLE value (given by vector $\boldsymbol{\alpha}$) is given to each AN, while the root mean square error (RMSE) is compared when the shadowing noise variance σ^2 in the path-loss is increased. The simulations are run independently η times. The network AN and TNs deployment is shown in Fig. 4.2.

In Fig. 4.3, the performance of LLS-opt and LLS-ref is analysed. For LLS-ref, the RMSE is given while choosing each AN as a reference AN at a time for all 20 TNs. It is seen that the selection of some ANs as reference ANs exhibits better performance than others, this is primarily due to larger PLE value for that particular AN. However, since the simulations show the average performance for all 20 TNs, a larger PLE does not guarantee a particular AN to be an optimal reference AN, since it also depends on the actual distance from the TN. On the other hand, the performance of LLS-opt supersedes that of LLS-ref.

In Fig. 4.4, the results obtained for the theoretical MSE for LLS and WLS are compared to the simulation for both algorithm respectively. It can be seen that theoretical MSEs accurately predicts the performance of the LLS and WLS algorithms.

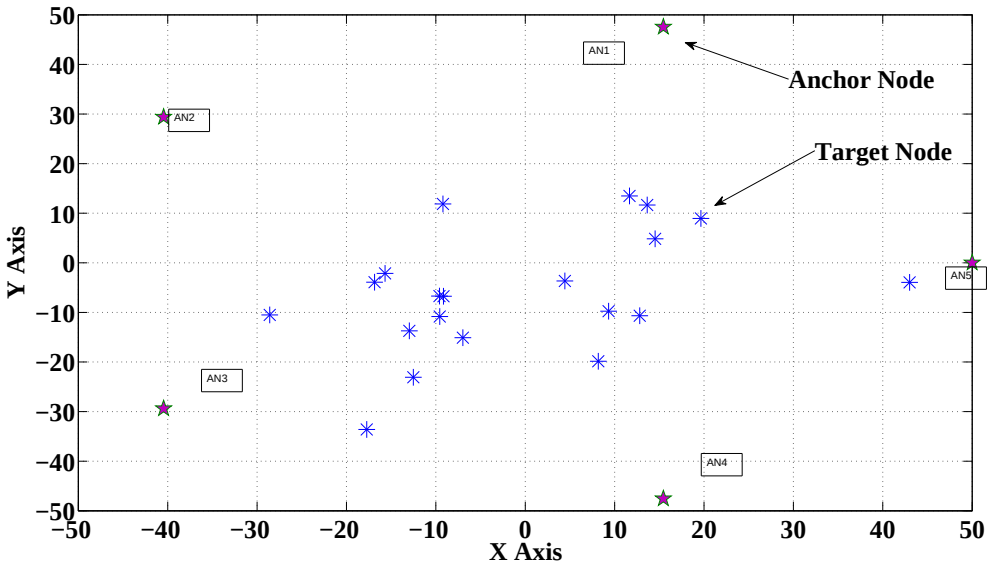

Figure 4.2: Network setup.

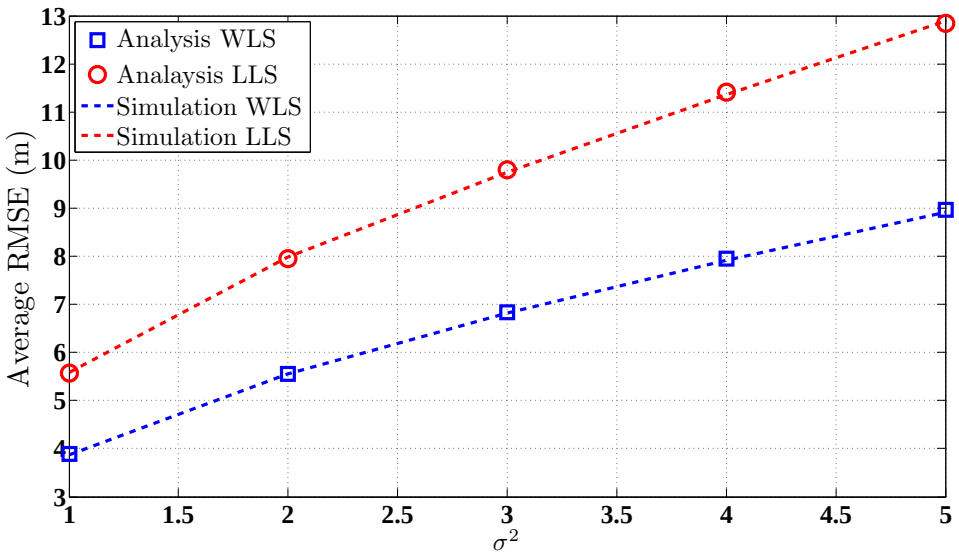

Figure 4.4: Performance comparison between theoretical MSE for LLS and WLS with simulation. $R = 50$ m, $\eta = 200$, $M = 5$, $\boldsymbol{\alpha} = [2.4, 2.6, 2.8, 3, 3.2]^T$.

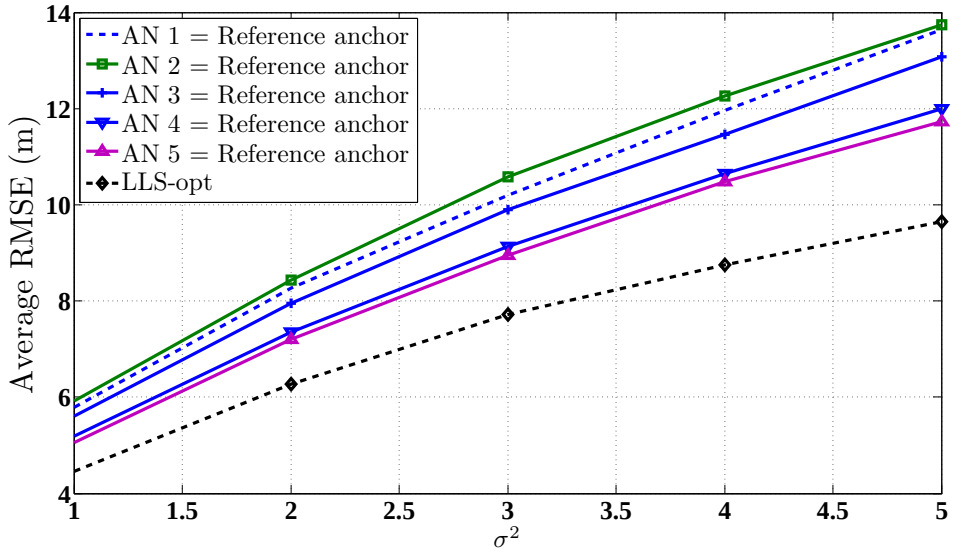

Figure 4.3: Performance comparison between LLS-ref for each AN as reference AN and LLS-opt. $R = 50$ m, $\eta = 200$, $M = 5$, $\boldsymbol{\alpha} = [2.4, 2.6, 2.8, 3, 3.2]^T$.

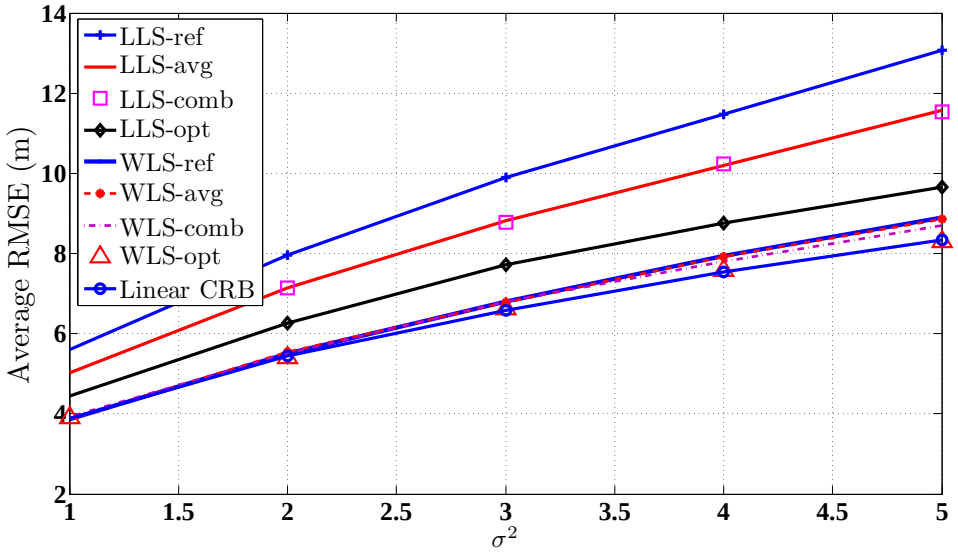

Figure 4.5: Performance comparison between different LLS and WLS implementations and linear CRB. $R = 50$ m, $\eta = 200$, $M = 5$, $\boldsymbol{\alpha} = [2.4, 2.6, 2.8, 3, 3.2]^T$.

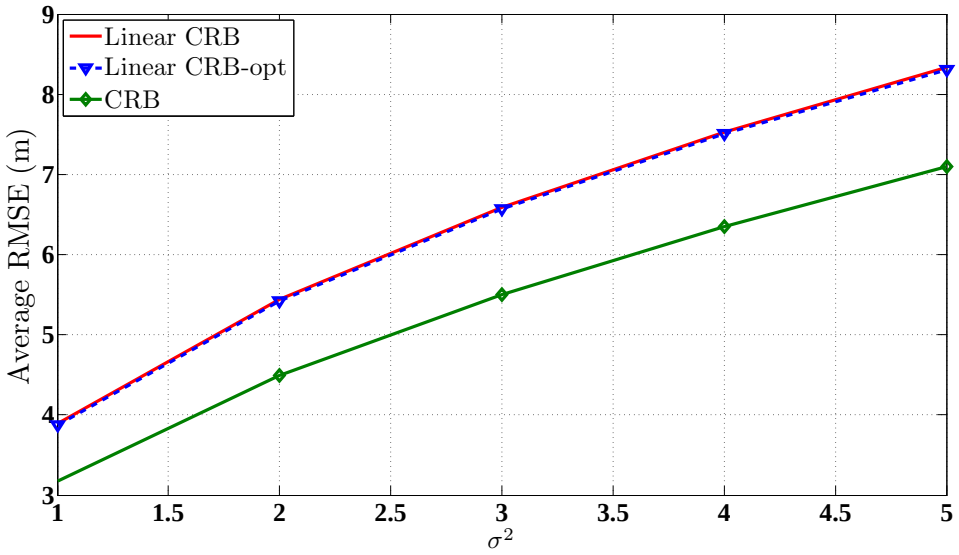

Figure 4.6: Performance comparison between linear CRB, linear CRB with optimal reference anchor and CRB. $R = 50$ m, $\eta = 200$, $M = 5$, $\boldsymbol{\alpha} = [2.4, 2.6, 2.8, 3, 3.2]^T$.

In Fig. 4.5, performances of the variants of LLS and WLS are compared with LLS-opt and WLS-opt. The linear CRB is also plotted for comparison. For LLS-ref and WLS-ref, AN-3 is randomly selected as the reference AN. As expected performance of LLS-avg and LLS-comb exceeds that of LLS-ref due to the averaging effect. However, the performance the LLS-opt surpasses all the other three LLS implementations. Interestingly, WLS-ref with reference AN-3 outperforms LLS-opt. As for the WLS, WLS-comb performs marginally better than WLS-avg and WLS-ref, both of which exhibit similar performance. While the WLS-opt performs better and approaches the linear CRB.

In Fig. 4.6, the CRB is compared with the linear CRB and as expected the performance of the linear CRB shows larger error than the exact CRB. Thus the linear CRB is a more realistic bound for the linear RSS estimator. On the other hand, the linear CRB changed little with optimal reference anchor selection.

4.8 Summary

The RSS based LLS localisation algorithm is a low complexity technique for node positioning in WSNs. In this chapter, performance analysis was carried out and improvements were proposed to the LLS method. The linear model was introduced and modified for three different LLS variants. Performance was improved with a WLS algorithm that uses the information present in the covariance matrix of the observations. Further performance improvement was achieved with an optimal reference AN selection technique. The performance of the WLS method was shown to be close to the linear CRB which was also derived. The linear CRB was shown to have larger error than the conventional CRB and thus realistically bounded the MSE of RSS location estimators operating on the linear model. Optimal anchor placement is discussed in next chapter.

5 Effects of anchor placement on mean-CRB for localisation

The material in this chapter has been published in the paper:

- N. Salman, H. K. Maheshwari, A. H. Kemp, M. Ghogho, "Effects of anchor placement on mean-CRB for localization," *The 10th IFIP Annual Mediterranean Ad Hoc Networking Workshop (Med-Hoc-Net),* pp.115-118, 12-15 June 2011.

5.1 Overview

Two widely used methods for range estimation are the time of arrival (ToA) and the received signal strength (RSS). Techniques to solve the range information for location estimation include the LLS method (chapter 3), the weighted LLS method (chapter 4) and the maximum likelihood (ML) approach (chapter 2). However the performance of these algorithms is bounded by the Cramer-Rao bound (CRB). The CRB puts a lower bound on the variance of any unbiased estimator. Apart from depending on the noise variance, the CRB for localisation also depends on the geometry of the anchor nodes (ANs) and the target node (TN). Since the lower bound is a function of the geometry of the network, it is

obvious that certain AN locations would offer better accuracy than others. In this chapter, the goal is to determine the optimal AN positions that will guarantee an overall optimal performance. The focus of this chapter is on ToA localisation. The ToA can be modelled based on an additive noise model (aNm) or a multiplicative noise model (mNm). The optimal AN placement for both models is investigated in this chapter.

This chapter is organized as follows, a review of the two noise models is given in section 5.2. In section 5.3, the CRB for localisation is discussed The simulation results are presented in section 5.4. In section 5.5, the LLS method is simulated and compared with the lower bound, which is followed by the conclusions.

5.2 Signal Models

A network consisting of N ANs is considered whose locations $\boldsymbol{\theta}_i = [x_i, y_i]^T$ for $i = 1, ..., N$ are known, this can be done by placing these ANs at predefined spots or their position can be determined via GPS. It is desired to determine the location of a TN $\boldsymbol{\theta} = [x, y]^T$. Then the estimated distance between each AN and the TN can be modelled either by the aNm or the mNm. The aNm is a widely accepted signal model, however the mNm is more suitable for practical propagation channels. The two noise models are discussed in the following subsections.

5.2.1 Additive noise model

The signal received at the TN from the i^{th} AN is given by

$$r_i(t) = A_i s(t - \tau_i) + n_i(t), \tag{5.1}$$

where A_i is the amplitude or attenuation of the signal, τ_i is the propagation delay and $n_i(t)$ is the thermal noise. The delay τ_i that is dependent on the distance

between the AN and the TN is given by

$$\tau_i(x, y, l_i) = \frac{1}{c}\sqrt{(x - x_i)^2 + (y - y_i)^2} + l_i, \tag{5.2}$$

where c is the speed of the electromagnetic wave $c \simeq 3 \times 10^8$ and l_i is non line of sight (NLoS) bias. The present work only considers the LoS case, thus $l = 0$. From (5.2), it is noted that the distance between i^{th} AN and the TN is given by

$$d_i = c\tau_i. \tag{5.3}$$

To include distances from N ANs, (5.3) is given in vector form

$$\mathbf{d} = [d_1, ..., d_N]^T. \tag{5.4}$$

Thus the estimated distance $\hat{d}_i$ can be represented as

$$\hat{d}_i = d_i + n_i, \tag{5.5}$$

where $n_i \sim \mathcal{N}(0, \sigma_i^2)$ is the additive white Gaussian noise with constant standard deviation σ_i, that is independent of d_i. Similarly, in vector form

$$\hat{\mathbf{d}} = \left[\hat{d_1}, ..., \hat{d_N}\right]^T. \tag{5.6}$$

Fig. 5.1 shows how the aNm effects the estimated distance or range.

5.2.2 Multiplicative noise model

For the multiplicative noise model (5.5) can be written as

$$c\hat{\tau}_i = c\tau_i + c\bar{n}_i. \tag{5.7}$$

Where $\bar{n}_i$ is Gaussian noise in the time estimates.

Then the CRB on the variance of the ToA estimate is given as [11]

$$\sigma^{\mathbf{2}}(\hat{\tau}) \geq \frac{1}{8\pi^2 \mathcal{B}^2 SNR}, \tag{5.8}$$

where $\mathcal{B}$ is the effective bandwidth of the signal and the received power from the i^{th} AN is given by [20]

$$P_i = P_t \frac{\nu}{d_i^{\alpha}}, \tag{5.9}$$

where ν is the frequency related loss. It is also dependent on antenna heights and other physical layer effects. P_t is the transmit power. α is the path-loss exponent (PLE), its value is generally taken between 2 to 5 depending on the type of environment. The signal-to-noise ratio (SNR) is hence given by

$$SNR = \frac{P_i}{N_0}, \tag{5.10}$$

where N_0 is the noise power. Putting the value of (5.9) in (5.10) and then back in (5.8), the standard deviation on the estimated distance is given by

$$\bar{\sigma_i} = \kappa d_i^{\frac{\alpha}{2}}, \tag{5.11}$$

where

$$\kappa = c\sqrt{\frac{N_0}{8\pi^2 \mathcal{B}^2 P_t \nu}}. \tag{5.12}$$

Following the distance dependent variance model, (5.5) can be written as

$$\hat{d}_i = d_i + \kappa d_i^{\frac{\alpha}{2}} \omega. \tag{5.13}$$

or

$$\hat{d}_i = d_i^{\alpha} \left(d_i^{1-\alpha} + \kappa d_i^{-\frac{\alpha}{2}} \omega \right)$$

Here ω is Gaussian random variable with zero mean and unit variance. Thus the noise model in (5.13) is multiplicative due to the term $d_i^{\frac{\alpha}{2}} \omega$. The variation in the estimated distance for the mNm is illustrated in Fig. 5.2.

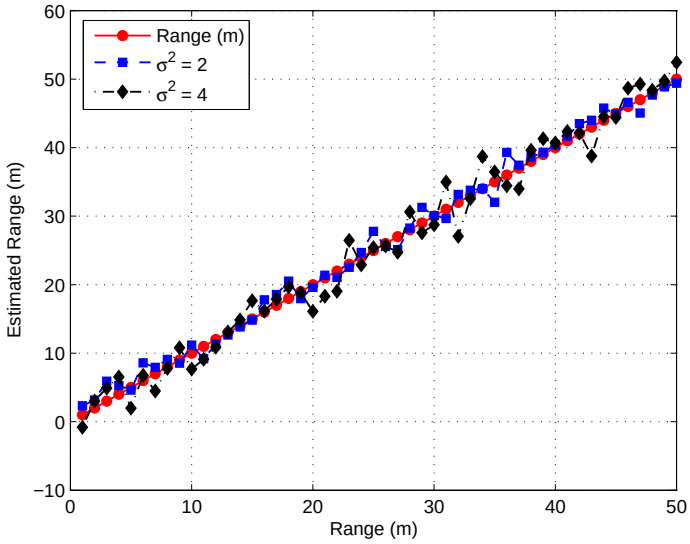

Figure 5.1: Simulation of estimated range for aNm.

5.3 Cramer-Rao Bound

The accuracy of $\hat{\boldsymbol{\theta}}$ being an unbiased estimate of $\boldsymbol{\theta}$ is bounded by

$$\text{var}(\hat{\theta}_i) \geq \left[\frac{1}{\mathbf{I}(\boldsymbol{\theta})}\right]_{ii}, \tag{5.14}$$

where $\boldsymbol{\theta} = [\theta_1\theta_2...\theta_p]^T$is the vector parameter to be estimated and $\mathbf{I}(\boldsymbol{\theta})$ is the $p \times p$ Fisher information matrix (FIM) and is defined as [39]

$$[\mathbf{I}(\boldsymbol{\theta})]_{ij} = -\,E\left[\frac{\partial^2 \ln p(\hat{\mathbf{d}}|\boldsymbol{\theta})}{\partial\boldsymbol{\theta}_i\partial\boldsymbol{\theta}_j}\right]; i,j = 1,2,..,p. \tag{5.15}$$

Where $p(\hat{\mathbf{d}}|\boldsymbol{\theta})$ is the likelihood function and $E\{.\}$ refers to the expected value and is taken w.r.t. $p(\hat{\mathbf{d}}|\boldsymbol{\theta})$ and the derivatives are taken at the true value of $\boldsymbol{\theta}$.

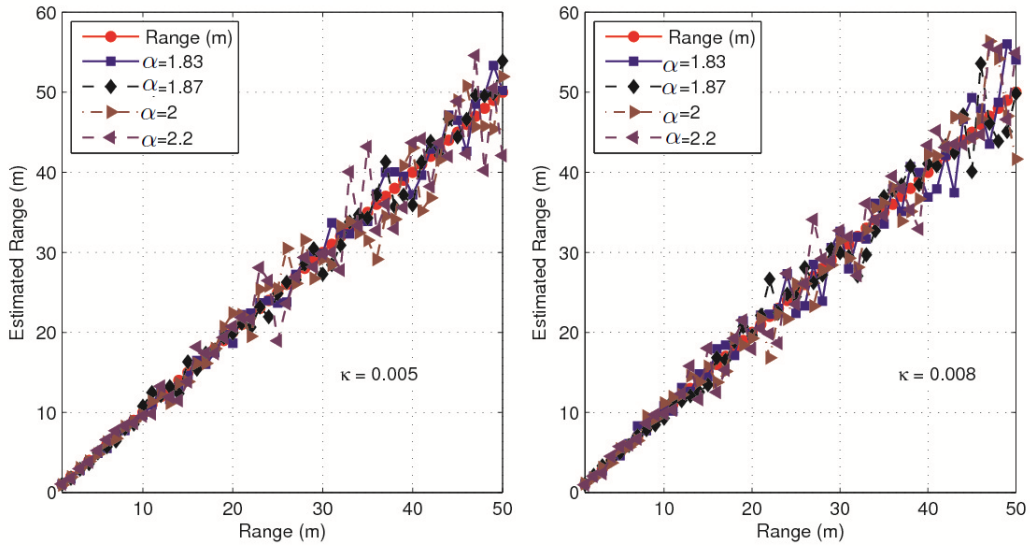

Figure 5.2: Simulation of estimated range for mNm.

The FIM for the aNm model is given by [45, 46, 28]

$$\mathbf{I}(\theta) = \frac{1}{\sigma_i^2}\begin{bmatrix} \sum_{i=1}^{N} \frac{(x-x_i)^2}{d_i^2} & \sum_{i=1}^{N} \frac{(y-y_i)(x-x_i)}{d_i^2} \\ \sum_{i=1}^{N} \frac{(y-y_i)(x-x_i)}{d_i^2} & \sum_{i=1}^{N} \frac{(y-y_i)^2}{d_i^2} \end{bmatrix} \tag{5.16}$$

or

$$\mathbf{I}(\theta) = \frac{1}{\sigma_i^2}\begin{bmatrix} \sum_{i=1}^{N} \cos^2(\Theta_i) & \sum_{i=1}^{N} \cos(\Theta_i)\sin(\Theta_i) \\ \sum_{i=1}^{N} \cos(\Theta_i)\sin(\Theta_i) & \sum_{i=1}^{N} \sin^2(\Theta_i) \end{bmatrix}, \tag{5.17}$$

where Θ_i being the angle of the TN with the i^{th} AN. The FIM for the mNm is given by [50]

$$\mathbf{I}(\theta) = \frac{1}{\bar{\sigma}_i^2}\begin{bmatrix} \sum_{i=1}^{N} \zeta_i \cos^2(\Theta_i) & \sum_{i=1}^{N} \zeta_i \cos(\Theta_i)\sin(\Theta_i) \\ \sum_{i=1}^{N} \zeta_i \cos(\Theta_i)\sin(\Theta_i) & \sum_{i=1}^{N} \zeta_i \sin^2(\Theta_i) \end{bmatrix}, \tag{5.18}$$

where $\zeta_i = 1 + \frac{\alpha^2\kappa}{2} d_i^{\alpha-2}$, which is distance dependent. Since the lower bound

in both noise models is a function of the geometry of the AN and the TN, it is obvious that certain AN locations would offer better accuracy than others. These optimal AN locations are discussed in the next section.

5.4 Optimal Anchor Positions

The estimation of different TN positions is subject to different accuracies. The aim is to find AN locations that would give us an overall best accuracy for all target positions. Thus the ANs that offers the minimum of the mean CRB are chosen. In the following subsection, these optimal AN locations are discussed.

5.4.1 Optimal anchor positions for aNm

Trilateration in a 2-D case requires a minimum of three ANs. Individual distance between each AN and the TN is represented by a circle or line of position (LoP). The point of intersection of these circles is the TN location. In order to get an insight on how the lower bound is affected by the relative angle between the target and the AN node, the CRB for every point in a 10×10 2-D plane is calculated for fixed AN positions. Furthermore, in order to achieve the AN positions that give the minimum mean CRB, all the combinations of ANs are taken. i.e.

$$C_r^n = \frac{n!}{r!(n-r)!}, \tag{5.19}$$

where n is the dimension of the area and r is the number of ANs.

The mean CRB is given by

$$mean\, CRB = \frac{1}{n^2} \sum_{i,j=1}^{n^2} CRB_{i,j}$$

for $i = 1, ..., n$ and $j = 1, ..., n$. Where $CRB_{i,j}$ is the CRB at the (x_i, y_j) TN position. Hence the mean CRB is the average CRB of the CRBs taken at all TN locations.

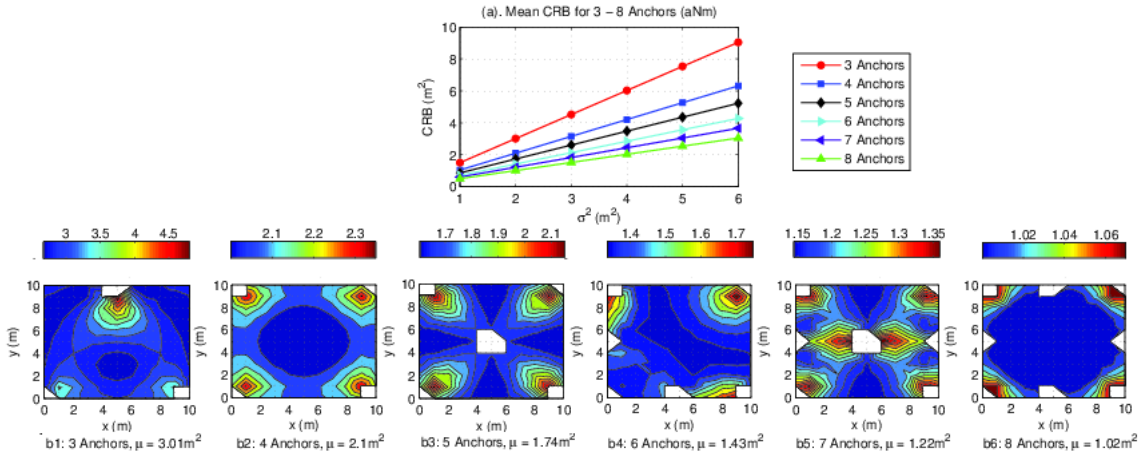

Figure 5.3: Optimal AN positions and corresponding CRB for aNm.

As an example, in the present case, an area of 10×10 is taken for case (b1) in Fig. 5.3, where 3 ANs are employed, a total combination of C_3^{100} =161,700 AN positions are obtained. It is well known that when all ANs are placed along the same line (x or y coordinates being the same), then the variance of the CRB rises to infinity and in such cases positioning algorithms such as the LLS fail to estimate the TN's coordinates. Thus in order to avoid this problem, all the collinear AN positions are not considered in the simulations. The number of such combination is given by $x' * C_r^{x'} + y' * C_r^{y'}$, where x', y' represent the lengths of x and y coordinates respectively. For case (b1) in Fig. 5.3, a total of 2,400 collinear AN positions are avoided. Fig. 5.3 shows the optimal AN positions for 3-8 ANs. The contour plots Fig. 5.3 (b1-b6) are obtained for a constant standard deviation for all cases i.e. $\sigma_i = \sigma = 2$. It is observed that when only 3 ANs are placed in a square area, the highest accuracy in the estimated location is achieved when the trio is placed at the corners of an equilateral triangle. This triangle is of maximum size as 2 ANs are placed at the corners of one side of the square area while the 3^{rd}

AN is placed at the centre of the opposite side. It is also noted that the bound increases as the TN goes near any of the AN nodes. The best location for 4 ANs is at the corners of the square area while the best location for an additional 5^{th} AN is the centre of the area. Similarly such symmetrical AN locations are exhibited in Fig. 5.3 (b4-b6) where 6, 7 and 8 ANs are used. The white points in the figures show the AN locations where the TN placement is avoided. It should be noted that these configurations are independent of rotation i.e. the same results are obtained if the entire set of ANs are simultaneously rotated clockwise or counter-clock wise by 90^0or 180^0. Fig. 5.3a displays the mean CRB as a function of variance. It is noted that as the number of ANs increase the variance effect on the mean CRB becomes smaller. Fig. 5.4 (b1-b6) illustrates the AN locations which exhibits the worst localisation accuracy and which gives the maximum mean CRB. It is observed that the variance of the estimator is the highest if all the ANs are placed in the same corner of a square area. It is also seen in 5.4a that the improvement in performance is negligible if the number of ANs is increased from 5 to 8 for such a poor network geometry. Furthermore, it is evident from both Fig. 5.3 and Fig. 5.4 that when the minimum 3 ANs are placed optimally (with mean CRB = 1.5063 and 9.0379 for σ^2= 1 and 6), it outperforms a poor deployment of 8 ANs (mean CRB = 13.562 and 81.375 for σ^2= 1 and 6).

5.4.2 Optimal anchor positions for mNm

The plot in Fig. 5.5a illustrates the mNm mean CRB as a function of the number of ANs placed at the optimal positions for the aNm. The contour plot for κ = 0.001 [50] and $\alpha = 4$ is given in Fig. 5.5 (b1-b6). The mean CRB for the mNm is lower with the aNm for ANs 5 and more. However this is not true for all values

κ of and α. The optimal AN placement for mNm is different than the aNm, as shown in Fig. 5.6 (a1-a3) for 3, 4 and 5 ANs. However, these optimal placements depend on the actual scale of the area, the constant κ and α. The mNm CRB becomes lower as values of κ and α are decreased. While both CRBs are almost identical for $\alpha = 2$. In a dense urban environments where $\alpha = 4$ to 5 or highly cluttered indoor scenarios, the mNm is a more suitable noise model. In such cases, results from Fig. 5.6 suggest that it is not always optimal to place the AN nodes at the corners as in Fig. 5.3. In fact, the optimality cannot even be guaranteed by the AN placement in Fig. 5.6 as they are for a particular dimension and for an assumed value of κ and α. Thus, for the mNm case, the values of κ and α need to be obtained experimentally before AN deployment. Finally, the worst AN placement for mNm is similar as that for aNm i.e. all ANs are placed at one corner of the area.

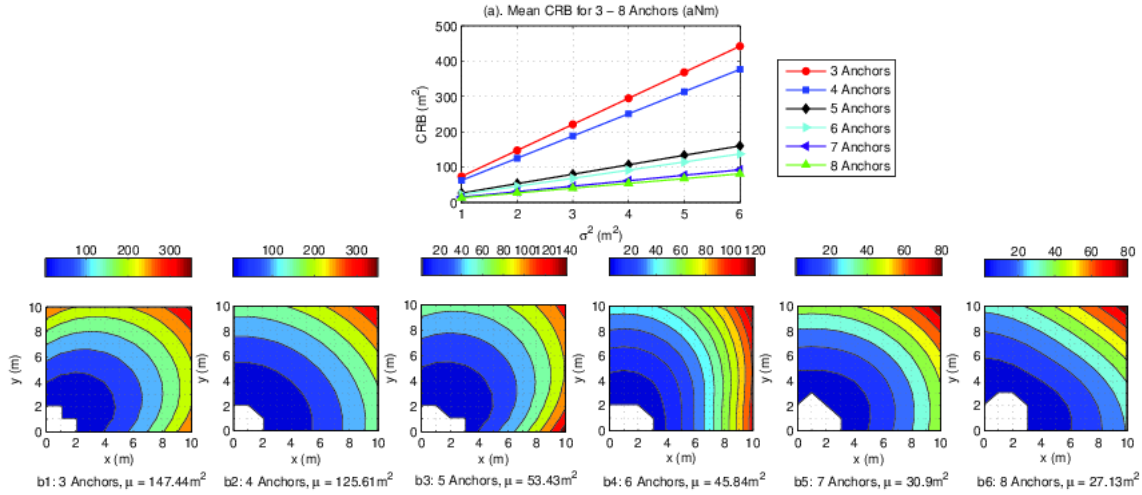

Figure 5.4: Poor AN positions and corresponding CRB for aNm.

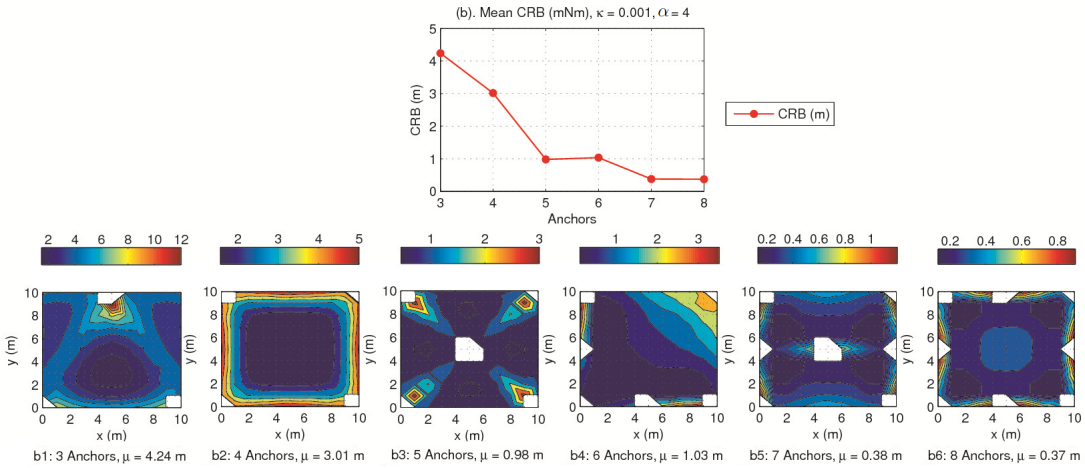

Figure 5.5: Suboptimal AN positions and corresponding CRB for mNm.

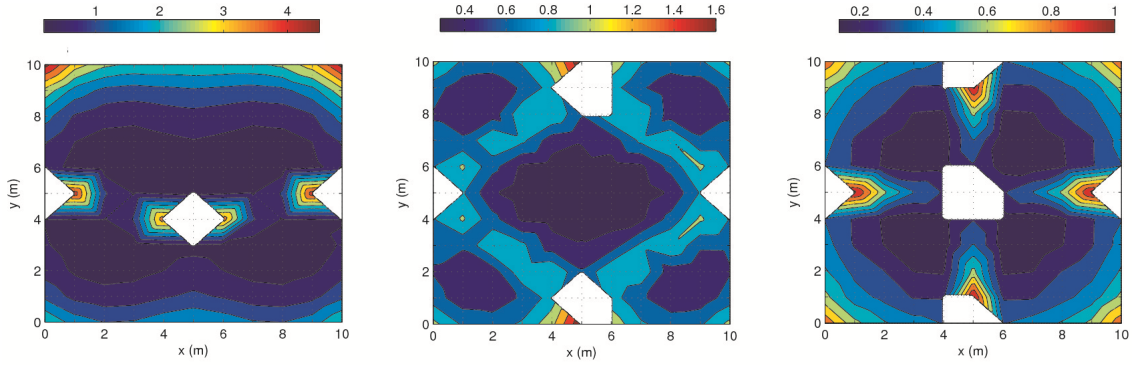

Figure 5.6: Optimal AN positions and corresponding CRB for mNm.

5.5 Performance of Linear Least Squares (LLS) Method at Optimal Anchor Positions

In this section, the performance of the LLS method for position estimation is compared with the mean CRB for optimal AN placement. The elements of the vector $\hat{d}_i$ in (5.5) are given by

$$\hat{d}_i = \sqrt{(x - x_i)^2 + (y - y_i)^2}, \tag{5.20}$$

where $\hat{d}_i$ represent the noisy estimated distances and the circles obtained from them do not intersect at a common point. In order to solve the LS problem (which is non-linear) for (x, y) coordinates, the distance equation of the r^{th} AN is fixed and all other distance equations are subtracted from it, yielding [28]

$$x_i^2 - x_r^2 + y_i^2 - y_r^2 - 2xx_i + 2xx_i - 2yy_i + 2yy_r = \hat{d}_i^2 - \hat{d}_r^2, \tag{5.21}$$

for $i = 1, ..., N-1$, $i \neq r$ and where $\varphi_{i,r} = x_{i,r}^2 + y_{i,r}^2$.

Similarly in matrix form

$$\mathbf{A}\boldsymbol{\theta} = 0.5\mathbf{b}, \tag{5.22}$$

where

$$\mathbf{A} = \begin{bmatrix} x_1 - x_r & y_1 - y_r \\ x_2 - x_r & y_2 - y_r \\ \vdots & \vdots \\ x_{N-1} - x_r & y_{N-1} - y_r \end{bmatrix}, \tag{5.23}$$

$$\boldsymbol{\theta} = \begin{bmatrix} x \\ y \end{bmatrix}$$

$$\mathbf{b} = \frac{1}{2}\begin{bmatrix} \varphi_1 - \varphi_r + \hat{d}_r^2 - \hat{d}_1^2 \\ \varphi_2 - \varphi_r + \hat{d}_r^2 - \hat{d}_2^2 \\ \vdots \\ \varphi_{N-1} - \varphi_r + \hat{d}_r^2 - \hat{d}_{N-1}^2 \end{bmatrix} \tag{5.24}$$

and the estimated coordinates of the TN is given by the vector

$$\hat{\boldsymbol{\theta}} = \left(\mathbf{A}^T\mathbf{A}\right)^{-1}\mathbf{A}^T\mathbf{b}. \tag{5.25}$$

The mean square error (MSE) is given by: $\text{MSE} = Tr\left\{E\left[\left(\hat{\boldsymbol{\theta}} - \boldsymbol{\theta}_0\right)\left(\hat{\boldsymbol{\theta}} - \boldsymbol{\theta}_0\right)^T\right]\right\}$, where $Tr(.)$ represents the trace of the matrix. Fig. 5.7(a) compares the MSE of the LLS method with the mean CRB for optimal AN positions. Fifty iterations are taken for each range measurement while the variance is incremented from 1 to 4 for aNm. The MSE for all TN locations is computed and its mean is compared with the mean CRB. The simulation uses the same setup of a 10×10 2-D plane as in the previous case. It is seen that although the number of ANs is increased from 4 to 5, it does not have a significant impact on the accuracy. Fig. 5.7(b) compares the MSE of LLS for mNm with the mean CRB for α= 4. The right y axis of Fig. 5.7(b) shows the mean MSE of the LLS method. It is observed that error is colossal for $\alpha = 4$. The effect of the different values of α is illustrated in Fig. 5.8, where the LS method for $\alpha = 2$ and 3 are simulated. As can be seen the LS offers less error for a smaller value of α.

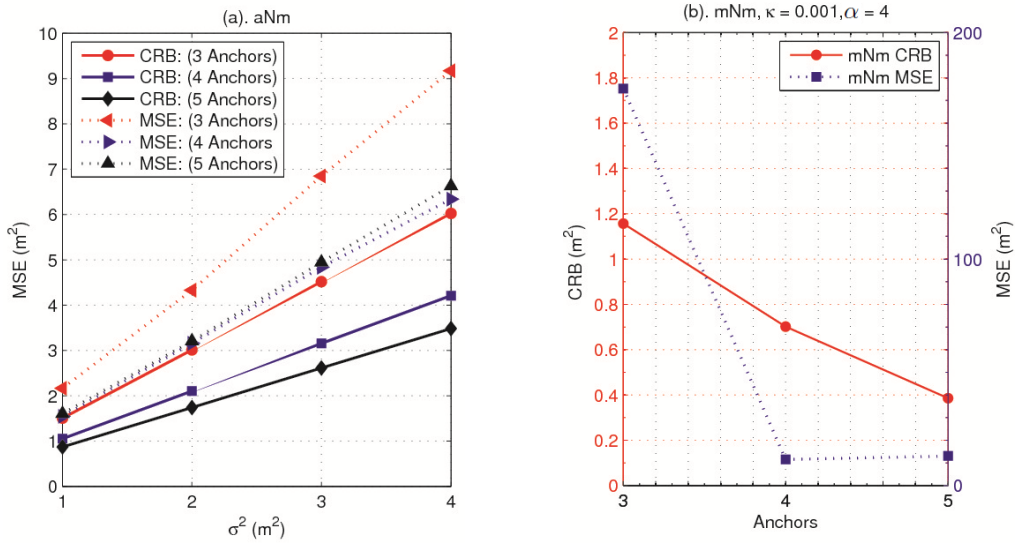

(a) **(b)**

Figure 5.7: Performance of the LS method for 3, 4 and 5 ANs for α= 2 and 3.

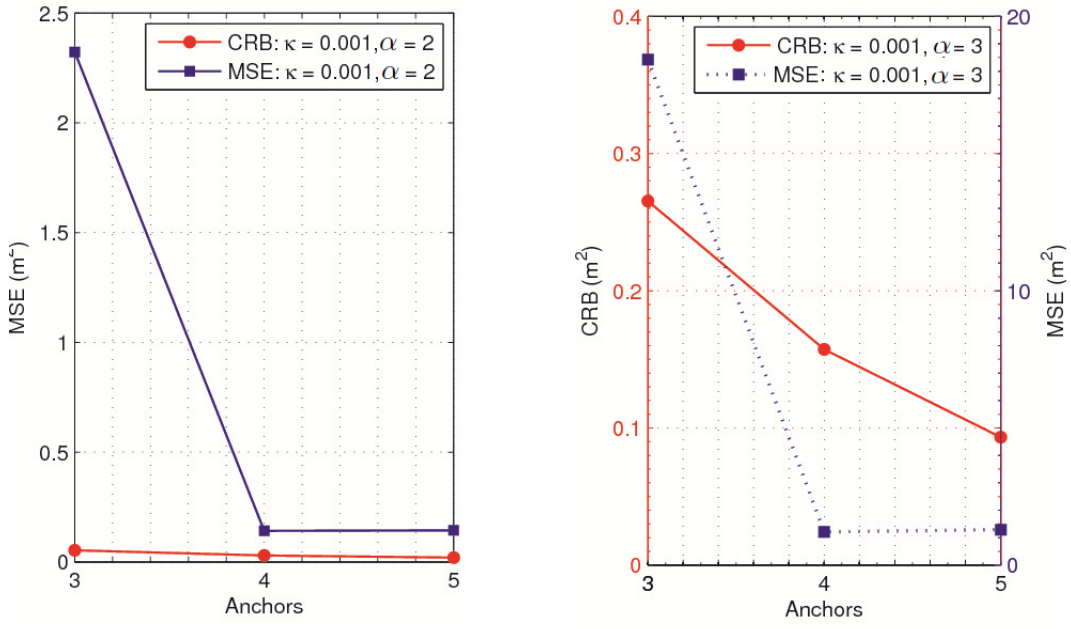

(a) **(b)**

Figure 5.8: Performance of the LS method for 3, 4 and 5 ANs for α= 2 and 3.

5.6 Summary

In this chapter, the impact of AN positions on the localisation of nodes was discussed. Based on extensive simulations, optimal AN location for both aNm and mNm have been achieved. It is evident from the simulations that for an aNm the CRB decreases as the TN is moved away from the ANs. Thus in a square area the lowest accuracy is observed near the AN while the highest accuracy is achieved at the centre of the area. On the other hand, for highly cluttered environments where the α value of 4-5 is taken, the mNm is more suitable. In such scenarios, the minimum mean CRB is not offered by ANs placed at the corners of a square area. Optimal AN placement in mNm depends on the dimension of the area and the value of κ and α. Although the tecnique used in this chapter is not analytical, however it can be best used to obtain optimal AN locations for unsymmetrical areas. For future work, the optimal AN selection using the RSS technique will be studied.

6 Geographic Routing in Localised Networks

The material in this chapter has been published in the papers:

- A. M. Popescu, N. Salman, and A. Kemp, "Energy consumption of geographic routing with realistic localisation," *Networks, IET*, vol. 1, no. 3, pp. 126–135, 2012.
- A. M. Popescu, N. Salman, and A. H. Kemp, "Geographic routing resilient to location errors," *Wireless Communications Letters, IEEE*, vol. 2, no. 2, pp. 203–206, 2013.

6.1 Overview

The constant need for energy efficiency in WSNs has led to the consideration of geographic based forwarding for routing in applications of large scale networks [51, 52]. However, until recently, the assumption of accurate location knowledge in the design of position-based algorithms was frequent, making this routing type unreliable in practical applications. Localisation solutions are either based on expensive GPS or affordable but less accurate local positioning systems (LPS).

The impact of location error on geographic routing has been considered in [51, 52, 53, 54, 55, 56, 57, 58].

This chapter focuses on the study of geographic routing because of its power saving features which makes it an ideal candidate for large scale WSNs. Early routing proposals assumed accurate location information readily available. Later algorithms considered the existence of location error and mathematically modelled it as either random uniform or Gaussian [51, 52, 53, 54, 55, 56]. In the first part of this chapter, geographic routing is studied when positioning is performed with specific localisation techniques i.e. with RSS or ToA. ToA and RSS are chosen because they have gained a lot of popularity over the years being based on inter-nodal ranges (R) and because they do not require costly equipment. Each technique is simulated using 2 different methods, LLS (chapter 3 and 4) and ML (chapter 2) based Levenberg Marquardt (LM) method (iterative). The chapter shows the loss rate (LR) of basic advance-based routing and the energy consumption of the networks with accurate locations and with position inaccuracy of various degrees. The results indicate that a general model for location errors is not sufficient for a correct algorithmic design as each localisation technique yields errors of a different degree, with a different impact on the routing performance.

The second part of this chapter proposes a solution to improve the performance of geographic routing in terms of packet delivery ratio (PDR) in realistic localisation conditions. A novel, low-complexity, error-resilient geographic routing method, named conditioned mean square error ratio (CMSER) routing is proposed with the intention to efficiently make use of existing network information and to successfully route packets when localisation is inaccurate. Next hop selection is based on the largest distance to destination (minimizing the number of forwarding hops) and on the smallest estimated error figure associated with

the measured neighbour coordinates. It is found that CMSER outperforms other basic greedy forwarding techniques. Simulation results show that the throughput for CMSER is higher than that of other methods; additionally it also reduces the energy wasted on lost packets by keeping their routing paths short.

Geographic routing with imprecise location measurements has been investigated by research literature in an attempt to improve its resilience to location errors by increasing the packet delivery ratio (PDR) and minimizing energy consumption. Two of the available forwarding techniques stand out, having different approaches: the least expected distance (LED)[58] and the maximum expected progress (MEP)[59] algorithms. While [59] focuses on increasing the throughput, the work in [58] aims to optimize power consumption.

[59] uses the objective function named maximum expectation progress (MEP) for positive advance. It determines the goodness of routing candidates based on progress to destination and location error characteristics. MEP uses a Gaussian location error model and assumes a known standard deviation of the location error (σ) for each node. Based on σ, the transmission range (R) and the measured inter-nodal distances $\hat{d}$, it estimates the probability of the real position of the forwarding node to be found within a circular area centered at the known erroneous location. The value of this probability (used as an indicator of the risk that the neihbour may be outside R in reality) and the amount of progress offered by the forwarding option help in choosing the best forwarding candidate.

The LED algorithm in [58] is presented as a novel, error-robust routing scheme, whose main aim is to preserve the power saving features of basic geographic forwarding. It is proven in [58] that whichever approach the position-based routing may have, either to optimize the energy spent per hop or for the overall chosen path, the energy-optimal forwarding position is the same. LED determines this

theoretical optimum and subsequently chooses as the next hop the neighbour whose real position is closest to it. The algorithm strategically incorporates location error into the forwarding objective function. It is assumed that the estimated coordinates of each node are affected by a Gaussian error of a given variance. As a consequence the erroneous distances between nodes are random variables characterized by the Rice distribution. LED calculates the expectation of the considered distances and chooses the node with the minimum expectation.

Although [59, 58] provide solutions for geographic routing in realistic localisation scenarios, performance degradation can still be considered severe and can be further reduced. The investigation in section 6.3 presents a comparative study of the various greedy forwarding techniques (the basis of the algorithms described above) and proposes the conditioned mean square error ratio (CMSER) algorithm as an alternative method to improve the overall performance while still coping with location errors. To be able to compare the routing techniques, all the algorithms forward with positive advance only, dismissing the possibility of backward progress.

The most forward within range algorithm (MFR) [60], a basic geographic routing algorithm without location error coping capabilities, is also used for comparison and it is considered energy efficient when using a fixed transmission power because it minimizes the hop count.

Simulations have shown that, under identical circumstances, the PDR of the proposed forwarding method CMSER is increased and the energy wasted on lost packets is limited. The throughput grows higher without the lost packets travelling in the network for a large number of hops, thus reducing the overall power consumption of the network.

6.2 Geographic Routing with ToA and RSS Localisation

Geographic routing depends on knowledge of location which is itself derived from measured or estimated distance either through RSS or ToA. The ranging techniques as well as the mathematical model have been described in chapter (2-5). The MATLAB simulation used for evaluation assumes 8 ANs, situated 20 m outside the network, in the corners and on the edges of the routing surface, one being placed in the centre. ANs do not participate in the routing process and for them $R \geq 623$m. Networks with different densities are considered and the variance of the estimated distance and shadowing path-loss is varied. The simulation uses the parameter values specified in table 6.1. The destination (D) is placed in the right upper corner of the square network. The events in the network are detected by source nodes (S). Their number determines the $S - D$ traffic connections and the congestion level in the networks. A static network is assumed, with randomly and uniformly distributed nodes.

As the network area is kept constant, the network density (calculated as number of in-range neighbours per node) is varied by a gradual increase of the total number of nodes (from 25 to 65 nodes). Each simulation consists in generating:

- A network with accurate location information and
- 5 networks with inaccurate location information, whose variance, σ_n^2 (ToA) and σ_w^2 (RSS) is increased from 2 to 10, with a step of 2.

This process takes place 300 times (similar to [58]) for each network size and all the results are averaged.

Packet forwarding is achieved through MFR routing, based on advance to D, but modified here so that no backward progress takes place. The algorithm assumes

Parameter Name (unit)	Value
Transmission R of Target Nodes (m)	100
Transmit power (mW)[58]	1.778
Path Loss Exponent	3
Standard Deviation for Shadowing	3.5
Sensitivity Threshold (dBm)[61]	-95
Packet Size (bits) [56]	1024
Data rate (kbits/s) [62]	250
Energy spent on Transmission (Joules/bit) [62]	2.5e-07
Energy spent on Reception (Joules/bit)[62]	1.5e-0.7
Network side length (m)	400
Number of trials	300
Number of packets per $S - D$ connection	10
Number of S	15
Minimum value of Backoff Exponent (minBE)[63]	3
Maximum value of Backoff Exponent (maxBE)[63]	5
Maximum number of Backoffs (maxCSMABackoffs)[63]	5

Table 6.1: Simulation parameters

Nodes	25	35	45	55	65
Density	3.5	5.2	6.7	8.2	9.8

Table 6.2: Network density (neighbours/node).

nodes which are aware of the location of S, D and of their neighbours (nodes within R). Nodes list their neighbours whose coordinates are known correctly or estimated.

Fig. 6.1a illustrates the forwarding of a node F with neighbours $F1$ and $F2$. The neighbour list of F is checked to see if it is empty and if D is listed as a neighbour. When it is not, F blacklists S and the previous hops within R. This has been simulated to avoid undesired loops and backward progress - sources of useless energy consumption. However, this implies a list of previous hops is forwarded in the header of each packet, slightly increasing its size. The remaining neighbours ($F1$ & $F2$) are possible forwarding options, but the one with actual progress (shorter distance to D than d) will be short-listed in a list of neighbours

with progress. The node with the most progress is the next hop ($d1$ in Fig. 6.1a).

Each transmitting node follows the same algorithm as illustrated in the simulation flow chart in Fig. 6.1b, which also shows that once the next hop is identified and transmission is attempted, the medium access control (MAC) layer's carrier sense multiple access with collision avoidance (CSMA/CA) mechanism comes into play. In agreement with the un-slotted version of IEEE 802.15.4 MAC layer [63], when inter-node communication is attempted, each sensor checks if the channel is idle or not before sending a packet. When found busy, the assessment is repeated. The channel status is determined through clear channel assessment (CCA) and the failure probability at node level is defined based on the number of sources S. If the MAC approves the transmission, the sending node either succeeds or fails, depending on the accuracy of the location knowledge it has.

The simulation makes use of a realistic log-normal shadowing channel model as in [58]. The model is considered to take into account multipath shadowing and fading effects which occur in wireless environments. Upper layers are not simulated.

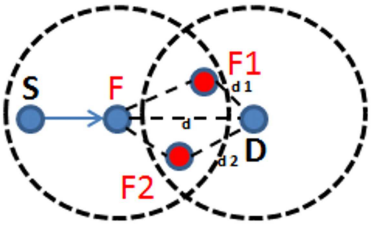

(a) Forwarding Example.

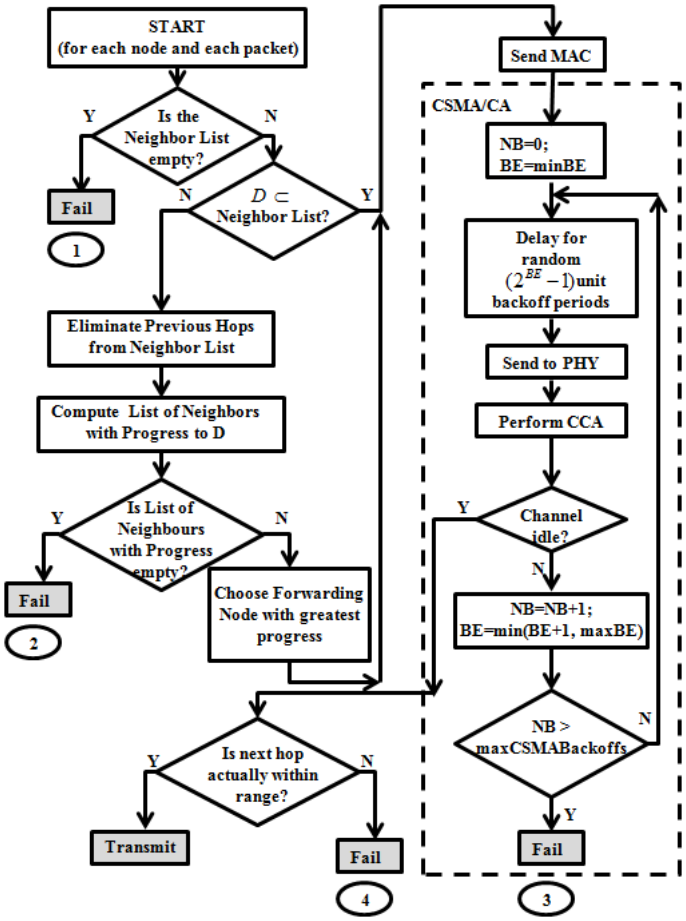

(b) Flow Chart.

Figure 6.1: Simulated Forwarding Algorithm.

It is expected that the results of the ML simulations have better accuracy, thus improving the routing process. ML localisation offers better accuracy at higher computational costs and is sometimes infeasible because it requires a good initial estimation which may not be achievable.

The loss rate (LR) is shown in Fig. 6.2 and Fig. 6.3. For lower densities, routing

performance is unsatisfactory in all cases and this is more pronounced as σ^2 increases. For ML localisation with RSS ranging (ML-RSS), even for the smallest σ_w^2, the LR reaches 89%, worse than for ML localisation with ToA ranging (ML-ToA) where the value is 81%. Although the LR for RSS ranging decreases with the increase in density, the figures show how the best value, with the smallest σ_w^2 reach 64% so more than half of the sent information is lost. This is because of the large errors introduced in the location estimates due to RSS measurements at longer distances. However, for both LLS-ToA and ML-ToA, the performance improves considerably when node density increases, reaching a LR of 26% for the worst case scenario of $\sigma_n^2 = 10$ of the LLS-ToA.

It is found that the performance of networks employing geographic routing, under the same relaxed traffic load, is considerably different for the positioning errors induced by ToA and RSS. While good connectivity is necessary for large scale networks, even when ensured, the routing outcome is seriously affected in terms of throughput when RSS is employed. If the networks are sparse, the loss rate can reach 80% to 90% regardless of the localisation method used. The failure causes have been studied and for each type, loss of connectivity is the fundamental reason. However, when the optimal density is ensured, inaccurate localisation is the most important cause for failure.

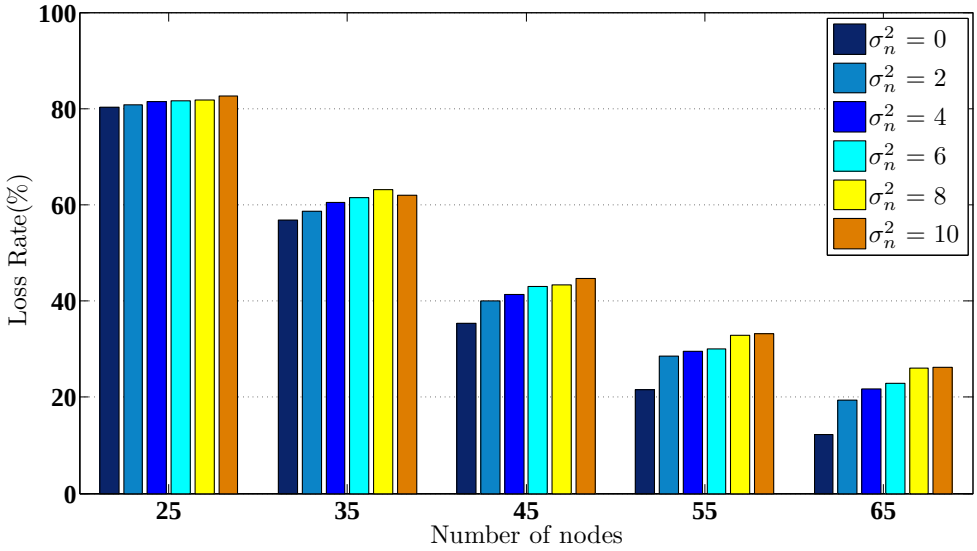

(a) For networks with ToA ranging.

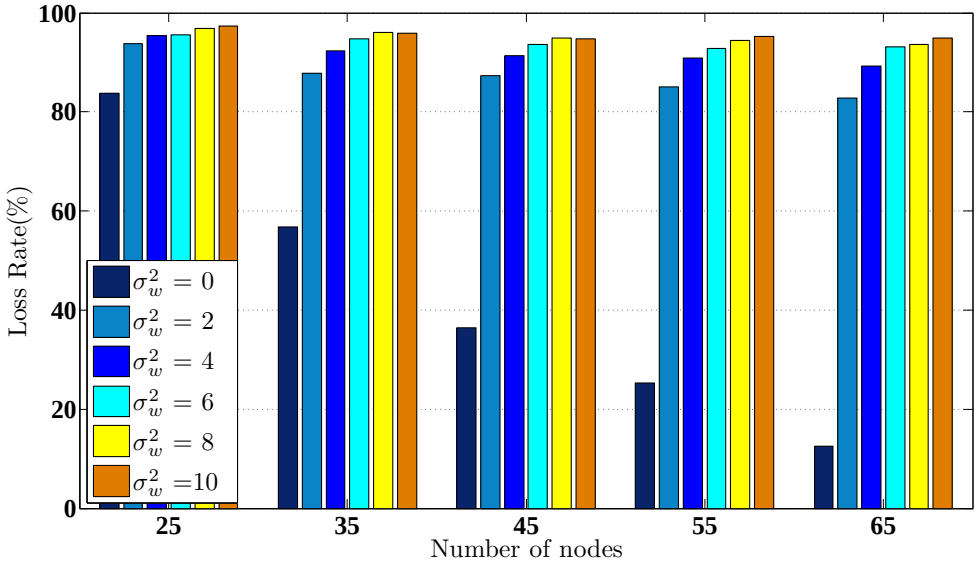

(b) For networks with RSS ranging.

Figure 6.2: Loss Rate (for LLS).

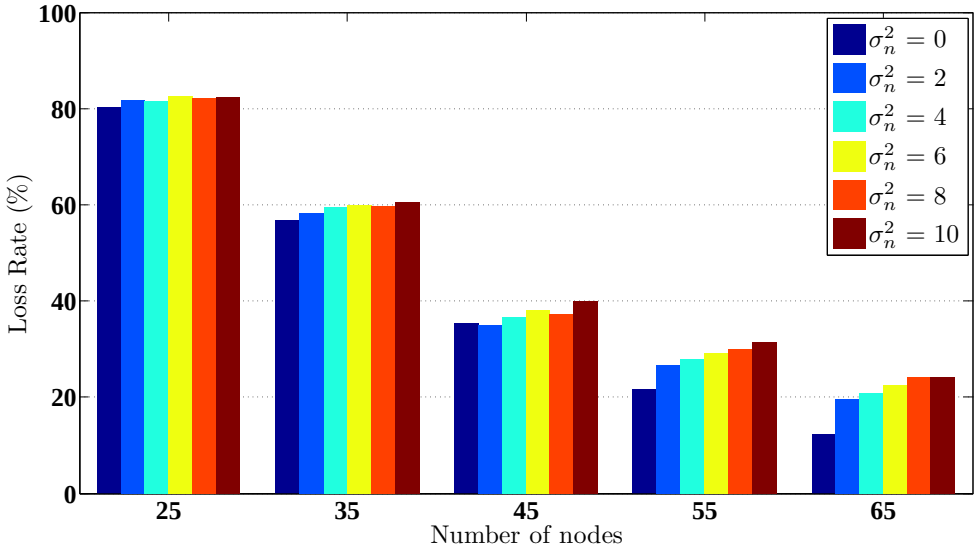

(a) For networks with ToA ranging.

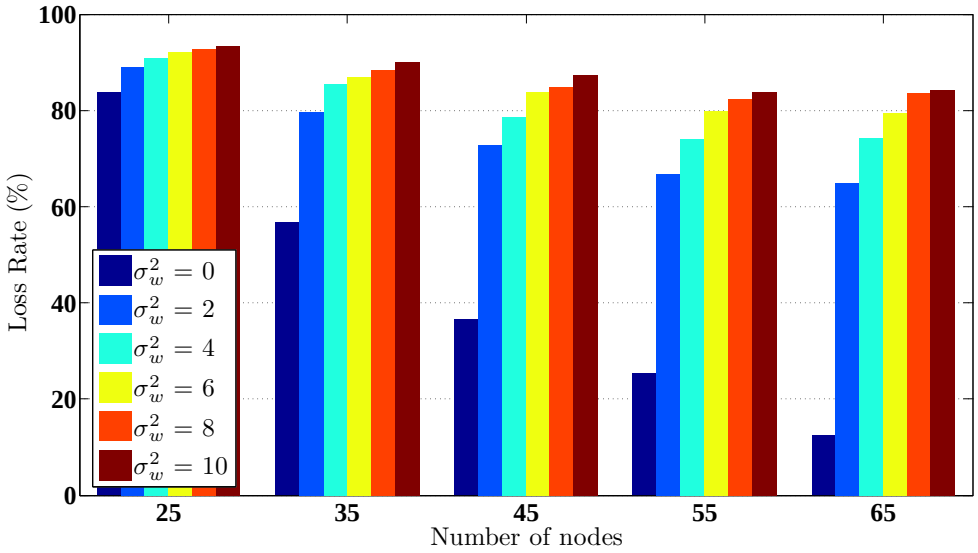

(b) For networks with RSS ranging.

Figure 6.3: Loss Rate (for ML).

The results of the present study are limited to the use of 8 anchor nodes, but a higher number of anchors involved in the localisation process would positively impact the positioning results and the routing. Also the findings herewith refer to a maximum of 65 nodes, larger and more congested networks, considering more practical issues, such as clock synchronization or the introduction of the ARQ

protocol would provide different results.

6.3 Geographic Routing Resilient to Location Errors

It has been concluded in section 6.2 that location errors have a significant impact on geographic routing performance. If the localisation is inherently erroneous, then the routing algorithm must be able to cope with these errors and provide quality of service. Here, it is considered that the location errors are independent Gaussian random variables and that the error variance of each node is different. Let there be a relay node S_i, with $i = 1, \ldots, I$, where I is the number of transmitting nodes along a routing path. Let F_j be a forwarding candidate of S_i, with $j = 1, \ldots, J$, where J is the number of neighbours of S_i with positive progress to destination D. In the two dimensional plane, S_i and F_j have the real coordinates $S_i\,(x_i,\, y_i)$ and $F_j\,(x_j,\, y_j)$ and the estimated locations $S_i^{'}\,(\hat{x}_i,\, \hat{y}_i)$ and $F_j^{'}\,(\hat{x}_j,\, \hat{y}_j)$, where $\hat{x}_i = x_i + W_i$, $\hat{y}_i = y_i + W_i$, $\hat{x}_j = x_j + W_j$ and $\hat{y}_j = y_j + W_j$. $W_i \sim \mathcal{N}\,(0,\, \sigma_i^2)$ and $W_j \sim \mathcal{N}\left(0,\, \sigma_j^2\right)$ are Gaussian random variables with zero mean with standard deviation σ_i and σ_j. For each node, it is considered that the error variance is equal on the x and y axes. The probability density function of the measured distance $\hat{d_{ij}}$ between 2 nodes ($S_i^{'}$and $F_j^{'}$) follows a Rice distribution

$$p\left(\hat{d_{ij}}\right) = \left(\frac{\hat{d_{ij}}}{\sigma_{ij}^2}\right) \exp\left(-\frac{\hat{d_{ij}}^{\,2} + d_{ij}^2}{2\sigma_{ij}^2}\right) I_0\left(\frac{\hat{d_{ij}} d_{ij}}{\sigma_{ij}^2}\right). \tag{6.1}$$

The estimated distance $\hat{d_{ij}}$ is given by (6.4) and d_{ij} is the accurate distance between S_i and F_j (6.3).

$$\hat{d_{ij}} = \sqrt{\left(\hat{x}_i - \hat{x}_j\right)^2 + \left(\hat{y}_i - \hat{y}_j\right)^2} \tag{6.2}$$

$$d_{ij} = \sqrt{\left(x_i - x_j\right)^2 + \left(y_i - y_j\right)^2}. \tag{6.3}$$

I_0 is the modified Bessel function of the first kind and order zero and $\sigma_{ij}^2 = \sigma_i^2 + \sigma_j^2$. The mean (expectation) of the estimated distance $\hat{d_{ij}}$ is

$$E\left(\hat{d}_{ij}\right) = \sigma_{ij}\sqrt{\frac{\pi}{2}} L_{\frac{1}{2}}\left(-\frac{d_{ij}^2}{2\sigma_{ij}^2}\right), \tag{6.4}$$

where $L_{\frac{1}{2}}(x)$ denotes the Laguerre polynomial (6.5) and I_1 is the modified Bessel function of the first kind and first order.

$$L_{\frac{1}{2}}(x) = \exp\left(\frac{x}{2}\right)\left[(1-x)\, I_0\left(-\frac{x}{2}\right) - x I_1\left(-\frac{x}{2}\right)\right]. \tag{6.5}$$

The variance of the estimated distance $\hat{d_{ij}}$ is

$$Var\left(\hat{d_{ij}}\right) = 2\sigma_{ij}^2 + d_{ij}^2 - \left(\frac{\pi\sigma_{ij}^2}{2}\right) L_{\frac{1}{2}}^2\left(-\frac{d_{ij}^2}{2\sigma_{ij}^2}\right). \tag{6.6}$$

According to the simple forwarding algorithm MFR presented in the section 6.1, when a node S_i has to choose among the available forwarding candidates with positive advance, the next hop F_j will be the one closest to the destination D, so the node with the largest distance d_{ij}. However, it is likely that the furthest node

from S_i will also be the nearest to the edge of R. Because all choices are made based on the estimated distances, the transmission is susceptible to failure and energy wastage. If a statistical error characteristic associated with the measured location of each node (a mean and error variance) is known and communicated along with the coordinates, then the forwarding decision can make use of this data.

Below a novel routing proposal to address the presence of location errors is made. Its aim is to minimize the effect of inherent positioning errors on the network throughput, when nodes use a fixed transmission power. To be able to analyse strictly the forwarding techniques, it is assumed that the communication is not affected by the environment.

It is proposed that S_i first calculates the mean square error (MSE) associated with all F_j with

$$MSE_{ij} = E\left(\hat{d}_{ij} - d_{ij}\right)^2 = E\left(\hat{d_{ij}}^2\right) - 2d_{ij}E\left(\hat{d_{ij}}\right) + d_{ij}^2, \tag{6.7}$$

where $E\left(\hat{d_{ij}}\right)$ is calculated with (6.4) and $E\left(\hat{d_{ij}}^2\right)$ is calculated as follows

$$E\left(\hat{d_{ij}}^2\right) = E(\hat{x}_i^2 - 2\hat{x}_i\hat{x}_j + \hat{x}_j^2) + E(\hat{y}_i^2 - 2\hat{y}_i\hat{y}_j + \hat{y}_j^2). \tag{6.8}$$

Using the second moments in (6.8), i.e. $E(\hat{x}_i^2) = x_i^2 + \sigma_i^2$, $E(\hat{y}_i^2) = y_i^2 + \sigma_i^2$, $E(\hat{x}_j^2) = x_j^2 + \sigma_j^2$ and $E(\hat{y}_j^2) = y_j^2 + \sigma_j^2$, (6.9) is obtained

$$E\left(\hat{d_{ij}}^2\right) = 2\sigma_i^2 + 2\sigma_j^2 + x_i^2 + x_j^2 + y_i^2 + y_j^2 - 2x_ix_j - 2y_iy_j. \tag{6.9}$$

The actual distance d_{ij} is not available as the accurate locations are unknown,

hence the calculations are made using the estimated coordinates instead. The next step is to calculate the mean square error ratio (MSER) associated with each forwarding candidate F_j and to detect the best choice as follows

$$MSER_{ij} = MSE_{ij}/\hat{d}_{ij}, \tag{6.10}$$

and finally

$$F_j = \arg\min\ (MSER_{ij})\,. \tag{6.11}$$

By choosing the neighbour F_j with the minimum value for MSER, a balance is obtained between the shortest distance to D and the smallest error of the next hop. In the special case of 2 forwarding options equally far from S_i, the next hop will be the node with the smallest error. If the error characteristics are the same, the next hop will be the furthest one from S_i. So, F_j is chosen depending on the scale of the error in comparison with the distance.

The algorithm can be further improved by considering that F_j, although optimal from the MSE point of view, can still be close to the edge of R, especially when few routing options are available. The routing selection can be refined by considering a condition similar to that of MEP, but redefined as follows: that the squared difference between R and the estimated distance to the neighbour node should be greater than the variance of the erroneous distance (6.12). The quadratic form is used to have the same unit of measurement. This is referred to as the CMSER algorithm. While in the simulation, the condition (6.12) when used independently

is referred to as COND.

$$\left(R - \hat{d_{ij}}\right)^2 > Var\left(\hat{d_{ij}}\right). \tag{6.12}$$

For a complete comparison LED is now based on the maximum $E\left(\hat{d}_{ij}\right)$ used to determine the F_j closest to D, instead of that used for the F_j closest to a predetermined energy-optimal forwarding position.

The PDR of the forwarding methods referred to as MFR, LED, COND, MSER and CMSER is analysed via MATLAB simulation when the nodes are erroneously localised with σ_i, $\sigma_j \in [0, \sigma_{max}]$. Nodes are randomly distributed over a network area of $200\,\mathrm{m}^2$. Several scenarios are studied, as described in table 6.3, where SE random sensing events take place. Each source sends 1 packet of 1024 bits in the network. The probability of correctly receiving any packet within R is 1, and 0 outside R. Performance is studied for different network densities (when the number of nodes N is varied), for different values of the maximum standard deviation of errors (σ_{max}) or different R. Each scenario consists of a network distribution with accurate node coordinates, where packet forwarding is made with MFR, and a number of η distributions with inaccurate locations (η being the number of iterations), where the errors have been modelled Gaussianly. The figures are obtained through averaging over η.

Table 6.3: Simulation Scenarios

Scenario	N	R(m)	σ_{max}(m) (% of R)	η	SE
1	50-600	40	8 (20%)	100	50
2	350	40	4-20 (10-50%)	100	50
3	200	10-100	5 (50-5%)	300	30

Fig. 6.4 presents the forwarding performance for different network densities. For

an optimal density of more than 200 network nodes, CMSER has a PDR between 70% to 80%. The MFR performs worst with approximately 10% PDR for all network densities. MSER and LED have a similar throughput with PDR values between 20% and 40%. It is however noticed that MSER has a slightly better performance. Looking strictly at COND an obvious improvement over the other methods is noticed, with a parallel behaviour to that of CMSER, but with a PDR below 50%. To indicate the reliability of the estimations, Fig. 6.4 illustrates the PDR with a 95% confidence level.

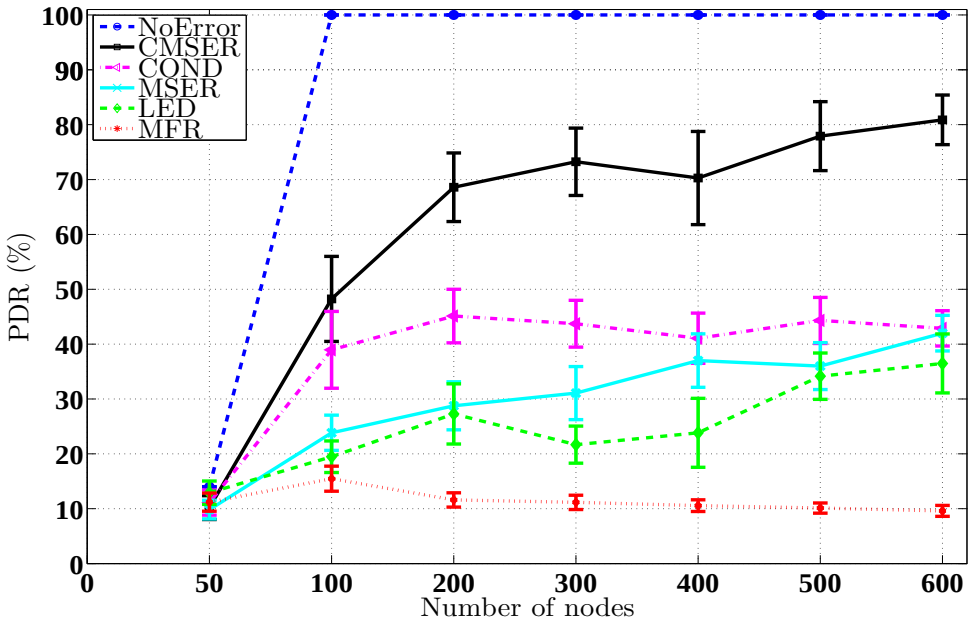

Figure 6.4: Routing performance for Scenario 1.

Looking at the PDR when σ_{max} is increased (Fig. 6.5), the performance degrades, as expected. The most severe performance degradation is that of LED, which for large errors behaves worse than MFR. COND has the second best performance maintaining a PDR of above 50% only for errors with σ_{max} up to 10% of R. CMSER is the best forwarding method here because its performance has the least abrupt degradation slope with the increase of errors. Although the PDR for

CMSER drops below 50% when σ_{max} is higher than 45% of R, it still maintains a significantly superior performance than that of the other methods.

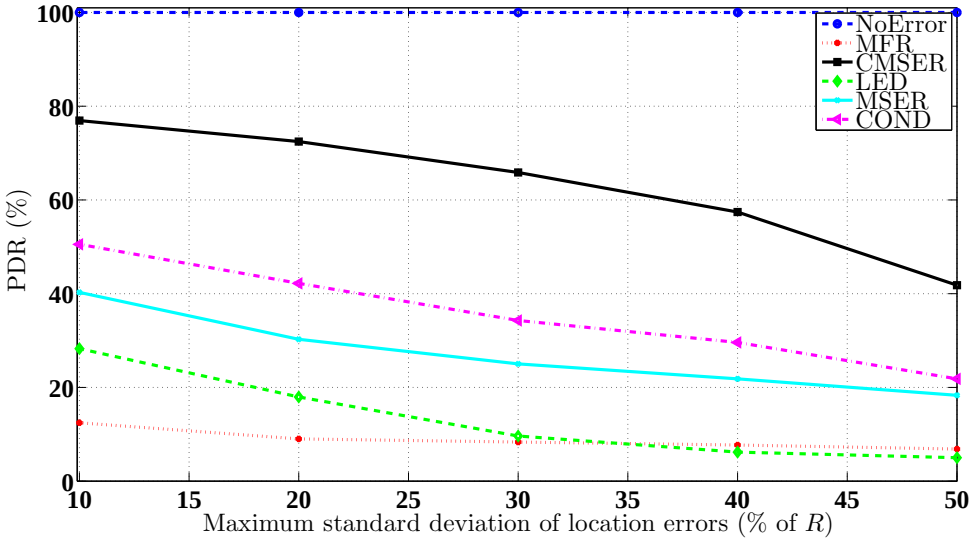

Figure 6.5: Routing performance for Scenario 2.

Varying the R (Fig. 6.6) within a reasonably dense network increases the potential forwarding options for each node. With more neighbours to choose from, the throughput also increases. For $R \leq 20$, all the considered forwarding methods fail to find neighbours to forward to and the routing fails. While for $R > 30$ CMSER increases its throughput progressively from 60% to almost 100% PDR, none of the other algorithms perform as well. The PDR curve for MFR remains detached below the rest of the algorithms for all values of R. The performance of CMSER, COND and LED is similar, but lower than for CMSER whose behaviour is constantly better than the rest.

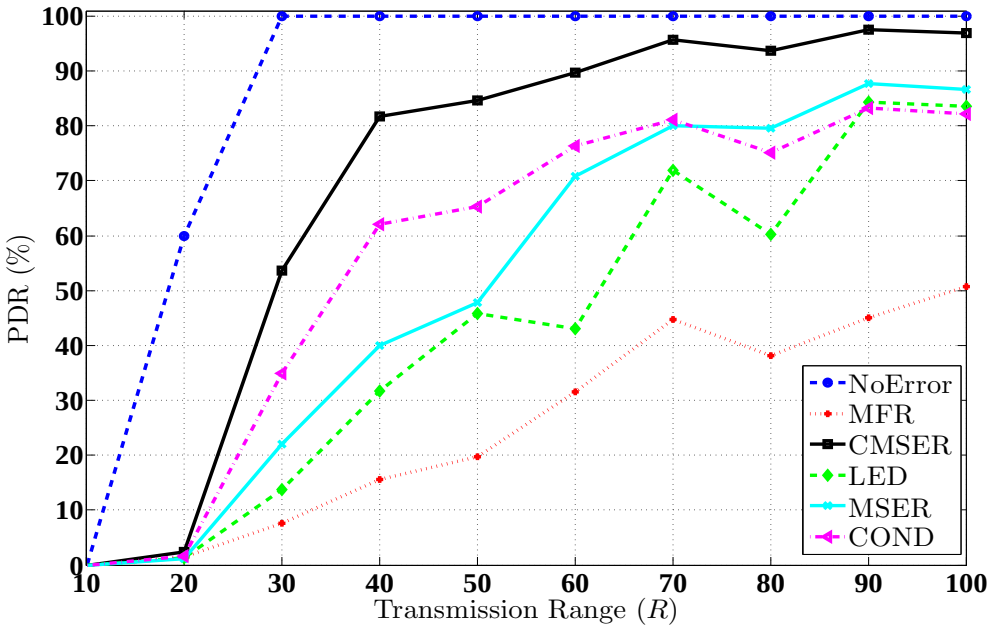

Figure 6.6: Routing performance for Scenario 3.

6.4 Summary

The design of new energy efficient algorithms as well as the analysis of the existing ones has to be made with realistic considerations of location errors. This is why the investigations of this chapter considered not only a statistical error model as previous work has, but the location error given by localisation techniques employed in real network design. It was found that geographic routing performance depends on the magnitude of the positioning errors as well as on the employed ranging methods, ToA or RSS. The differences in localisation influence both the PDR and the energy wastage of the networks.

Making geographic routing algorithms resilient to location error is imperative as this type of routing is theoretically energy efficient and very suitable to large scale networks. CMSER's performance in terms of throughput is considerably

better when compared to other basic greedy routing techniques such as those employed by MFR, MSER, COND and LED. The MATLAB simulations results confirm that CMSER outperforms other algorithms when the network objective is to increase packet delivery. CMSER makes use of the notion of maximum progress to destination, but gives more importance to the probability of success when coordinates are affected by location error. As a consequence, the energy spent on lost routing packets is considerably decreased. While the paths of the received packets of CMSER may be longer, the routes of the lost packets are kept short, being surpassed only by MFR, which does not cope with location error at all.

7 Conclusions and Future Work

7.1 Conclusions

This thesis focused on low complexity and low powered localisation of nodes in wireless networks. A major part of the thesis utilized the received signal strength (RSS) measurements for range estimation. Where the attention was given to environments with unknown path-loss model. This was followed by another aspect impacting location accuracy i.e. anchor node (AN) and target node (TN) network geometry. Finally, the impact of localised nodes on the geographic routing was discussed and algorithms were developed to mitigate the impact of location error.

For unknown path-loss models or models with unknown path-loss exponent (PLE), the natural strategy was to estimate the PLE alongside the location coordinates. However, first an theoretical analysis of incorrect PLE assumption was required to highlight its impact on location coordinates. This was done for a high complexity maximum likelihood (ML) estimator and for a low complexity linear least squares (LLS) estimator. For both methods it was shown that the simulation results are in agreement with the error analysis results and that both show degraded performance when α was incorrectly assumed. Performance degradation was even worse when the assumed PLE value was smaller than the correct value.

The next step was to jointly estimate the location coordinates and the PLE. Thus this was done for both the ML and LLS estimators. For the ML type estimator, the low complexity joint estimator (LCJE) was developed that operated on the Lavenberg-Marquardt (LM) method which is a modification to the Gauss-Newton (GN) method. Furthermore, in order to utilize the on hand data available about the PLE, the PLE was considered as a random variable and a MAP estimator was proposed. Simulation results proved that the MAP performs better in estimating α at low signal-to-noise ratio (SNR) and has a faster convergence in location estimation. As for the LLS technique, a simplistic technique to estimate the PLE by optimizing a single variable function was devised, this technique was referred to as the linear joint estimator (LJE). Simulation results showed that this technique had acceptable performance though the estimates were biased. In order to achieve even better accuracy, the LJE result was used as the initial estimate for more computationally intense but optimal algorithm and showed via simulation that it performed considerably better with a smaller number of iterations in comparison with an arbitrary initial estimate. Furthermore, in order to optimize the performance of the LLS algorithm, optimization techniques such as optimal anchor selection and weighted least squares (WLS) algorithms were also proposed.

In order to compare the mean square error (MSE) of estimators, the Cramer-Rao bound (CRB) has been extensively used as a benchmark. For the MAP estimator where the PLE was assumed to be a random variable, the conventional CRB could not have been used as a performance bound, hence a modified bound i.e. the hybrid Cramer-Rao bound (HCRB) was derived. The the HCRB for a random α was shown in general to be lower than the CRB due to the additional information provided about α. Yet when the TN was at equal distance from all ANs both bounds showed similar performance. As for the LLS algorithm the

conventional CRB again could not be used as a lower bound hence a linear CRB was derived. The error in the linear CRB was shown to be considerably larger than the conventional CRB.

Further CRB analysis was done on the impact of AN/TN geometry on location accuracy. It has been previously established that the relative angle of the TN with ANs had an impact on the accuracy of the estimated location of the TN. Thus, the goal was to formulate a mechanism that would guarantee minimum error due to network geometry or to place the ANs at optimal positions. Optimal AN positions were achieved that guaranteed best accuracy for the entire network area via extensive simulation. This is done via choosing the placement of ANs that offered the minimum mean CRB.

Inaccuracy in localisation estimates impacts the applications in the upper layers. Location based routing has been favoured in energy efficient WSNs. Conventional geographic routing algorithms are based on the assumption of accurate location knowledge making this routing type unreliable in practical applications. Thus impact of location error on geographic routing parameters such as the loss rate (LR) was done via simulation. It was found that geographic routing performance depends on the magnitude of the positioning errors as well as on the employed ranging methods, ToA or RSS. The differences in localisation influence both the LR and the energy wastage in the networks.

The next natural step was design algorithms that are resilient to location error. Thus an algorithm conditioned mean square error ratio (CMSER) was developed to counter the effects of location error. CMSER's performance in terms of throughput was considerably better when compared to other basic greedy routing techniques such as those employed by most forward within range (MFR) and least expected distance (LED). Overall energy costs were also kept down to a

minimum. CMSER makes use of the notion of maximum progress to destination, but gives more importance to the probability of success when coordinates are affected by location error. As a consequence, the energy spent on lost routing packets was considerably decreased. While the paths of the received packets of CMSER may be longer, the routes of the lost packets were kept short, being surpassed only by MFR, which does not cope with location error at all.

7.2 Future Work

Although localisation of wireless nodes has been a well studied subject, there still remains room for further research. Some current trends and topics for future research are highlighted below.

Cooperative localisation

Low cost and hence low powered node localisation is a critical requirement for WSNs. In a large and low powered sensor network, some TNs may not be in range of all the ANs. Thus, a method in which the in-range TNs can work in a peer-to-peer manner to localise the out of range nodes is required. This type of localisation scheme is known as cooperative localisation. One of the main problem in cooperative localisation is error propagation i.e. error in one node will show up in another node. In [64] Nayef Al-sindi proposed an error propagation aware algorithm in which only those nodes with small errors are used in a peer-to-peer manner. In [65] D. Niculescu proposed a range free algorithm which takes into account an approximated distance between two nodes rather than a metric distance. This approximated distance depends upon node density of the network. Another method used for cooperative localisation is multidimensional

scaling (MDS). MDS has its origins in psychometric and is recently introduced in node localisation. It uses the spectral decomposition of a doubly centred distance matrix. A rotated, translated and shifted configuration of the true configuration is obtained, which can be brought back to its original position subject to the availability of minimum 3-4 ANs for 2D-3D systems respectively. [66] and [67] uses classical MDS for localisation, using spectral decomposition. In [68] Shang, et al. proposed a new centralized algorithm called MDS-MAP(C), where C is for centralized. MDS-MAP(C) has three steps. In the first step shortest distance between all the nodes are calculated via Dijkstra or Floyd warshall algorithm. These shortest distances are used to construct the distance matrix. In the second step classical MDS is applied on this distance matrix to get relative configuration of the nodes. In the third step this relative configuration is rotated, shifted and translated to its original position by the help of ANs. The authors also propose a distributed version of their system in [69] which is known as the MDS-MAP(P) where P is for patched. In MDS-MAP(P) the whole network is divided in small sub-networks. MDS-MAP is applied on each section to get relative configuration. These relative configurations are patched together by using common nodes between two neighbouring sub-networks, forming the relative map of the full network which is then translated and rotated to its original position. This map stitching technique for localisation was introduced in [70]. The MDS algorithm involves spectral decomposition of a doubly centred distance matrix thus for large number of nodes a large matrix is obtained. For example for a network of hundred nodes a 100×100 matrix is formed. Performing spectral decomposition on such a matrix is computationally not efficient, thus iterative technique like SMACOF (Scaling by MAjorization aCOmplicated Function) [71] is used. In [72] the author combined ML estimator and SMACOF, and showed that the estimator converges faster and gives better estimation of the node position. In [73] the

author uses a weighted multidimensional scaling approach that does not involve spectral decomposition and shows better results than classical MDS.

Whichever localisation approach is used, cooperative localisation is often seen as a failure to produce appreciable results. This may be due to node failure, due to the effect of harsh environments or due the effect of improper placement of ANs in random deployment. Considerable amount of work is needed to be done in these areas, to limit the node failures, to improve the geometric dilution of precision (GDOP) and to overcome the effect of the harsh environment on localisation. Another issue that affects the accuracy of localisation nodes is the use of erroneous AN positions. Small amount of work is done on how to mitigate this error and needs to be addressed in future research.

Hybrid ToA-RSS Localisation

A recent trend is the design of efficient hybrid (ToA & RSS) location systems. This research area is still in its infancy. Since we inherently have the RSS measurements even in ToA systems, it is thus logical to manipulate both for increased accuracy. With N number of ANs and M number of TNs, we will have $N \times M$ estimates of RSS and ToA ranges. The next step is to either filter out or deprioritize erroneous samples of the observed data. For efficient design of hybrid (ToA & RSS) location systems, one way for example can be the design of algorithms that identify and reject non line of sight (NLoS) ToA estimates or giving higher weights to links with a smaller estimated PLE.

Multipath mitigation

Indoor environments face two main propagation challenges: multipath and NLoS The former significantly affects the accuracy of ToA based localisation techniques

for low bandwidth systems such as IEEE 802.11 – WLAN. Thus to enable accurate ToA-based ranging, multipath mitigation algorithms are required to provide better time-resolution and accurate distance estimation. Thus an extensive evaluation of existing multipath mitigation algorithms needs to be investigated to assess the limitations of existing techniques and their practicality in implementation.

Multipath mitigation algorithms are based on noise and signal sub-space decomposition techniques and the major approaches in literature are based on two algorithms for high-resolution delay estimation which are MUltiple SIgnal Classification (MUSIC) and Estimation of Signal Parameters Via Rotational Invariance Techniques (ESPRIT) [74, 75]. Recently different variants of MUSIC and ESPRIT have been proposed for different system implementations which are typically based on singular value decomposition (SVD) and eigen value decomposition (EVD) methods. The implementations are usually grouped under time-domain (cross-correlation method) [76] versus frequency domain (channel estimation method) [77]. Thus for future work capabilities of the existing multipath decomposition algorithms operating in realistic propagation conditions can be investigated. Finding the most suitable and practical approach is the desirable outcome.

Bibliography

[1] J. Proc, "Decca navigator," online: http://www.jproc.ca/hyperbolic/decca.html).

[2] D. of transportation United States Coast Guard, "Loran-c user handbook 1992 comdtpub p16562.6," online: http://www.navcen.uscg.gov.

[3] P.-U. of Colorad at Boulder, "Global positioning system overview," online: http://www.colorado.edu/.

[4] J. Proc, "Omega," online: http://www.jproc.ca/hyperbolic/omega.html.

[5] T. navigation Ltd, "Gps tutorial," online: http://www.trimble.com/gps/index.shtml.

[6] W. R. F. Myron Kayton, *Avionics navigation systems 2nd edition*. Wiley-IEEE, 1997.

[7] H. Trond JACOBSEN, "The russian vlf navaid system alpha, rsdn-20," online: http://www.vlf.it/alphatrond/alpha.htm.

[8] I. G. group, online: http://www.insidegnss.com/glonass.

[9] K. O'Neil, "Galileo - european satellite navigation system," Advanced Aviation Technology Ltd. online: http://www.aatl.net/publications/galileo.htm.

[10] S. Pandey, "A survey of lcalization techniques for wireless networks," *journal of chinese institute of engineers*, vol. 29, pp. 1125–1148, 2006.

[11] s. g. Zafer sahinoglu and ismail guvenc, Eds., *Ultra-wide band positioning systems, theoretical limits, ranging algorithms and protocols.* Cambridge University Press, 2011.

[12] J. R. C. Savarese and K. Langendoen, "Robust positioning algorithms for distributed ad-hoc wireless sensor networks," in *USENIX Tech. Annu. Conf.*, Jun. 2002.

[13] D. Niculescu and B. Nath, "Dv based positioning in ad hoc networks," *Telecommun. Syst*, vol. 22, pp. 267–280, 2003.

[14] I. Akyildiz, W. Su, Y. Sankarasubramaniam, and E. Cayirci, "A survey on sensor networks," *Communications Magazine, IEEE*, vol. 40, no. 8, pp. 102–114, 2002.

[15] P. Juang, H. Oki, Y. Wang, M. Martonosi, L. S. Peh, and D. Rubenstein, "Energy-efficient computing for wildlife tracking: design tradeoffs and early experiences with zebranet," *SIGOPS Oper. Syst. Rev.*, vol. 36, no. 5, pp. 96–107, Oct. 2002. [Online]. Available: http://doi.acm.org/10.1145/635508.605408

[16] F. Michahelles, P. Matter, A. Schmidt, and B. Schiele, "Applying wearable sensors to avalanche rescue," *Computers & Graphics*, vol. 27, p. 2003, 2003.

[17] N. Patwari, J. Ash, S. Kyperountas, A. Hero, R. Moses, and N. Correal, "Locating the nodes: cooperative localization in wireless sensor networks," *Signal Processing Magazine, IEEE*, vol. 22, no. 4, pp. 54–69, 2005.

[18] N. Patwari, A. Hero, M. Perkins, N. Correal, and R. O'Dea, "Relative location estimation in wireless sensor networks," *Signal Processing, IEEE Transactions on*, vol. 51, no. 8, pp. 2137–2148, 2003.

[19] G. G. Maria-Gabriella Di Benedetto, *Understanding Ultra Wide Band Radio Fundamentals.* Prentice Hall; 1 edition, 2004.

[20] M. M. Simon O. Haykin, *Modern Wireless Communications*. Prentice Hall, 2004.

[21] G. Mao, Fidan, and B. D. Anderson, "Wireless sensor network localization techniques," *Computer Networks*, vol. 51, no. 10, pp. 2529 – 2553, 2007. [Online]. Available: http://www.sciencedirect.com/science/article/pii/S1389128606003227

[22] D. Dardari, A. Conti, U. Ferner, A. Giorgetti, and M. Win, "Ranging with ultrawide bandwidth signals in multipath environments," *Proceedings of the IEEE*, vol. 97, no. 2, pp. 404–426, 2009.

[23] IEEE, "Ieee std 802.15.4-2007 (amendment to ieee std 802.15.-2006)."

[24] G. C. Carter, "Coherence and time delay estimation," *Proceedings of the IEEE*, vol. 75, no. 2, pp. 236–255, 1987.

[25] A. Muqaibel, A. Safaai-Jazi, A. Bayram, A. M. Attiya, and S. Riad, "Ultrawideband through-the-wall propagation," *Microwaves, Antennas and Propagation, IEE Proceedings*, pp. 581–588, 2005.

[26] Z. S. Sinan Gezici, "Uwb geolocation techniques for ieee 802.15.4a personal area networks," *MERL Report*, 2004.

[27] J. Riba and A. Urruela, "A non-line-of-sight mitigation technique based on ml-detection," in *Acoustics, Speech, and Signal Processing, 2004. Proceedings. (ICASSP '04). IEEE International Conference on*, vol. 2, 2004, pp. ii–153–6 vol.2.

[28] I. Guvenc and C.-C. Chong, "A survey on toa based wireless localization and nlos mitigation techniques," *Communications Surveys Tutorials, IEEE*, vol. 11, no. 3, pp. 107–124, 2009.

[29] P. Bergamo and G. Mazzini, "Localization in sensor networks with fading

and mobility," in *Personal, Indoor and Mobile Radio Communications, 2002. The 13th IEEE International Symposium on*, vol. 2, 2002, pp. 750–754 vol.2.

[30] A. Sayed, A. Tarighat, and N. Khajehnouri, "Network-based wireless location: challenges faced in developing techniques for accurate wireless location information," *Signal Processing Magazine, IEEE*, vol. 22, no. 4, pp. 24–40, 2005.

[31] R. Ouyang, A.-S. Wong, and C.-T. Lea, "Received signal strength-based wireless localization via semidefinite programming: Noncooperative and cooperative schemes," *Vehicular Technology, IEEE Transactions on*, vol. 59, no. 3, pp. 1307–1318, 2010.

[32] S. Mazuelas, A. Bahillo, R. Lorenzo, P. Fernandez, F. Lago, E. Garcia, J. Blas, and E. Abril, "Robust indoor positioning provided by real-time rssi values in unmodified wlan networks," *Selected Topics in Signal Processing, IEEE Journal of*, vol. 3, no. 5, pp. 821–831, 2009.

[33] G. S.-G. A. Bel, J.L. Vicario, "Localization algorithm with on-line path loss estimation and node selection," *Sensors*, pp. 6905–6925, 2011.

[34] X. Li, "Rss-based location estimation with unknown pathloss model," *Wireless Communications, IEEE Transactions on*, vol. 5, no. 12, pp. 3626–3633, 2006.

[35] K. Pahlavan and A. Levesque, *Wireless Information Networks*. New York: John Wiley & Sons, Inc, 1995.

[36] T. Rappaport, *Wireless Communications: Principles and Practice*. Englewood Cliffs, NJ: Prentice-Hal, 1996.

[37] H. Hashemi, D. Tholl, and G. Morrison, "Statistical modeling of the indoor radio propagation channel." in *Vehicular Technology Conference, 1992, IEEE 42nd*, 1992, pp. 338–342 vol.1.

[38] C. W. Helstrom, *Statistical theory of signal detection.* Pergamon Press, 1st edition, 1960.

[39] S. M. Kay, *Fundamentals of Statistical Signal Processing: Estimation Theory.* Upper Saddle River, NJ: Prentice Hall, Inc., 1993.

[40] G. A. F. Seber and C. J. Wild, *Nonlinear Regression.* Hoboken, NJ: Wiley-Interscience, 2003.

[41] S. Ghassemzadeh, R. Jana, C. Rice, W. Turin, and V. Tarokh, "A statistical path loss model for in-home uwb channels," in *Ultra Wideband Systems and Technologies, 2002. Digest of Papers. 2002 IEEE Conference on*, 2002, pp. 59–64.

[42] K. L. B. H. L. Van Trees, *Bayesian Bounds for Parameter Estimation and Nonlinear Filtering/Tracking.* Wiley-IEEE Press, 2007.

[43] J. Caffery, J.J., "A new approach to the geometry of toa location," in *Vehicular Technology Conference, 2000. IEEE-VTS Fall VTC 2000. 52nd*, vol. 4, 2000, pp. 1943–1949 vol.4.

[44] Z. S. Ismail Guvenc, Sinan Gezici, "Fundamental limits and improved algorithms for linear least-squares wireless position estimation," *Wireless Communications and Mobile Computing*, 2010.

[45] Y.-T. Chan, H. Yau Chin Hang, and P.-C. Ching, "Exact and approximate maximum likelihood localization algorithms," *Vehicular Technology, IEEE Transactions on*, vol. 55, no. 1, pp. 10–16, 2006.

[46] C. Chang and A. Sahai, "Estimation bounds for localization," in *Sensor and Ad Hoc Communications and Networks, 2004. IEEE SECON 2004. 2004 First Annual IEEE Communications Society Conference on*, 2004, pp. 415–424.

[47] S. Venkatesh and R. Buehrer, "A linear programming approach to nlos error mitigation in sensor networks," in *Information Processing in Sensor Networks, 2006. IPSN 2006. The Fifth International Conference on*, 2006, pp. 301–308.

[48] J. Wu, N. Mehta, and J. Zhang, "Flexible lognormal sum approximation method," in *Global Telecommunications Conference, 2005. GLOBECOM '05. IEEE*, vol. 6, 2005, pp. 3413–3417.

[49] L. Fenton, "The sum of log-normal probability distributions in scatter transmission systems," *Communications Systems, IRE Transactions on*, vol. 8, no. 1, pp. 57–67, 1960.

[50] T. Jia and R. Buehrer, "A new cramer-rao lower bound for toa-based localization," in *Military Communications Conference, 2008. MILCOM 2008. IEEE*, 2008, pp. 1–5.

[51] K. Seada, A. Helmy, and R. Govindan, "On the effect of localization errors on geographic face routing in sensor networks," in *Proceedings of the 3rd international symposium on Information processing in sensor networks*, ser. IPSN '04. New York, NY, USA: ACM, 2004, pp. 71–80. [Online]. Available: http://doi.acm.org/10.1145/984622.984633

[52] R. Shah, A. Wolisz, and J. Rabaey, "On the performance of geographical routing in the presence of localization errors [ad hoc network applications]," in *Communications, 2005. ICC 2005. 2005 IEEE International Conference on*, vol. 5, 2005, pp. 2979–2985 Vol. 5.

[53] S. Kwon and N. B. Shroff, "Geographic routing in the presence of location errors," *Comput. Netw.*, vol. 50, no. 15, pp. 2902–2917, Oct. 2006. [Online]. Available: http://dx.doi.org/10.1016/j.comnet.2005.11.008

[54] M. Witt and V. Turau, "The impact of location errors on geographic routing

in sensor networks," in *Proceedings of the International Multi-Conference on Computing in the Global Information Technology*, ser. ICCGI '06. Washington, DC, USA: IEEE Computer Society, 2006, pp. 76–. [Online]. Available: http://dx.doi.org/10.1109/ICCGI.2006.87

[55] B. Peng, R. Mautz, A. Kemp, W. Ochieng, and Q. Zeng, "On the effect of localization errors on geographic routing in sensor networks," in *Communications, 2008. ICC '08. IEEE International Conference on*, 2008, pp. 3136–3140.

[56] B. Peng and A. Kemp, "Impact of location errors on geographic routing in realistic wsns," in *Indoor Positioning and Indoor Navigation (IPIN), 2010 International Conference on*, 2010, pp. 1–7.

[57] Y. Kim, J.-J. Lee, and A. Helmy, "Modeling and analyzing the impact of location inconsistencies on geographic routing in wireless networks," *SIGMOBILE Mob. Comput. Commun. Rev.*, vol. 8, no. 1, pp. 48–60, Jan. 2004. [Online]. Available: http://doi.acm.org/10.1145/980159.980168

[58] B. Peng and A. Kemp, "Energy-efficient geographic routing in the presence of localization errors," *Computer Networks*, vol. 55, no. 3, pp. 856 – 872, 2011. [Online]. Available: http://www.sciencedirect.com/science/article/pii/S1389128610003415

[59] R. Marin-Perez and P. M. Ruiz, "Effective geographic routing in wireless sensor networks with innacurate location information," in *Proceedings of the 10th international conference on Ad-hoc, mobile, and wireless networks*, ser. ADHOC-NOW'11. Berlin, Heidelberg: Springer-Verlag, 2011, pp. 1–14. [Online]. Available: http://dl.acm.org/citation.cfm?id=2032462.2032464

[60] H. Takagi and L. Kleinrock, "Optimal transmission ranges for randomly

distributed packet radio terminals," *Communications, IEEE Transactions on*, vol. 32, no. 3, pp. 246–257, 1984.

[61] Jennic, "www.jennic.com/products/modules."

[62] A. M. Popescu, G. I. Tudorache, and A. Kemp, "Performance study of node placement for geographic routing in wsns," in *Communication Technologies Workshop (Swe-CTW), 2011 IEEE Swedish*, 2011, pp. 13–18.

[63] N. Salman, I. Rasool, and A. Kemp, "Overview of the ieee 802.15.4 standards family for low rate wireless personal area networks," in *Wireless Communication Systems (ISWCS), 2010 7th International Symposium on*, 2010, pp. 701–705.

[64] N. Alsindi, K. Pahlavan, and B. Alavi, "An error propagation aware algorithm for precise cooperative indoor localization," in *Military Communications Conference, 2006. MILCOM 2006. IEEE*, 2006, pp. 1–7.

[65] D. Niculescu and B. Nath, "Ad hoc positioning system (aps) using aoa," in *INFOCOM 2003. Twenty-Second Annual Joint Conference of the IEEE Computer and Communications. IEEE Societies*, vol. 3, 2003, pp. 1734–1743 vol.3.

[66] W. Shi and V. Wong, "Mds-based localization algorithm for rfid systems," in *Communications (ICC), 2011 IEEE International Conference on*, 2011, pp. 1–6.

[67] C.-H. Wu, W. Sheng, and Y. Zhang, "Mobile sensor networks self localization based on multi-dimensional scaling," in *Robotics and Automation, 2007 IEEE International Conference on*, 2007, pp. 4038–4043.

[68] Y. Shang, W. Rumi, Y. Zhang, and M. Fromherz, "Localization from connectivity in sensor networks," *Parallel and Distributed Systems, IEEE Transactions on*, vol. 15, no. 11, pp. 961–974, 2004.

[69] Y. Shang and W. Ruml, "Improved mds-based localization," in *INFOCOM 2004. Twenty-third AnnualJoint Conference of the IEEE Computer and Communications Societies*, vol. 4, 2004, pp. 2640–2651 vol.4.

[70] O.-H. Kwon and H.-J. Song, "Localization through map stitching in wireless sensor networks," *Parallel and Distributed Systems, IEEE Transactions on*, vol. 19, no. 1, pp. 93–105, 2008.

[71] P. J. F. G. I. Borg, *Modern Multidimensional Scaling: Theory and Applications*. Springer, 2005.

[72] X. Li, "Collaborative localization with received-signal strength in wireless sensor networks," *Vehicular Technology, IEEE Transactions on*, vol. 56, no. 6, pp. 3807–3817, 2007.

[73] F. Chan and H. So, "Efficient weighted multidimensional scaling for wireless sensor network localization," *Signal Processing, IEEE Transactions on*, vol. 57, no. 11, pp. 4548–4553, 2009.

[74] R. Schmidt, "A signal subspace approach to multiple emitter location and spectral estimation," Ph.D. dissertation, Standford University, 1981.

[75] R. Roy and T. Kailath, "Esprit-estimation of signal parameters via rotational invariance techniques," *Acoustics, Speech and Signal Processing, IEEE Transactions on*, vol. 37, no. 7, pp. 984–995, 1989.

[76] F. Bouchereau, D. Brady, and C. Lanzl, "Multipath delay estimation using a superresolution pn-correlation method," *Signal Processing, IEEE Transactions on*, vol. 49, no. 5, pp. 938–949, 2001.

[77] X. Li and K. Pahlavan, "Super-resolution toa estimation with diversity for indoor geolocation," *Wireless Communications, IEEE Transactions on*, vol. 3, no. 1, pp. 224–234, 2004.